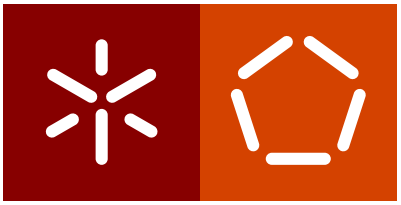

Universidade do Minho
Escola de Engenharia
Departamento de Eletrónica Industrial

Ana Raquel Mendonça de Sá Correia

Functional Electrical Stimulation for Gait Rehabilitation

November 2018

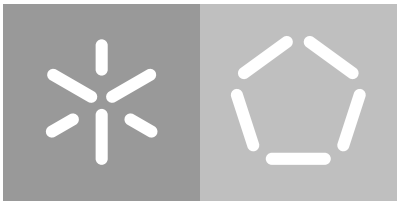

Universidade do Minho
Escola de Engenharia
Departamento de Eletrónica Industrial

Ana Raquel Mendonça de Sá Correia

Functional Electrical Stimulation for Gait Rehabilitation

Master dissertation
Master Degree in Industrial Eletronics and Computers

Dissertation supervised by
Professora Doutora Cristina P. Santos

November 2018

ACKNOWLEDGEMENTS

To my father and grandfather - thank you for the support and for all the help and knowledge you provided.

I would like to thank my advisor, Professor Cristina P. Santos, for the opportunity to work on this project, for all the guidance and for encouraging me to always work towards the best possible results. I would also like to thank Professor Jorge Martins, from IST, for providing the stimulator that made this project possible and for all the advice and help given.

To the doctoral student Joana Figueiredo, i would like to thank you for all the valuable input and support, and for always taking the time out to help. I would also like to thank everyone in the laboratory, for being welcoming and making it a fun place to work in.

A special thank you to my sister, for her valuable help in the design of this thesis, for volunteering as a test subject and for all the encouragement and support along the way.

Thank you to my friends Joana, Mariana and Beatriz, for the never-ending advice and for all the trips and moments we shared. It would not have been possible without you.

I would also like to thank Inês, Primo and Tiago, for all the memorable times we spent together throughout these 5 years. Working with you was as rewarding as it was enjoyable.

Finally, a special thank you to my mother and the rest of my family and friends, for their endless support throughout this journey.

ABSTRACT

Conditions that can lead to a **full or partial motor function loss**, such as stroke or multiple sclerosis, leave people with disabilities that may interfere severely with lower body movements, such as gait. **Drop Foot (DF)** is a gait disorder that results in a reduced ability or total inability to contract the *Tibialis Anterior (TA)* muscle, **causing an inability to raise the foot during gait**. One of the most effective methods to correct DF is **Functional Electrical Stimulation (FES)**. FES is a technique used to reproduce the activation patterns of functional muscles, in order to **create muscular contractions through electrical stimulation of the muscles' nervous tissue.**

FES has first been introduced in 1961. However, the available commercial FES systems still do not take into account the fact that the **gait differs from subject to subject**, depending on their **physical condition**, **muscular fatigue** and **rehabilitation stage**. Therefore, they are **unable to provide a personalized assistance to the user**, delivering constant stimulation pulses that are only based on gait events. Consequently, they promote the **early onset of fatigue** and **generate coarse movements**. This thesis aims to tackle the aforementioned issues by developing a **FES system for personalized DF correction**, tailored to each individual user's needs through the use of a **Neural Network (NN)**.

A Non-Linear Autoregressive Neural Network with Exogenous inputs (NARX Neural Network) was used to model the dynamics of the electrically stimulated TA muscle, in a **novel approach that uses both the foot angle and the foot velocity**. The model was combined with a **Proportional Derivative controller** to help compensate for any external disturbances. In order to create more natural movements, **reference trajectories** were obtained by recording the foot angle and velocity of **healthy subjects walking at different speeds**.

The system has been validated with a healthy subject walking at 3 different speeds on a treadmill: 1 km/h, 1.5 km/h and 2 km/h. It was **able to track the desired trajectory for every speed**, thus creating a **more natural movement** and **effectively correcting DF gait**.

Keywords: *Functional Electrical Stimulation; Drop Foot; Artificial Intelligence-based control; Closed-loop Control.*

RESUMO

Condições que podem levar a **perdas totais ou parciais de funções motoras**, como o acidente vascular cerebral ou a esclerose múltipla, deixam as pessoas com incapacidades que podem interferir severamente com movimentos dos membros inferiores, como a marcha. **Pé Pendente (PP)** é um distúrbio da marcha que resulta numa incapacidade de contrair o músculo TA, causando uma **incapacidade de contrair o pé durante a marcha**. Um dos métodos mais eficientes para corrigir o PP é a **Estimulação Elétrica Funcional (EEF)**. EEF é uma técnica utilizada para reproduzir os padrões de ativação dos músculos funcionais, de modo a **gerar contrações através de estimulação elétrica do tecido nervoso muscular**.

EEF foi introduzida pela primeira vez em 1961. No entanto, os sistemas comerciais de EEF disponíveis no mercado não têm em conta que a **marcha difere dependendo do sujeito**, da sua **condição física, da fadiga muscular e da fase de reabilitação**. Posto isto, são **incapazes de fornecer uma assistência personalizada ao utilizador**, aplicando pulsos de estimulação constantes baseados apenas nos eventos da marcha. Consequentemente, promovem o **início precoce da fadiga e geram movimentos bruscos**. Esta dissertação tem como objetivo a resolução dos problemas mencionados acima, com o desenvolvimento de um **sistema personalizado de EEF para a correção do PP**, adaptado às necessidades individuais de cada utilizador através do uso de uma **Rede Neuronal (RN)**.

Uma Rede Neuronal Auto-Regressiva com inputs Externos foi utilizada para modelar a dinâmica do músculo TA eletricamente estimulado, com uma **abordagem inovadora que utiliza o ângulo do pé e a velocidade do pé**. O modelo foi combinado com um **controlador Proporcional Derivativo**, para compensar quaisquer perturbações externas. De modo a gerar movimentos mais naturais, a **trajetória de referência** foi obtida gravando o ângulo e a velocidade do pé de **sujeitos saudáveis a andar a diferentes velocidades**.

O sistema foi validado com um sujeito saudável a andar a 3 velocidades diferentes numa passadeira: 1 km/h, 1.5 km/h e 2 km/h. Foi capaz de seguir a trajetória desejada para todas as velocidades, **gerando um movimento mais natural e efetivamente corrigindo a marcha de PP**.

Keywords: *Estimulação Eléctrica Funcional; Pé Pendente; Controlo baseado em Inteligência Artificial; Controlo em Malha Fechada.*

CONTENTS

LIST OF FIGURES

LIST OF TABLES

ACRONYMS

AFO Ankle-Foot Orthosis. 32

BP Back Propagation. 26

CC Contralaterally Controlled. 29

DF Drop Foot. ix, x, xiii, xiv, 2, 3, 4, 5, 6, 7, 15, 16, 18, 23, 28, 30, 32, 34, 35, 37, 39, 40, 43, 44, 45, 46, 51, 52, 53, 54, 55, 58, 64, 83, 84, 88, 90, 92, 96, 97, 102, 104, 105, 104, 105, 107, 108, 109, 111, 112, 113, 114

EMG Electromyography. vii, ix, 15, 17, 18, 21, 30, 31, 32, 33, 34, 37, 40, 83

FES Functional Electrical Stimulation. ix, xiv, xv, 1, 2, 3, 4, 5, 7, 9, 10, 11, 12, 13, 15, 16, 17, 18, 19, 20, 21, 24, 25, 26, 29, 31, 32, 36, 37, 39, 40, 41, 43, 57, 58, 88, 104, 105, 111

FRN Filtered Random Noise. xi, xv, 64, 67, 69, 71, 72, 71, 72, 73, 74, 75, 77, 78, 81, 108

FSR Forse-sensing Resistor. 15, 16, 40

FTDI *Future Technology Devices International Ltd.*. 45

GA Genetic Algorithm. 26

GOF Goodness of Fit. 67, 69, 95

ILC Iterative Learning Control. ix, 28

IMU Inertial Measurement Unit. x, xiii, 15, 16, 37, 40, 45, 46, 49, 50, 52, 53, 54, 66, 84, 89, 90, 91, 94, 111, 113

IRC Isometric Recruitment Curve. 19

MCU Microcontroller Unit. x, 43, 44, 45, 46, 48, 49, 50, 51, 52, 53, 58

MISO Multiple Input Single Output. 22, 23

MLP Multilayer Perceptron. 59, 61, 62, 63, 69

MSE Mean Square Error. 23, 69

MSU Modular Stimulation Unit. x, xv, 38, 40, 45, 47, 48

NARX Non-Linear Autoregressive with Exogenous input. 58, 59

NARX Neural Network Non-Linear Autoregressive Neural Network with Exogenous input. x, xi, xii, 58, 59, 60, 61, 62, 63, 64, 65, 67, 69, 71, 74, 75, 77, 80, 81, 82, 90, 91, 92, 95, 98, 99, 105, 111, 112

NN Neural Networks. 3, 6, 7, 27, 41, 53, 58, 59, 60, 62, 81

NRMSE Normalized Root Mean Square Error. 67

PD Proportional Derivative. xii, xiii, 53, 57, 83, 90, 91, 92, 95, 96, 97, 99, 100, 101, 105, 108, 112

PID Proportional Integral Derivative. 19, 24, 25, 26, 27, 41

PRBS Pseudo-Random Binary Sequences. 64

PRMS Pseudo-Random Multi-Level Sequences. xi, xv, 64, 67, 69, 71, 72, 73, 74, 81

RISE Robust Integral of the Sign of the Error. 29

RMSE Root Mean Square Error. 24, 27, 33, 34

RNN Recurrent Neural Network. 59

ROM Range of Motion. x, 53, 64, 81

RSA Residual Stimulation Artifact. 30, 31

SISO Single Input Single Output. 22, 23

SRT Successful Run Time. 29

STR Staircase Ramps. 64

TA *Tibialis Anterior*. x, xi, 2, 4, 5, 6, 16, 23, 24, 25, 32, 34, 40, 43, 44, 45, 46, 48, 53, 54, 57, 58, 61, 62, 65, 66, 67, 69, 74, 77, 80, 81, 84, 98, 105, 108, 111, 112

TR Triangular Ramps. xi, 64, 66, 81, 94

1

INTRODUCTION

1.1 MOTIVATION

Conditions that can lead to **full or partial motor loss**, as is the case of Cerebral Palsy, Stroke, Multiple Sclerosis, Amyotrophic Lateral Sclerosis, Muscular Dystrophy, Poliomyelitis, Muscular Atrophy and Spinal Cord Injuries, leave people with disabilities that **interfere severely with their daily activities** (Melo et al. (2015)). According to the World Health Organization, of the 15 million people that suffer a stroke worldwide every year, **5 million remain permanently disabled**. The Portuguese Society of Cerebrovascular Accident, reported that 16% of stroke patients develop slight to moderate disabilities while 41% lose their independence completely. Furthermore, a study conducted in the United Kingdom (Godwin et al. (2011)) concluded that the yearly rehabilitation cost for each stroke patient averaged at 13 000 €. When it comes to multiple sclerosis, the World Health Organization estimates that it affects 2.5 million people worldwide, while in Portugal, it affects over 8 thousand people. A global study on multiple sclerosis (Giovannoni and Pepper (2015)) found that, in Germany, a person spends around 5000 € every year for non-medical treatments, which is the case of rehabilitation. The disabilities that come as a consequence of these conditions can affect upper limb movements, which is the case of grasp, or **lower limb movements, such as gait**. They affect the patients' quality of life and, in some cases, may even lead to a loss of independence. Hence, there is a **growing need for more economic and effective rehabilitation methods**.

If the disability is caused by a disruption in the neural pathways, but the muscles remain fully functional and contain excitable nerves, they are still able to contract, despite being paralyzed or paretic. These contractions can be achieved with Neuromuscular Electrical Stimulation, NMES, which aims at reproducing the activation pattern of functional muscles. However, in order to use these contractions for a useful task, **Functional Electrical Stimulation (FES)** is necessary, as it is a form

of NMES used specifically to produce a useful movement (Sheffler and Chae (2007)). Additionally to reproduce muscle patterns, FES is also commonly used to benefit breathing, intestinal, urinary, and sexual functions (de Souza et al. (2017)).

Functional Electrical Stimulation (FES) can replace the central nervous system, generating the necessary potential to induce a muscular contraction (Kesar et al. (2008)). It works by **stimulating the nervous tissue of the paralyzed muscle so that it contracts**, consequently generating movement. The pulses with which they are stimulated can have different parameter values, such as amplitude, frequency or width. Being able to **vary the pulse's parameters in real-time** is important, given the **non-linear behaviour muscles exhibit while being electrically stimulated** (Hunt et al. (1998)). It should also be taken into account that different muscles have different characteristics and, therefore, need different stimulation patterns.

Drop Foot (DF) is a gait disorder that results in a reduced ability or total inability to contract the TA muscle. Subjects affected by DF are more prone to falls, since they **cannot lift the foot off the ground completely**. In the case of the elderly, this lack of mobility can even be fatal. It is estimated that 75% of the people that survive a stroke are affected by some kind of lower limb weakness and, of those, 20% are affected by DF (Johnson et al. (2004)). If the DF is caused by damaged nerves, **FES can have a crucial part in achieving a partial or full recovery**, since the electric pulses delivered to the muscle help strengthen the synaptic connections of the spinal cord (Brend et al. (2015)). However, if it is the consequence of a progressive neurological disease, it will affect the patient throughout his life.

Even though FES has been used since 1961, when the first system to correct drop foot was created by Liberson, W. T.; Holmquest, H. J.; Scot, D.; Dow (1961), most of the recently developed systems still use **pre-programmed movements**, not only to assist gait but also to generate hand movements (Burridge et al. (2007), Khattar et al. (2012), Van Swigchem et al. (2011), Venugopalan et al. (2015)). Taking into account the fact that **muscular activation patterns are different for every subject**, depending on their **physical condition**, **muscular fatigue** and **rehabilitation stage** (Gorgey et al. (2009)), it is important to provide a **personalized assistance for each user**.

FES devices for DF correction are meant to be simple and easy to use, being usually constituted by **two electrodes**, one placed on top of the *Common Peroneal* nerve and the other placed on top of the TA muscle, connected to a **small-sized stimulator**, a **sensor** and a **controlling unit**. The aim of such systems is to provide a **convenient and ergonomic** way for the subject to achieve a normal gait pattern that can be **integrated in his daily activities**. The DF correction systems currently available in the

market **fail to take into consideration the time-variant dynamics of the electrically stimulated muscles** (Hunt et al. (1998)), the **onset of muscular fatigue** and any **external disturbances** (Melo et al. (2015)), by applying a constant stimulation pulse that only depends on the gait phase. This **deprives the user of an assisted-as-needed experience** and **promotes the early onset of fatigue**. Hence, the systems fail to deliver optimal excitation patterns for the muscle's nervous system, **generating non-natural coarse movements** (Brunetti et al. (2011)). Therefore, the applied stimulation intensity must be **adequate to every user**, increasing and decreasing depending on the desired movement, **mimicking the biological behaviour**. This makes the subject more motivated and invested in his own recovery, since when constant high stimulation pulse values are applied constantly, fatigue onsets faster and the subject may even feel a slight discomfort on the area where stimulation is being applied.

In order to provide a FES **rehabilitation treatment that is tailored for each user**, **models** are created in order to capture the dynamics of the electrically stimulated muscle. There are two types of models that are used for FES systems: mechanistic or biomechanical models and empirical or black-box models. Although mechanistic models are based on the physiological properties of the muscle, they require more parameters and more complex calibration routines. **Empirical models**, on the other hand, only **describe the relationship between the stimulation pulse and the corresponding muscular movement**, which means they are less complex (Previdi (2002)). Nonetheless, they can be just as accurate and precise, since they only sacrifice the level of detail when compared to the mechanistic models (Luzio de Melo (2014)). Therefore, more recently, empirical models, in particular **Neural Networks (NN)**, have been extensively used to model both upper limb and lower limb muscles (Azura et al. (2016), Yassin et al. (2017), Yilei et al. (2006), Popov et al. (2015), Imatz-ojanguren et al. (2016)).

These **models** are able to **capture the dynamics of the modeled muscle** and are **created specifically for each subject**. The result is a control strategy that is able to determine which pulse value is more adequate to apply to the subject, depending on the desired movement. This represents a personalized alternative that is able to **delay muscular fatigue**, since the necessary pulse value is predicted by the model at every given moment. Furthermore, the **models are usually combined with a controller**, in order to compensate any external disturbances that may occur (Chang et al. (1997)).

It it important to further research on the most adequate control strategies, so that the patient can not only feel comfortable when wearing the system but also have a **personalized long-lasting experience**. Although the system developed in this project

is meant to correct DF, in the long run, it could treat more than one specific gait pathology. More stimulators can be used simultaneously to address more complex pathologies and it could possibly be combined with a powered knee orthosis, in order to help patients with paraplegia stand up or even walk.

1.2 PROBLEM STATEMENT

DF is a gait disorder that results in a reduced ability or total inability to contract the TA muscle. This results in a **failure to raise the foot and toes**, which is called dorsiflexion. It is most commonly a result of a disruption in the nerve pathways, which means the nerves in the leg muscles remain fully functional. FES can act in place of the central nervous system, generating action potential to induce muscular contraction (Hayashibe et al. (2011)). For DF correction, it works by **stimulating the nervous tissue of the TA muscle** so that it contracts, consequently raising the foot and toes. A diagram of a DF correction system using FES can be seen in Figure 1.1.

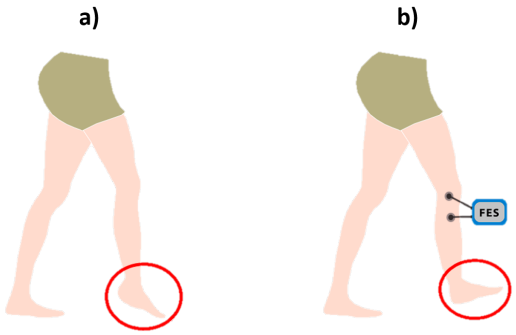

Figure 1.1: DF correction diagram using FES: a) DF without FES and b) DF correction using FES.

The current DF correction systems available in the market provide an open-loop control strategy that applies constant stimulation pulse values that only depend on the gait event. Hence, they are **not tailored to the user's needs, fail to compensate any external disturbances** and **promote the early onset of fatigue**. Furthermore, by applying a constant stimulation pulse, the movements are more coarse and unnatural.

In addition to this, even though in the research field there have been advancements in order to create more adaptable FES systems, there is still room for improvements. In the case of DF correction, a **dynamic model of the TA muscle has not yet been in used**.

This project aims at solving this problem, by providing the user with a **personalized assistance with the creation of a dynamic model**. Additionally, a controller will be combined with the model, in order to **compensate any real-time external disturbances**. The **gait patterns of healthy people** will also be acquired and fed into the controller, so the DF patients can have a **gait that is as close to the natural one as possible**.

1.3 GOALS AND RESEARCH QUESTIONS

The purpose of this work is the creation of a **wearable FES system for real-time DF correction**, so patients can **achieve a healthy gait pattern**. The system should be **personalized to each user's needs**, be able to **provide assistance at different walking speeds** and be **comfortable** for daily use. Thus, to achieve this main objective, three main questions must be answered:

- **How to provide a personalized experience for each user?**

  To adapt the system to the user's needs, it is necessary to find the best way to **model the electrically stimulated muscles**, so that the model can not only be **tailored to the user's anatomical characteristics**, but can also be incorporated in a **real-time control strategy**. Therefore, a **novel way to model the electrically stimulated TA muscle** will be proposed.

- **How to provide a comfortable long-lasting experience for each user?**

  To increase user comfort it is necessary to **delay the onset of fatigue** and create a **light wearable system** that does not constrain the user's daily movements. In order to do this, an **assisted-as-needed control strategy** should be implemented, so the system only delivers the necessary stimulation at any given moment. Furthermore, a light stimulator that allows **real-time update of pulse parameters** should be used for this system.

- **How to ensure a natural gait pattern?**

  To **prevent coarse movements** and **generate a gait pattern similar to the natural one**, it is necessary to study the gait pattern of healthy subjects and find a way to reproduce it with FES. Moreover, it is also necessary to determine if the **gait pattern changes depending on the walking speed of the subject**.

Based on the previous identified research questions, several goals were established in order to develop the aforementioned system:

Goal 1 Study DF and the muscles affected by this pathology;

Goal 2 Research of the best muscle modeling and control strategies for DF correction;

Goal 3 Identify the most adequate stimulator to integrate in the system;

Goal 4 Select the most adequate sensor for gait event detection and foot movement tracking;

Goal 5 Select the most adequate microcontroller unit to implement the control strategy;

Goal 6 Implement and test the chosen strategy to model the electrically stimulated TA muscle;

Goal 7 Track the foot movement of healthy subjects during gait at different speeds;

Goal 8 Based on the foot movement acquired on the previous stage, create a reference trajectory for the control strategy;

Goal 9 Implement and test the chosen control strategy;

Goal 10 Compare the performance of the model alone with the performance of the model combined with the controller;

Goal 11 Validate the control strategy with a healthy subject;

1.4 CONTRIBUTIONS

What distinguishes this project from both the commercial and the research prototypes available for DF correction, is the use of a *Neural Networks (NN)* to create a novel dynamic model for the TA muscle, using both the foot angle and the foot angular velocity. This creates a **personalized experience for the users**, since the model is tailored to the specific dynamics of their electrically stimulated TA muscle, allowing the system to **adapt the stimulation parameters to the user's anatomy**.

This project won the 1st place in the Fraunhofer Portugal Challenge in the MsC category and has also yielded an article that has been submitted to the Robotics and Automation Letters.

1.5 THESIS' OUTLINE

This thesis proposes a novel approach to DF correction, using a NN-based control, that models the individual dynamics of the electrically stimulated TA muscle, thus creating a personalized experience for the user. This thesis contains six chapters in total.

Chapter 2 contains a summary of the main FES features, and how they are applied throughout the literature, as well as the main control strategies found in FES systems used to generate functional movements.

Chapter 3 begins with a global view of the created system, to which follows a more in depth look into all of the components.

Chapter 4 presents the personalized muscular model created with a NN, along with the method that was used in its creation. Different models are tested in order to assess which one is better fit for the real-time control strategy.

Chapter 5 uses the model created in the previous chapter, in order to implement the real-time trajectory tracking control strategy for DF correction. Static and gait trials are conducted with a healthy subject in order to determine the performance of the controller.

Chapter 6 concludes the thesis, with an analysis of the work developed and a guideline for future work.

2

STATE OF THE ART

In this chapter the commercial and research existent Functional Electrical Stimulation (FES) systems will be examined. In particular, the sensors used, the stimulators and its parameters and the control strategies. The chapter begins with an explanation of what FES is, its characteristics and what it is used for. It is followed by the types of stimulation used in FES systems, along with its benefits, and the type of sensors used in the different systems. It is followed by an extensive study of all the control strategies used with FES systems. Finally, the commercial systems that exist in the market and the systems created in the research field will be presented, and the chapter ends with a discussion of the content that was presented.

2.1 INTRODUCTION

FES is used to **produce functional muscular movements**, by activating the muscles with an electrical pulse, generating the necessary movements to produce a useful task. Thus, a paralyzed muscle, once excited, can produce movements that the person could no longer produce on its own. This technique is used in rehabilitation, to assist lower limb or upper limb movements, in order to rehabilitate the muscles and nerve pathways, so that the users can ultimately produce the same movements on their own, if possible (Brend et al. (2015)). However, despite being generally said that FES stimulates the muscle, the unit that is stimulated is normally the nerve, rather than the muscle. This happens because the activation threshold for muscle fiber is much greater, compared to the activation threshold of nerve cells (Peckham and Knutson (2005)), as can be seen in Figure 2.1. Sometimes the muscle fibre is in fact stimulated, but that is reserved for cases when the muscle is denervated (Eberstein and Eberstein (1996)).

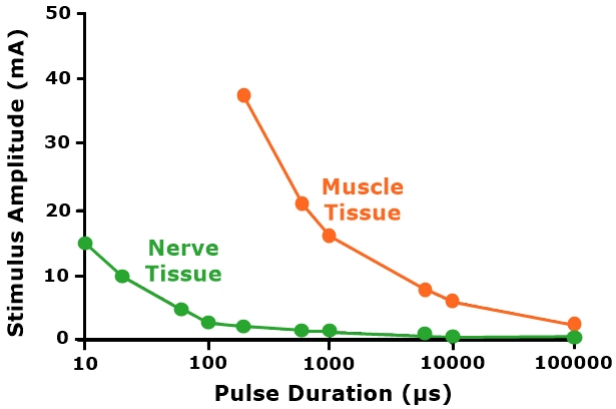

Figure 2.1: Stimulus amplitude necessary to produce a muscle response. Adapted from Peckham and Knutson (2005).

A FES system is constituted by three main components: the **actuator or stimulator**, the **sensor** and the **control unit**. The actuator **creates and delivers the pulses** to the desired muscle; the sensors **track the joint's kinematic movements** and in the case of gait correction systems, **detect the gait events** and the control unit implements the control strategy that sends **the pulse parameters of the actuator**, so that the resultant movement is in accordance to what is expected. The components of FES and their main functions can be seen in Figure 2.2.

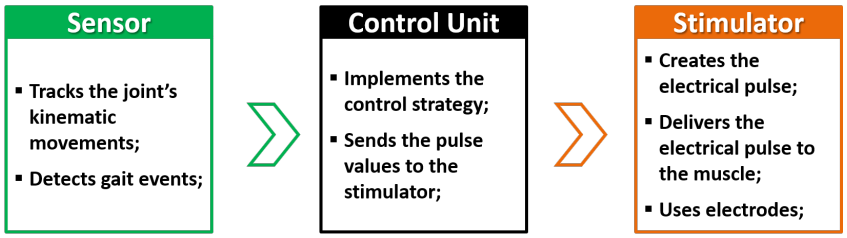

Figure 2.2: FES components and their main functions.

2.2 ACTUATOR

In a FES system, the actuator is generally an **electrical stimulator** that generates a **series of electrical pulses** to be **delivered to the muscle through electrodes**, creating a muscular movement. The electrical stimulator is constituted by 3 stages: the *Pulse Generator*, which can be an oscillator circuit or a microcontroller that allows the control of the pulse's parameters - frequency, width and amplitude -, the *Waveform Modulator*

which modulates the pulse with a carrier signal, in order to make it more adequate to stimulate muscles and the *Output Stage*, that amplifies the pulse to high-level voltage or current.

The generated stimulation should be biphasic, so that there are no charge imbalances in the skin, which can damage the tissue (Low et al.). The classical stimulation pulse shape is rectangular with a typical stimulation pulse often having a ramping up and down of stimulus, to avoid sudden muscular responses (Melo et al. (2015)). These types of pulses are more **commonly used in open-loop FES systems**, where a physician or the subject calibrates the pulse parameters - frequency, amplitude and width - to comfortable levels, and these values are **constantly applied throughout the stimulation**. The classical FES waveform is depicted in Figure 2.3.

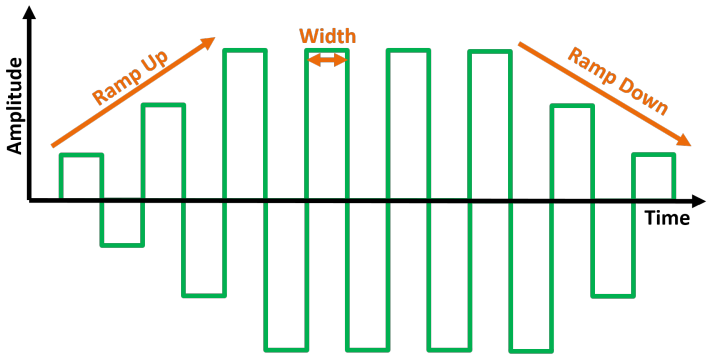

Figure 2.3: Typical FES waveform with balanced charges.

As more FES systems are being created, the tendency is shifting towards **closed-loop control strategies** that are able to provide a **personalized assisted-as-needed assistance** to the user. Therefore, the classic FES waveform is no longer the most recommended, since the **pulse must ideally vary in accordance to the movements** being made, the speed at which they are being made and the user of the system (Seel et al. (2016b)). The waveform of a stimulation pulse generated during closed-loop control, can have different widths, frequencies or amplitudes, as it should adapt to the user's movements. This type of adaptable FES pulse can be seen in Figure 2.4.

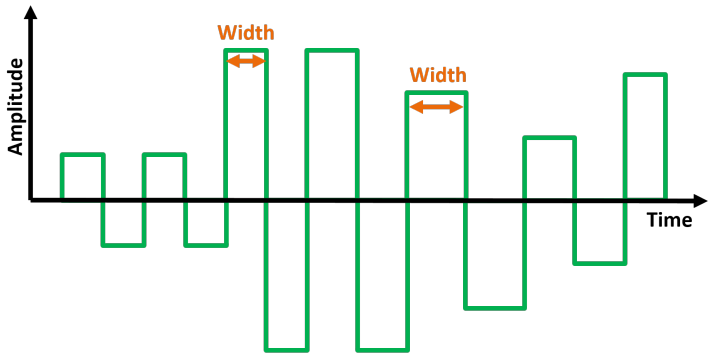

Figure 2.4: Adaptable FES waveform with balanced charges.

2.2.1 *Stimulation Parameters*

There are three stimulation parameters in a FES pulse: **frequency**, **amplitude** and **width**. **Frequency** is directly connected to **force generation**, meaning that higher pulse frequencies generate higher muscle force. However it is also associated with **muscle fatigue**, having been proved in various studies that **lowering stimulation frequency results in less fatigue** of the stimulated muscle (Gorgey et al. (2009), Gregory et al. (2007), Kesar et al. (2008)). Even though high frequencies increase the rate of muscle fatigue, frequencies that are too low create a series of muscular twitches. Therefore, a balance must be found when choosing the stimulation frequency, so that the muscle does not fatigue too quickly, but there is still a smooth muscular contraction.

Both the **pulsewidth** and the **pulse amplitude** are linked to **muscle fiber recruitment**, which in turn results in **stronger muscle contractions** (Doucet et al. (2012)). However the necessary pulsewidth and amplitude values to produce a movement vary from case to case, **depending on the different pain thresholds of the user, the electrode-skin interface and the muscular groups being stimulated** (Sheffler and Chae (2007)).

The reviews made by Melo et al. (2015) and Meng et al. (2017), collected the information of a large amount of commercial and research stimulators' parameters. Table 2.1 was created, in order to provide a more global look at the pulse's parameter values. This table was based on the data obtained on the reviews and on the data of other stimulators created for research in Chen et al. (2004) and Simonsen et al. (2016)).

Table 2.1: FES pulse parameters' most common and maximum values

Parameter	Definition	Unit	Common Values	Maximum Value
Frequency	Number of pulses produced per second	Hertz (Hz)	20 - 50 Hz	200 Hz
Width	Time span of a single pulse	Second (s)	0 - 500 us	1000 us
Amplitude	Intensity of the pulse	Ampere (A)	0 - 100 mA	260 mA

2.2.2 *Types of Stimulation*

There are currently **three types of stimulation** that are used in FES: **conventional** stimulation, **asynchronous** stimulation and **sequential** stimulation. Conventional stimulation only uses **one channel to stimulate a muscle group**, while both asynchronous and sequential stimulation use **multiple channels**. This is done in order to divide the stimulated muscle into different groups of muscle units, using multiple electrodes to stimulate the same area covered by one single electrode in conventional stimulation (Nguyen et al. (2011)), which is depicted in Figure 2.5.

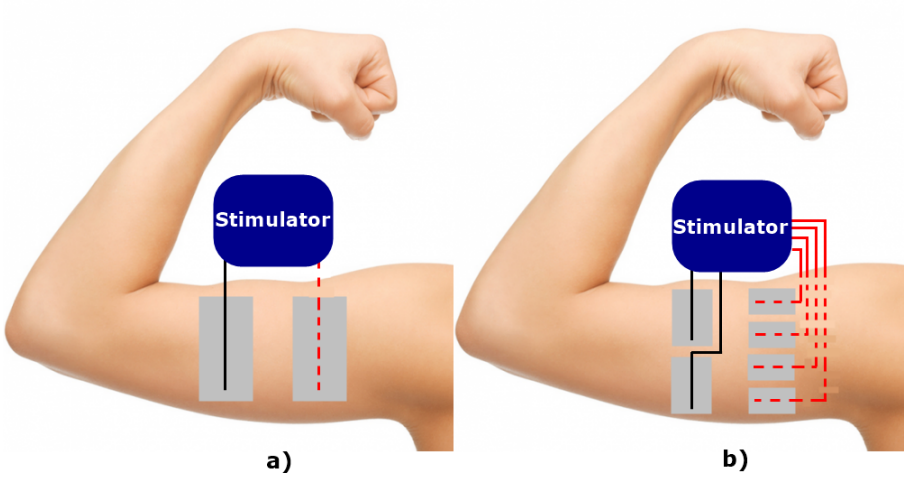

Figure 2.5: Electrode placement for a) conventional stimulation b) asynchronous or sequential stimulation. The active electrode is represented by the red dotted line.

In **sequential stimulation pulse trains are delivered sequentially** to each stimulation channel, while in **asynchronous stimulation the active stimulation**

channel is switched after each individual pulse is delivered (Downey et al. (2014)). Figure 2.6 depicts the different pulses corresponding to the different types of stimulation.

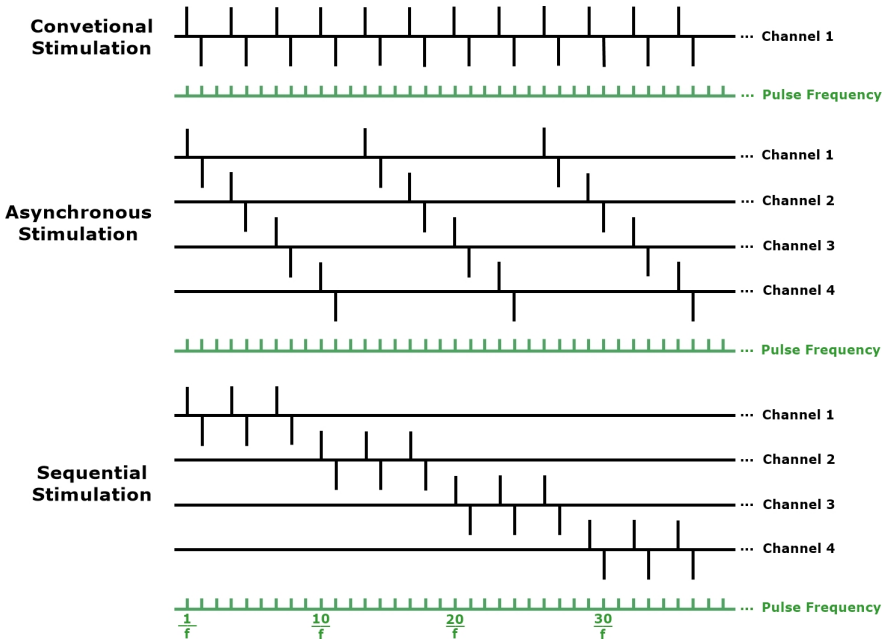

Figure 2.6: Different types of stimulation: conventional, asynchronous and sequential. Adapted from Downey et al. (2015b).

The **sequential and asynchronous** stimulation methods have been **proved to reduce muscle fatigue** caused by FES (Pournezam et al. (1988), Popović and Malešević (2009) Nguyen et al. (2011), Maneski et al. (2013), Downey et al. (2014), Downey et al. (2015a)). The study conducted in Pournezam et al. (1988) indicated that the lower the frequency applied in each channel, the faster the muscle recovery time was and the longer it took for the muscle to become fatigued. This study was backed by Popović and Malešević (2009), which **compared conventional stimulation with multi-pad asynchronous stimulation**, and concluded that with the latter a **better resistance to muscle fatigue was achieved**. Furthermore, Nguyen et al. (2011) used three different fatigue measures in one patient to compare the conventional stimulation with four electrode **sequential stimulation**, and concluded that during sequential stimulation the **fatigue took 280% more time to onset**, when using a stimulation frequency of 40Hz. Following the same concept and stimulation frequency, Maneski et al. (2013) noted that asynchronous stimulation doubles the time interval before fatigue sets in, when compared to the conventional one.

Although the fatigue related benefits produced by **asynchronous or sequential stimulation** have been extensively proven in various studies, Downey et al. (2014) points out that these two types of stimulation, on account of being delivered in pulses of lower frequency when compared to the conventional one, **may cause a force ripple in the stimulated muscle**. This force ripple happens when the muscle contractions are not fully fused, resulting in a more coarse/unstable movement, which can be solved by higher frequency stimulation pulses, like the ones applied by conventional stimulation. This force ripple may be a problem when feedback control is necessary (Downey et al. (2015a)), however efforts must be made in order to **substitute conventional stimulation by sequential or asynchronous stimulation** on closed-loop FES systems, as it allows patients to use the systems for longer periods of time.

2.3 SENSORS

The **sensors** provide information about the **joint's kinematic parameters**, based on the joint movements. They are generally used to measure the angle or the torque of the controlled joint. In gait assistance, they are used to **detect the gait events**, so the system knows when to apply stimulation. The most commonly used sensors in FES systems are **Forse-sensing Resistor (FSR)s and foot switches** for gait event detection; gyroscopes, accelerometers, **Inertial Measurement Unit (IMU)s** and goniometers for joint angle estimation; **Electromyography (EMG)** signals for muscle activation and dynamometers or transducers for joint torque calculation. There are however, other sensors that are not as widespread, but that have also provided some good results. Magnetic sensors were used in (Chen et al. (2004)) to calculate the ankle angle and computer vision was used in (Simonsen et al. (2016)) to detect hand opening and closing events.

2.3.1 *FSRs*

*Forse-sensing Resistor (FSR)*s are sensors that change resistance when a force is applied to them. They are usually **used to detect gait events**. By being placed on the foot of the patient, they can detect when a specific part of the foot is in contact with the ground, which is usually linked to a specific gait event. The foot switch is the **most frequent sensor for gait event detection found in commercial DF systems**, and it consists of a FSR that is placed under the heel and can easily recognize the stance

or the swing phases (Meng et al. (2017)). Figure 2.7 depicts a wireless FES system to correct DF, where the wireless foot switch can be seen and the actuator is wrapped around the dorsiflexor muscles.

Apart from gait event detection, in (Knutson et al. (2012)) FSRs were used to detect hand opening, in a system designed to control hand movements in stroke patients. It uses a glove with FSRs in the healthy hand, to **measure the degree of hand opening** and replicates these movements in the affected hand with electrical stimulation.

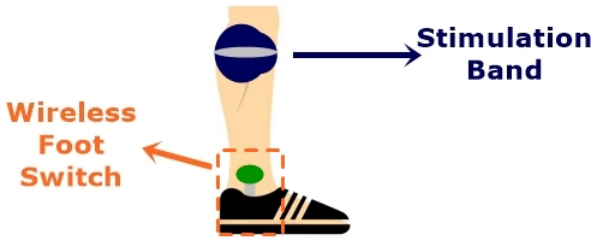

Figure 2.7: Wireless FES system to correct DF with foot switch.

2.3.2 *Inertial Sensors*

Inertial sensors are used to **monitor gait (Rueterbories et al. (2014)) and to provide information about the joint's kinematic movements**, since they can provide the **joint's angle, angular velocity and acceleration**. They are frequently small in size, have low power consumption and are widely available on the market (Sprager and Juric (2015)).

The *WalkAide*® system is an open-loop commercial system for DF correction that uses an inertial sensor embedded in the stimulation band that is placed around the *Tibialis Anterior* (TA) muscle, to detect the gait phases. This is an improvement for the patient, as the system only has one wearable component, being able to be used in activities that do not require shoes, improving the user's quality of life. In Seel et al. (2016b) and Seel et al. (2016a) an Inertial Measurement Unit (IMU) is used to detect gait events and to estimate the foot angle, simultaneously. In Watanabe and Tadano (2017) and in Basith et al. (2016) inertial sensors are used to estimate the knee angle in closed-loop fuzzy control strategies.

Using inertial sensors to detect gait events and estimate the angle of the joint is an **effective way to reduce the number of sensors** that are placed on the subject, creating **more ergonomic and efficient systems**.

2.3.3 *Electromyograpy Sensors*

Electromyography (EMG) sensors measure muscular activation by calculating the voltage potential measured by two electrodes placed side-by-side on the muscle. The bioelectric or EMG signals of the muscles provide the **user's intention of movement**, being ideal for subjects with intact neural pathways. However, paraplegic and tetraplegic subjects are not able to generate EMG signals, and some patients with paralyzed limbs cannot provide EMG signals with an amplitude big enough to be measured correctly with the electrodes. Therefore, in order to use these sensors, the **subject still has to retain voluntary muscular contractions** that can be measured by the system. EMG signals provide the muscular activation that is used as input for the control strategies in Hsieh et al. (2009), Yeom and Change (2011) and Chen et al. (2013), used to control the ankle movement. A FES system with EMG sensors is depicted in Figure 2.8.

Although EMG signals are used in orthosis and exoskeletons to control the movement of the joints, they are less used in wearable FES systems due to the **complexity of signal acquisition and processing**. The proximity of the electrodes that deliver the stimulation pulse to the muscle and the ones used to acquire the EMG signals makes it **harder to remove the stimulation artifacts from the acquired signal**, since the **signal acquisition system is monitoring the same muscle that is being stimulated**. Some commercial systems, that will be discussed further in the chapter, also monitor the EMG signals of healthy limbs to reproduce the movements in the affected limbs with FES.

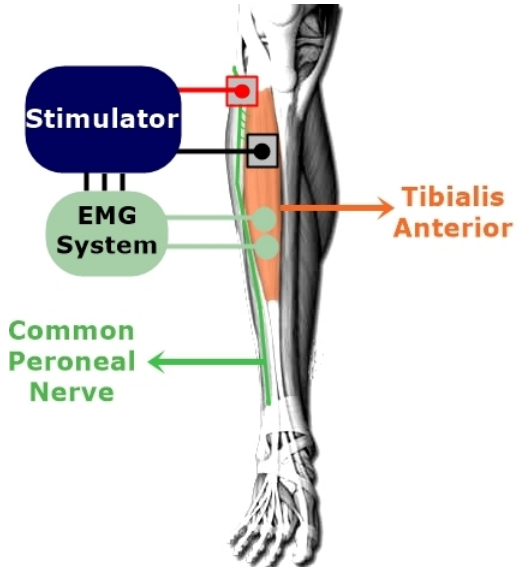

Figure 2.8: FES system with EMG sensors.

2.4 CONTROL STRATEGIES

In FES systems, the **control unit communicates with the sensors and with the stimulator**, and is the component where the control strategy is implemented. In this section, the control strategies found in the literature will be analyzed, in order to assess what **still needs to be done in the scope of DF correction** and to determine what control strategies yield the best results.

When it comes to FES control strategies, there are different control combinations that can be used, which can mainly be divided in **trajectory tracking control strategies** and **EMG-based control strategies**. **Trajectory tracking control aims at following a defined joint trajectory**, reducing the error between the desired trajectory and the real one as much as possible. **EMG-based control focuses on controlling a joint based on the bioelectric signals of a muscle**, which represent the **movement intentions of the user**. The downsides of EMG-based control are the fact that some patients that require FES are paraplegic, tetraplegic or simply do not have an EMG signal amplitude big enough to be acquired by the system, rendering this control useless in those types of patients and the **complexity of signal acquisition and processing**. Although **trajectory tracking control generally does not take into account the movement intentions** of the user, it can be used with any patient. There is also a possibility to **combine the trajectory tracking control strategy with the EMG signals**, using

the bioelectrical signal to create a muscular model and tracking the desired trajectory based on that model.

The **control strategy can use only a controller**, in order to control a joint's torque or angle. The diagram for this strategy is depicted in Figure 2.9, where Td represents the desired reference trajectory, e represents the error between the desired trajectory and the real trajectory, Tr, and u represents the controller variable. The most common controllers in FES systems are the Proportional Integral Derivative (PID) or fuzzy controllers, however, using a simple controller introduces a big time-delay in trajectory tracking control (Ferrarin and D'Acquisto (1996)), not being useful for real-time control purposes, such as gait.

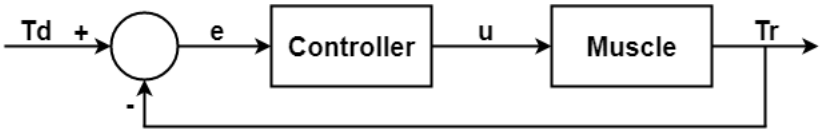

Figure 2.9: Feedback closed-loop controller.

There is also the possibility of **using just a model, in open-loop configuration**, to control a joint using FES. When it comes to the model, a diversity of them are used in the literature ((Fujita et al. (1998), Imatz-ojanguren et al. (2016), Chang et al. (1997), Chen et al. (2004), Azura et al. (2016), Previdi (2002), Yassin et al. (2017), Yilei et al. (2006)), Kesar et al. (2008), Li et al. (2015), Quintern et al. (1997), Tu et al. (2017)). The **biomechanical models** are the most complete ones,since they require more complex calibration routines, that may not always be feasible in subjects with pathologies. The model **calibration routine** is necessary in order to **match the model's parameters to the user's anatomical characteristics**. The biomechanical model more widespread in literature is the **Hill-type muscle model**, which is formed by three independent factors: the force-length relationship, the force-velocity relationship and the nonlinear muscle activation dynamics under isometric contraction (Le et al. (2010)). The nonlinear muscle activation dynamics are frequently modeled with a **Hammerstein structure**, which comprises a static nonlinearity in series with a linear dynamic. This structure is used mostly due to the **nonlinear nature of electrically stimulated muscles** and due to its connection to biophysics. The static nonlinearity, $f(u)$, represents the Isometric Recruitment Curve (IRC) - static gain relation between stimulus activation level, $u(t)$, and the output torque, when the muscle is in an isometric contraction, $w(t)$. The linear dynamics, $G(q)$, represent the muscle contraction dynamics, which are combined with

the *Isometric Recruitment Curve (IRC)* to output the generated torque, $y(t)$ (Le et al. (2010)). The Hammerstein structure can be seen in Figure 2.10.

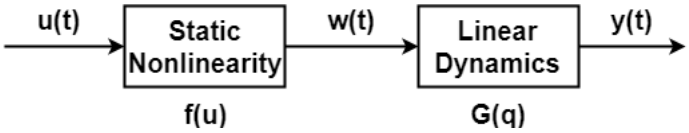

Figure 2.10: Hammerstein structure.

As an alternative for complex biomechanical models, **empirical or black-box models** started to be used to model the dynamics of the electrically stimulated muscle, since the transparency of the model is not as important as its accuracy (Previdi (2002)). A black-box model is a model that is viewed in terms of its inputs and outputs, often by means of a transfer function. In FES systems, the **stimulation parameter** delivered to the skin is the **input** and the **joint movement** that it generated, be it torque or angle, is the **output**.

A neural network is a type of black-box model. It can be trained with the input and output data of the stimulated muscle, in order to output the correct stimulation pulse depending on the desired trajectory. **Neural networks** tend to have **good performance controlling the joint's movements**, regardless of the muscular nonlinear behaviour (Chen et al. (2004)). Instead of neural networks, other type of nonlinear functions can be used to model the electrically stimulated muscle dynamics (Previdi (2002), Luzio de Melo (2014)). A diagram of FES using a model to control the joint can be seen in Figure 2.11, where *Td* represents the desired reference trajectory, *Tr* represents the real trajectory and *Us* represents the model variable.

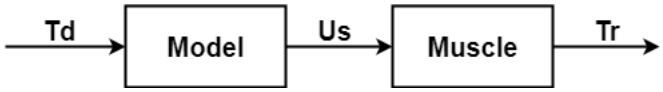

Figure 2.11: Diagram of a FES system open-loop control using a model.

Ultimately, a **model performs better in controlling a joint's movement than just a controller**, because some tracking errors do exist, but the time lag which appears when using just a controller does not (Quintern et al. (1997)). Nonetheless, **combining a model with a controller provides the best tracking performance**, since the **controller is able to compensate for any modeling errors** that inevitably occur in real-time and the **model avoids time delays**. This type of control is depicted in Figure 2.12, where *Td* represents the desired reference trajectory, *e* represents the error between the desired

trajectory, *Td*, and the real trajectory, *Tr*, *Uc* represents the controller variable, *Um* represents the model variable and *Us* represents the final pulse value applied to the muscle.

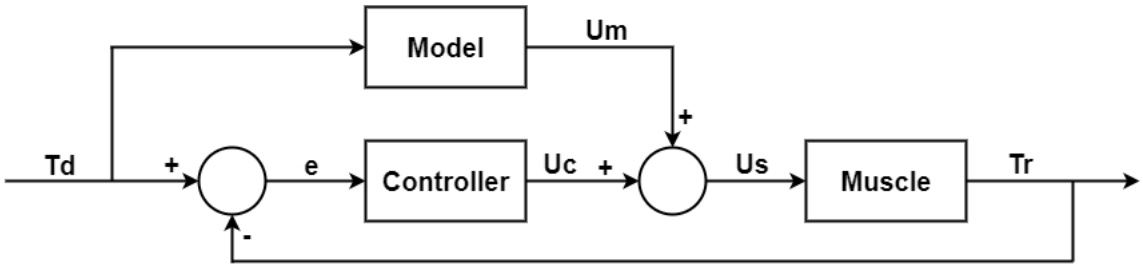

Figure 2.12: Control diagram of a model combined with a controller.

All these different control configurations will be discussed in the following sections, being divided in *Trajectory Tracking Control Strategies*, *EMG-based Control Strategies* and *EMG-based Trajectory Tracking Control Strategies*. There will also be presented tables gathering the most important details of each control strategy discussed.

2.4.1 *Trajectory Tracking Control*

The aim of this control is to **follow a provided trajectory**, trying to eliminate the error between the desired trajectory and the real trajectory. The trajectories that are normally used in FES control are either the **joint's angle or the joint's torque**. This type of control has the advantage of also being able to be used in paraplegic or tetraplegic subjects, since it **does not require bioelectric signals from muscles**, which these subjects cannot provide.

The following subsections will analyze the different trajectory tracking controls that are more commonly used in literature, all of which can be seen in Table 2.2, arranged by year.

Table 2.2: Trajectory tracking control strategies

Article	Control Implemented	FES Controlled Variable	Feedback sensor	Validation Method	Controlled Variable
Ferrarin and D'Acquisto (1996)	PID Control	Pulse Width	Electrogoniometer	-	Knee Angle
Quintern et al. (1997)	Inverse Biomechanic Model-based PID Control	Pulse Width	Electrogoniometer	5 subjects with spinal cord injury	Knee Angle
Chang et al. (1997)	Neural Network plus PID Control	Pulse Amplitude	Potentiometer	1 healthy subject & 1 paraplegic subject	Knee Angle
Chen et al. (2004)	Neural Network plus Fuzzy Control	Pulse Intensity	Magnetic-Resistive Position Sensor	3 subjects w/ Hemiplegia & 1 healthy subject	Ankle Angle
Knutson et al. (2012)	Contralaterally Controlled FES	Pulse Duration	Bend Sensors	9 subjects w/ hemiplegia	Hand Opening
Qiu et al. (2014)	PID Control	Pulse Intensity	Electronic Goniometer	5 healthy subjects	Knee Angle
Downey et al. (2015b)	RISE-based Control	Pulse Width	Optical Encoder	4 healthy subjects	Knee Angle
Seel et al. (2016b)	Iterative Learning Control	Pulse Intensity	Inertial Measurement Unit	6 subjects w/ Drop Foot	Ankle Angle
Simonsen et al. (2016)	Closed-Loop Control	Pulse Duration	Kinect Sensor	9 subjects w/ Stroke	Hand Opening and Grasping
Basith et al. (2016)	Fuzzy Logic Control	Pulse Duration	Accelerometers and Gyroscopes	2 healthy subjects	Knee Angle
Watanabe and Tadano (2017)	Fuzzy Control	Pulse Intensity	Inertial Sensor	3 healthy subjects	Knee Angle
Tu et al. (2017)	Hammerstein Model-based Fuzzy Control	Pulse Width	Two-axis Wire Potentiometer	3 healthy subjects	Ankle Angle

Fuzzy Logic Control Strategies

In order to control the knee flexion angle, a fuzzy logic control strategy was designed by Basith et al. (2016). **Two fuzzy controllers were designed**, depending on what joint movement was meant to be performed: a *Single Input Single Output (SISO)* controller for maximum hip flexion, maximum hip extension, maximum knee flexion and maximum ankle plantarflexion movements, and a *Multiple Input Single Output*

(MISO) controller for maximum knee extension and maximum ankle dorsiflexion. The controllers were designed for seven muscles, with each of the target angles taken from previous studies in the literature, and the **output of the controllers was the duration of the stimulation pulse**. The SISO controllers' input was the error between the desired joint angle and the current joint angle and the MISO controllers' input was the error and also the desired range of joint - difference between the maximum joint angle obtained in the current cycle and the target angle. The **rules sets** for the fuzzy logic controllers were **designed following the nature of the gait movement**.

Although both the MISO and SISO controllers were designed, in this study the SISO **controller for knee flexion angle** was the only one tested. In order to test it, the *Bicefs Femoris Long Head* muscle was stimulated in two healthy subjects. The control was tested in three trials for each subject. The **constant target angle** was always achieved within 2 to 10 cycles with a *Mean Square Error (MSE)* of less than 7°. The study also concludes that the stimulation's **pulse parameters vary according to the subject's physical characteristics**, since subject B, being heavier and taller than subject A, required a higher pulse voltage. Furthermore, it is stated that the **pulse's parameters should be adjusted during the stimulation in order to compensate muscle's fatigue**, instead of just the pulse duration, considering it was noted that **the muscle reacted differently to the exact same pulse duration in different occasions**. Although the results of this study were not extremely positive, it does give important insight as to why the focus of FES control strategies should be on the pulse's parameters and why open-loop strategies are not the most adequate when using FES.

The aim of the study conducted in Chen et al. (2004) was to **correct DF** in hemiplegic patients. In order to do that, a **neural network with a fuzzy logic controller** was used. The approach used was a black-box control, since the **data used for the neural network learning process was obtained by stimulating the TA muscle with random pulse intensity values** and recording the ankle angle it generated. The neural network is used to **estimate the necessary stimulation intensity** and its input is the **desired ankle angle**. After the muscle responds to this stimulation, the ankle angle is measured by the sensor and the error input for the fuzzy controller is the difference between the desired angle and the ankle angle generated by the stimulation. The **fuzzy controller will provide a stimulation intensity based on this error**, in order to correct any discrepancy between the pulse delivered to the muscle and the actual movement it provoked. The control diagram can be seen in Figure 2.13, where θd is the desired ankle angle, θr is the real ankle angle, In is the pulse intensity predicted by the model,

If is the pulse intensity output by the controller and *Is* is the pulse intensity applied to the muscle.

In this study **two other control strategies were compared** to the neural network with fuzzy logic control, in order to evaluate the performances. The first control tested was an **open-loop control, using only the neural network** previously created. The network was trained offline with the data obtained by stimulating the TA muscle with random pulse intensity values and simultaneously recording the ankle angles. It was concluded that the neural network benefited from a lower learning rate, as it produced better learning results. The second control strategy tested was a **neural network with a *Proportional Integral Derivative (PID)* controller** and the Kp, Kd e Ki values were obtained with continuous tests to obtain the best values. **The neural network with PID controller performed better than the neural network alone**, having a lower *Root Mean Square Error (RMSE)*. The **neural network with the fuzzy controller had the best performance of the three control strategies** tested. Although **the RMSE values do not differ greatly from the neural network with PID controller to the neural network with the fuzzy controller**, the PID controller's parameters took a lot of time to tune correctly.

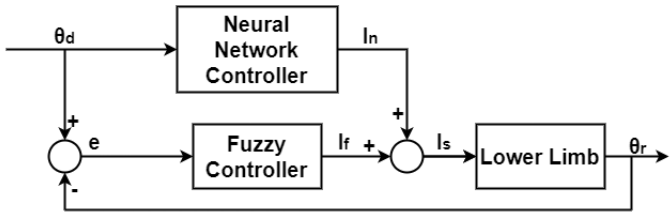

Figure 2.13: Neural network plus fuzzy logic control diagram. Adapted from Chen et al. (2004).

A **hip-knee exoskeleton was combined with FES to induce ankle movement** in Tu et al. (2017). Both the **plantarflexion and the dorsiflexion movements**, which are the lowering and raising of the foot and toes, respectively, were controlled in this work. The response of the electrically stimulated muscle was **modeled with a Hammerstein structure**. For the plantarflexion movement, the *Soleus* and the *Gastrocnemius* muscles were stimulated in a coordinated manner, and **for the dorsiflexion movement the TA muscle was stimulated**. **Each muscle was modeled individually** and a fuzzy controller was used for each one, in order to determine the necessary pulsewidth in order to follow the desired trajectory. Since the *Gastrocnemius* and the *Soleus* muscles control the same movement, coordination parameters needed to be found in order to assess which muscle had the biggest influence in the plantarflexion movement, thus

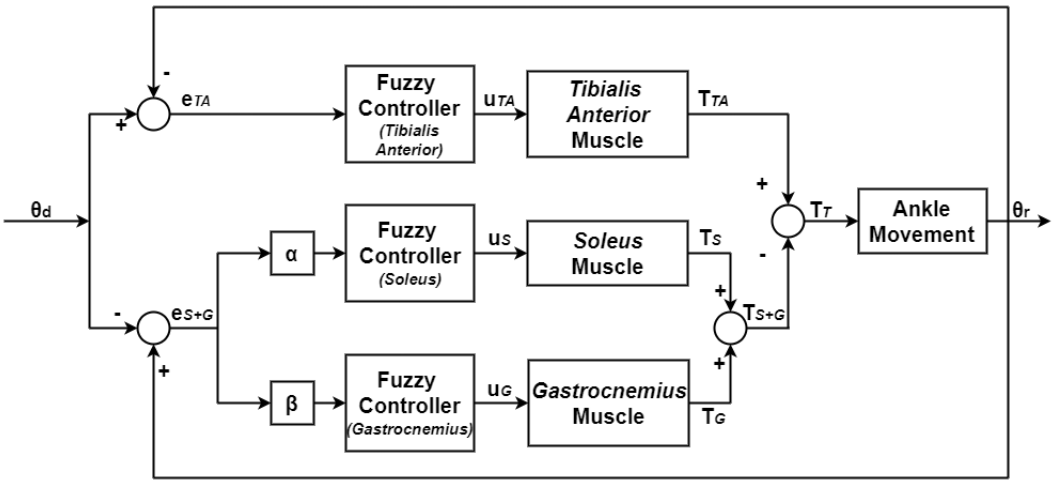

Figure 2.14: Control diagram for plantarflexion and dorsiflexion. Adapted from Tu et al. (2017).

rehabilitating the ankle movement properly. The study concluded that a parameter value of 0.7 for the *Soleus* muscle and a parameter value of 0.3 for the *Gastrocnemius* muscle produced the best control performance, which indicates that **the *Soleus* muscle has more substantial influence in the plantarflexion movement**.

The **control of the ankle angle was based on a desired trajectory** and the control diagram can be seen in Figure 2.14, where θd is the desired ankle angle, θr is the real ankle angle, e_{TA} and e_{S+G} are the tracking error, α and β are the coordinating parameters for the *Soleus* and the *Gastrocnemius*, respectively. U_{TA}, U_S and U_G are the control variables for the TA, *Soleus* and *Gastrocnemius* muscles, respectively; T_{TA}, T_S and T_G are the torque values for the TA, *Soleus* and *Gastrocnemius* muscles respectively and T_T is the total combined of torque produced by the 3 muscles to generate the ankle movement.

The results showed that the **controller was able to track the desired trajectory better in the first 5 seconds**, when the muscle required a smaller stimulation pulsewidth to generate the same movements when compared with the pulsewidth required after 55 seconds of stimulation. This was probably **caused by the onset of muscle fatigue** in the dorsiflexor and plantarflexor muscles, which seems to increase the longer FES is applied to the muscles.

Along with the fuzzy controller, PID controllers are also used extensively in FES systems. The latter will be analyzed in the next section.

PID Control Strategies

Ferrarin and D'Acquisto (1996) implemented a **closed-loop PID controller** to control the knee angle. The parameters were calculated with the Ziegler-Nichols method and the **input of the controller was the error between the desired angle and the measured one**. Three configurations were possible in this work: **constant angle reference, predefined variable angle reference and a Master-Slave configuration**, where the angle reference was controlled in real-time by a joint of another subject. By analyzing the frequency response of the implemented control, it was concluded that it **can only be used to control slow movements, since the time delay does not allow for fast movements to be controlled with favorable results**.

In Qiu et al. (2014) **three different PID controllers with three different parameter tuning algorithms were compared**, one based on a *Back Propagation (BP)* neural network, one based on the *Genetic Algorithm (GA)* and one using the traditional Ziegler-Nichols method. The aim was to **control the knee joint angle with a FES stimulator**. The two controllers with adjustable parameters (BP and GA), had significantly better results, with the GA PID controller performing better in the beginning of the simulations. The classic PID controller has also been compared with a fuzzy controller in Watanabe and Tadano (2017). The article focuses on FES for cycling rehabilitation, by **controlling the angle of the knee**. **Both controllers were tested for constant value control and trajectory tracking control**. In the constant value control the performance of the controllers was pretty similar and acceptable. In the tracking control, however, the fuzzy controller performed better. Ultimately, **the performance of the two controllers for fast tracking control was not satisfactory**.

These studies corroborate what was concluded in Ferrarin and D'Acquisto (1996) and Chang et al. (1997), that the basic FES control without a model is not the most adequate method to compensate angle error in real-time during gait, mainly due to its time delay in trajectory tracking.

Quintern et al. (1997) combined a **PID controller with an inverse biomechanical model** to control the **knee angle**. The controlled pulse variable was the width and the PID controller parameters were found in a computer simulation. The control was tested in isometric conditions and with a freely swinging shank. In order to compare the performance of the controller, a **closed-loop control using only the PID controller** was used. The performance of this controller had a **significant time lag of 330 ms and 130 ms** for the freely swinging shank and the isometric conditions, respectively, when compared to the **much smaller 30 ms time lag of the PID controller combined with**

the inverse model when controlling the freely swinging shank. Thus, it was concluded that the **inverse model can improve the controller's performance significantly**, as it can compensate for the nonlinearities of the electrically stimulated muscle and, if the target angle is constant, it can also compensate for time delays. The control loop diagram can be seen in Figure 2.15, where θd is the desired ankle angle, θr is the real ankle angle, Um is the pulse value predicted by the model, Uc is the pulse value output by the controller and u is the pulse value applied to the muscle.

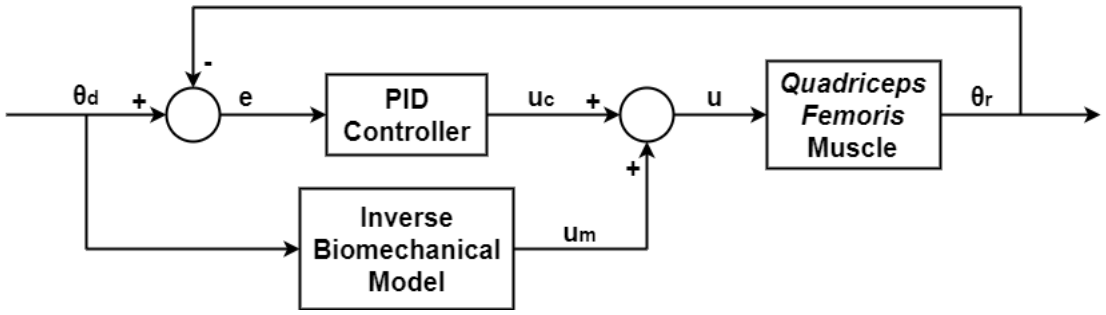

Figure 2.15: Control diagram of PID control with inverse biomechanical model. Adapted from Quintern et al. (1997)

In Chang et al. (1997) a **PID controller with a NN** was implemented in order to control the knee angle. The multilayered feedforward time delay NN was trained with the signals acquired from stimulating the muscle with different amplitude pulses and the resulting knee angles. The PID controller parameters were tuned using the Ziegler-Nichols method. In order to assess the performance of the controller, besides the PID controller with the neural network, **the PID controller and the neural network were also tested alone**, with two **sinusoidal references of 0.5 and 1 Hz**. With the reference of 1 Hz the neural network was able to follow the desired trajectory, after overcoming an initial tracking time lag, presenting a RMSE of 8.15°. With the reference of 0.5 Hz it was able to track the trajectory without a time lag, presenting a RMSE of 6.73°. The **PID controller alone presented a higher time lag when tracking both the 0.5 and 1 Hz references**, presenting a RMSE of 17.86° and 19.75°, respectively, which corroborates the results presented in Ferrarin and D'Acquisto (1996). The **PID controller with the neural network presented the best results**, being able to **improve the performance of the neural network controller**, presenting a RMSE of 7.24° and 5.32°, for the 0.5 Hz and 1 Hz trajectory, respectively. This shows that the PID controller is able to compensate any modeling errors that can occur. The **PID controller alone was the one that presented the biggest average tracking error** and

the PID controller with the neural network had the smallest error, being only slightly smaller than the one of the neural network controller alone.

Iterative Learning Control

The study in Seel et al. (2016a) aims to **correct DF during gait**. The ankle angle is the tracked variable and the pulse amplitude is the controlled variable. However, in order to avoid discrepant pulses, the pulsewidth varies proportionally to the amplitude, while the frequency remains constant. The ILC aims at improving the performance of tasks with a periodic nature (Seel et al. (2011)), which is the case of gait, by **analyzing previous strides and learning from it**. This way, the delay that seems to be inherent to controllers that are not supported by a model (Ferrarin and D'Acquisto (1996), Chang et al. (1997)) is compensated, since **the controller is able to determine the duration of previous strides and stimulate the muscles even before the swing phase begins**, in order to correct the ankle pitch angle. Given the difference, e, between the desired angle θ_d and the real angle, θ_r, the ILC controller increases/decreases whether the number of time samples before the swing phase of the next step the stimulation is applied, δ, or the stimulation parameters, U_c. The control strategy can be seen in the diagram of Figure 2.16.

This control was tested with six subjects with DF walking in real-time and the **reference trajectory was obtained from data of the gait of healthy subjects**. The gait proved to be within the desired range of values after the first stride, and **remained within the reference values, even if the muscles were fatigued**.

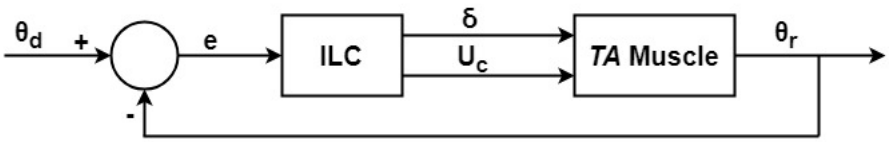

Figure 2.16: Diagram of the ILC.

In Seel et al. (2016b) the work was continued, this time controlling **the pitch angle of the ankle and the roll angle**, as depicted in Figure 2.17. For this purpose a **decentralized ILC** was implemented, in order to correct both joint angles. In order to do this, the *Tibialis Anterior* and the *Fibularis Longus* muscles were stimulated. The system was tested with four subjects with DF, and concluded that in order **for the ankle joint to be at optimum position, both muscles must be stimulated simultaneously**. However, the contribution of each muscle must be determined,

similarly to what was done to correct plantarflexion in Tu et al. (2017). The ILC proved, once again, that it was able to maintain the ankle angles within the desired healthy range while compensating muscular fatigue.

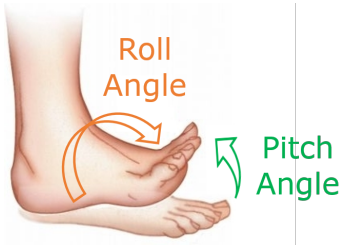

Figure 2.17: Roll and pitch angles of the ankle.

Asynchronous Closed-Loop Control

Downey et al. (2015b) designed a **closed-loop controller for asynchronous stimulation and compared it with conventional stimulation**. The aim of this study was to **track a desired angle trajectory for the knee joint**, for which a model was created. In order to avoid torque discontinuities in the knee joint, when switching channels, there was a brief period of time when both channels were simultaneously activated, each with a percentage of the input pulse value, creating a smooth transition. The controller was designed based on *Robust Integral of the Sign of the Error (RISE)*, which **switched between the stimulation channels while implementing the chosen transition period**, aiming at following the defined trajectory. The controls were tested on four healthy subjects: the asynchronous stimulation with 4 channels, with a 16 Hz pulse frequency in each channel, and the conventional stimulation with a 64 Hz pulse frequency in one channel. Although the tracking errors of both controllers were very similar, with the biggest difference being 0.82°, **the *Successful Run Time (SRT)* of the asynchronous stimulation averaged at more then double the time of the conventional one**. This study shows that asynchronous stimulation is, in fact, able to delay the on-set of fatigue on electrically stimulated muscles. However, the control was only tested on a modified leg extension machine. In order to obtain more precise results, asynchronous stimulation should be tested in real-time gait, as the authors suggest.

Contralateral Control

Knutson et al. (2012) implemented *Contralaterally Controlled (CC)* FES to **improve hand opening in hemiplegic stroke patients**. This type of control **stimulates the hand extensors of the paretic hand proportionally to the hand opening of the healthy hand**. The **healthy hand wears a glove with bend sensors**, that detect the degree of hand opening. The **duration of the stimulation pulse is controlled** based on the opening of the healthy hand. The system was tested in 9 hemiplegic subjects during 6 weeks, **showing a hand opening degree improvement of about** 17°, which increased to 27.8° 3 months after the end of the treatment. Although this type of control cannot be used in real-time gait for lower limbs, since the legs cannot perform the same movement at the same time, **patients can use it to train movements while sitting or laying down**, hopefully matching the paretic limb movements' to the healthy ones, becoming increasingly closer to physiological movements.

Vision-based Closed-Loop Control

Although the control designed in Simonsen et al. (2016) cannot yet be used for DF correction during gait, it is an interesting approach to rehabilitation with FES. A **closed-loop system for the rehabilitation of hand opening and grasping movements** of hemiparetic patients was designed, using a *Kinect*® sensor. The sensor was able to **differentiate between the hand and the object to be handled**. When the hand was at the correct distance from the object, a pulse would stimulate the correspondent muscles in order to open the hand and then another pulse would stimulate the hand grasping muscles, when the hand was in the correct position to grasp the object. The duration of the pulses would vary according to the time it took for the subject to open the hand and to place the object on a specified area, in the case of hand opening and grasping, respectively. The subjects were asked to grab two cylinders, one with 40 mm of diameter and the other with 75 mm. **The system was able to increase the percentage of successful grasps** with the small cylinder, but was unable to do the same with the larger cylinder. This was mainly because the larger cylinder needed the hand to open wider, and most patients were unable to perform this movement.

Although a control using a *Kinect*® sensor is not yet able to be used to correct gait pathologies, it **can be used in the rehabilitation of specific movements, in both upper and lower limbs**.

Table 2.3: EMG-based control strategies

Article	Control Implemented	FES Controlled Variable	Feedback sensor	Validation Method	Controlled Variable
Hsieh et al. (2009)	EMG-controlled FES	Pulse Intensity	EMG Muscle Signal Activation	1 hemiplegic subject	-
Yeom and Change (2011)	Autogenic EMG-controlled FES	-	EMG Muscle Signal Activation	1 healthy subject	Ankle Torque
Hayashibe et al. (2011)	Hammerstein Model-based Dual Predictive Control	Pulse Width	Calibrated Dynamometer	Simulation	Ankle Torque
Johnson and Fuglevand (2011)	EMG-based Prediction Control	Pulse Width Pulse Frequency	Force Transducer/ Goniometer	5 subjects	Thumb Torque/ Angle
Chen et al. (2013)	EMG-based Self-adaptive Open-loop Control	Pulse Width	Goniometer	1 subject w/ drop foot	Ankle Angle
Li et al. (2015)	Hammerstein Model-based Predictive Control	Pulse Width	EMG Muscle Signal Activation	1 healthy subject	Muscle Activation

2.4.2 *EMG-based Control Strategies*

The aim of EMG-based control strategies is to **detect the user's intentions and reproduce the activation pattern of the muscles**, by electrically stimulating the muscles with a pulse proportional to the EMG signals. This control **requires complicated hardware**, since the *Residual Stimulation Artifact (RSA)* needs to be removed from the acquired EMG signal, in order to obtain the real movement intention of the subject. An EMG signal with a substantial amplitude is also fundamental, meaning that **paraplegic, tetraplegic or subjects with weak muscular bioelectric signals cannot use the system**. When compared to trajectory tracking control, it is more intuitive, because the subject controls the stimulation pulse depending on his movement intentions.

The following subsections will analyze the different EMG-based controls that are more commonly used in literature, all of which can be seen in Table 2.3.

Proportional EMG-based Control

Yeom and Change (2011) developed a **new filtering technique to remove the RSA from the acquired EMG signal**, in order to generate **ankle dorsiflexion** movements proportional to the muscle activation signal. The acquired EMG signal passed through three stages before being able to generate the proportional stimulation pulse: an EMG blanking stage to filter the main stimulation artifact, since it would saturate the EMG acquisition system, an amplification and filtering stage, commonly used in ordinary EMG acquisition systems, and finally an adaptative Gram-Schmidt Prediction-Error-Filter, to remove the remaining RSA. This was the **first time an adaptive filter was used in the rehabilitation FES field to cause ankle dorsiflexion**.

The system was tested on a healthy subject. The EMG electrodes were placed on the TA muscle and the stimulation electrodes were placed in the region of the *Common Peroneal* nerve. **The *Common Peroneal* nerve was stimulated with a gain 80 times higher than the EMG signal**. In order to measure the ankle torque, an *Ankle-Foot Orthosis (AFO)* was placed on the subjects leg. **The system was able to stimulate the nerve in accordance to the acquired muscle activation signal**. Furthermore, the EMG signal of the TA muscle was compared with and without stimulation, and they were found to be identical, which means the novel Gram-Schmidt Prediction-Error-Filter performs as expected. Although the system performs well with a healthy subject, it should be tested on subjects with drop foot, since **they may not be able to generate a muscle activation signal with the required amplitude**, as the authors point out.

In Hsieh et al. (2009) both the **dorsiflexion and plantarflexion movements were controlled** based on the muscles' EMG signals. In order to do this, the TA muscle and the *Gastrocnemius* muscles were stimulated with FES, for dorsiflexion and plantarflexion, respectively. The **stimulation was triggered by the acquired residual EMG signals of the muscles**, which influenced the pulse's amplitude accordingly. The system was tested on a hemiplegic subject and, after 12 weeks of training, the **mean gait velocity had doubled, the stride length had improved significantly and the subject, who could not walk without support previously, could walk independently on level ground**.

Chen et al. (2013) created a **system for DF correction**, that consists of **stimulating the TA muscle with stimulation envelopes obtained from EMG signals acquired from healthy subjects walking at different speeds**. The control used a step frequency prediction algorithm, in order to apply to the TA muscle the corresponding EMG envelope, thus **generating a gait pattern close to the healthy one**. Although the

system was open loop, **by varying the stimulation envelope based on the step frequency, it was able to perform better than gait without FES assistance and gait assisted by FES using a classic trapezoidal envelope**, when tested in a patient with DF. The **subject was able to increase his step frequency by 4 steps per minute**, when aided by the system. This shows the EMG signals of healthy subjects provide yield better results when compared to the that the classical trapezoidal FES stimulation pulse.

The objective of the study conducted in Johnson and Fuglevand (2011) was the **creation of a generalized transfer function between the EMG and stimulation patterns** (pulse amplitude and frequency) with one subject, that could be extended to other subjects. Another goal was to find an optimized transfer function for individual subjects. The **thumb joint** was used for this test, because it only has one extensor and one flexor muscle. In order to find the optimized transfer function of each subject, first, the relation between the EMG signals and the joint's torque was found. Second, the relation between the stimulation patterns and the joint's torque was found. Since both relations have something in common, the torque, a transfer function between EMG signals and stimulation parameters was found. In order to create the generalized transfer function, the stimulation parameters, frequency and amplitude, were multiplied, creating a normalized current. The normalized relation between normalized torque and current was related to the EMG and torque relationship, creating the generalized transfer function.

In order to assess the performance of the optimized transfer function, the subjects' desired torque trajectory was compared to the real one, obtaining the average RMSE value of 16°, showing that the system is able to reproduce the torque trajectories for each subject. To evaluate the performance of the generalized transfer function, the previously recorded EMG data was used to generate the correspondent pulse, then was applied to all the subjects, including the subject whose data was used to generate the transfer function. The best predictions occurred for the subject that was used to create the function. For the other subjects, however, the RMSE in this case was significantly larger, about 31°. **The transfer function was also used to generate a desired angle joint movement**. In this case, the RMSE was very close to the one of the optimized transfer function, about 18.5° for the subject who generated the generalized function. **For one of the other test subjects, the joint movement was extremely identical to the desired one, even though the generalized transfer function was created with data from another subject**. The results are promising, indicating that **the system could be used to generate joint movements in paraplegic subjects, since**

an optimized transfer function cannot be used in such subjects, because they do not have EMG signals in paralyzed muscles.

While in Hayashibe et al. (2011) the Hammerstein model was used to model both the excitation dynamics and the contraction dynamics of the muscle, in Li et al. (2015) only the excitation dynamics are modeled. In this work, the torque of the ankle joint is ignored and the **aim is to follow a predefined muscle activation trajectory**. **The Hammerstein model is used to model the excitation dynamics of the muscle** and the parameters are estimated with a Kalman filter. The model is identified by stimulating the TA muscle group with gradually increasing pulse width until the plateau is reached, while measuring the correspondent EMG values. **The predictive controller's input is the desired muscle activation and the output is the stimulation pulse to be applied to the muscle**, so that the desired trajectory is followed. In Figure 2.18 the diagram for this control strategy is presented, where EMG_d is the desired muscle activation, EMG_p is the EMG activation predicted by the excitation model, EMG_r is the real muscle activation, e is the error between EMG_d and EMG_p, and u is the stimulation control variable.

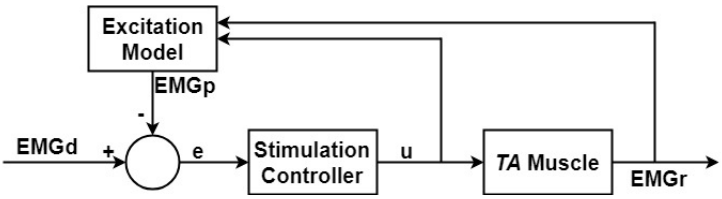

Figure 2.18: Model predictive control strategy. Based on Li et al. (2015).

Four different muscle activation patterns were tested: random amplitude level with constant contraction duration, random amplitude level with random contraction duration, a natural pattern with continuous contraction and an actual TA muscle contraction pattern. The developed control was **tested with one able-bodied subject** and it was found to **perform well for all the patterns** it was tested with, with an average RMSE of 0.0523.

2.4.3 *EMG-based trajectory tracking control*

In Hayashibe et al. (2011) **dual predictive control** was used in order to track a desired **ankle torque trajectory for DF correction**. The muscular dynamics of the subjects were modeled with the **Hammerstein model**. In this study, two models were created, the **excitation model**, which predicted the EMG signal based on the pulse

width of the stimulation pulse, and the **contraction model**, which predicted the ankle torque based on the TA muscle's EMG signal. The **initial model parameters, for each model, were identified with the data of two healthy subjects**. In order to gather the data, each subjects' TA muscle was stimulated with different pulse widths, while the EMG activity of the TA muscle was recorded and the ankle's torque was measured. Two controllers were designed, the activation controller and the stimulation controller. The activation controller was fed the desired torque trajectory value and the torque value of the joint predicted with the contraction model. The EMG signal calculated by the activation controller and the EMG signal predicted with the excitation model were then fed to the stimulation controller, that calculated the pulse width stimulation in order to achieve the desired trajectory. The control diagram can be seen in Figure 2.19, where T_d is the desired torque trajectory, T_p is the torque predicted by the contraction model, T_r is the real torque and e_a is the error between the desired torque trajectory, T_d and the torque predicted by the contraction model, T_p; EMG_d is the EMG signal calculated by the activation controller, EMG_p is the EMG signal predicted by the excitation model, EMG_r is the real EMG signal, e_s is the error between EMG_d and EMG_p, and u is the stimulation control variable.

The parameters of both the contraction and the excitation models could be updated in real-time using a Kalman filter. **The control was tested in a simulated environment**, with the identified muscle model used to simulate the muscle response. The results were good, since **the dual predictive controller was able to generate suitable control signals, even when the contraction and excitation model parameters were not updated**. This showed the stability of the model when the parameters were static and when they were time-varying. The downside of this study was that **the control strategy was not tested in real subjects**, probably due to the difficulty to find a portable torque sensor that could be easily inserted in the system. The results, although very good, were only obtained in a simulated environment.

2.5 FES SYSTEMS

A wide range of FES systems has been created since the first one in 1961 (Liberson, W. T.; Holmquest, H. J.; Scot, D.; Dow (1961)), however, the only ones available in the market for the treatment of specific pathologies **do not provide closed-loop assistance**. Currently, the only commercial lower limbs neuroprostheses available in the market are the ones used to treat DF. That is the case of the *Bioness L-300*® and the *WalkAide*®

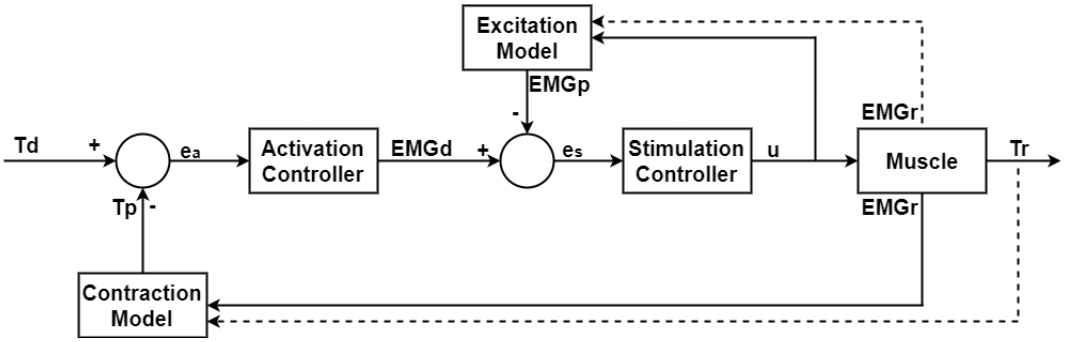

Figure 2.19: Dual predictive control diagram. Based on Hayashibe et al. (2011).

wireless systems, both created to correct DF. These systems are constituted by a band with electrodes, that straps over the dorsiflexor muscles, and a sensor for gait event detection. While the *Bioness L-300*® uses a foot switch sensor to detect the event, the *WalkAide*® uses an inertial sensor embedded in the band, making the system even more portable by only containing one wearable component. *Bioness Inc.* also created a wireless device that helps affected patients regain more natural hand movements, the *Bioness H-200*®. The device is controlled by a hand-held control unit that allows the user to choose the movement he wants to perform, be it reach, grasp or pinch. The stimulator then applies the stimulus in a precise sequence, in order to achieve the movement. Although these systems help the users regain movements, they provide constant stimulation pulses that do not take into account muscle fatigue.

The existing FES systems have been divided into two categories: commercial systems and non-commercial systems. The next section will present the commercial and non-commercial existing FES systems, as well as their characteristics.

2.5.1 *Commercial Systems*

VIVALTIS created a line of portable and wireless electrical stimulators, *PHENIX*®. The stimulators, referred to as PODs, **allow real-time change of the stimulation parameters** while also providing biofeedback of the muscular movement. All the products available allow a pulse intensity of up to 100 mA, have a pulse width range from 30 ms to 300 ms and a pulse frequency range from 1 Hz to 400 Hz, except for *PHENIX Nano Portable*®, that has a pulse width range of up to 4000 µs and a pulse frequency up to 150 Hz. The *PHENIX*® stimulators can be used to **treat a wide range**

of pathologies, depending on the user's necessities. The system can be seen in Figure 2.20 (a).

Fesia Technology created a system specific for the treatment of DF, the *FesiaWalkPHENIX®*. The system consists of an IMU, to detect gait events, and a stimulator, which **uses an electrode matrix to help delay the onset of fatigue**. The stimulator can generate pulses of up to 80 mA of amplitude, 100Hz of frequency and a width from 150 µs to 750 µs. The stimulator can be controlled wirelessly and has a friendly graphical interface (Malešević et al. (2017)). The system can be seen in Figure 2.20 (b).

XFT Medical created a system **based on biofeedback** to rehabilitate hand movements. The stimulation pulses generated are based on the EMG signals of the muscles. The system is equipped with **mirror therapy**, which means that the **person can also control the affected limb with the unaffected one**, allowing a greater freedom of movements, that may not be achievable just by controlling the affected limb with its own EMG signals.

The *FESarray®* stimulator, created by *Tecnalia* (Serbia (2011)), is a commercial device that allows multi-channel functional electrical stimulation, via an array of electrodes. This device allows **asynchronous stimulation**, which has been **proven to reduce fatigue** in users when compared to conventional stimulation (Popović and Malešević (2009), Nguyen et al. (2011), Maneski et al. (2013)). The frequency of the pulse created by this device ranges from 1 to 50 pulses per second, the amplitude can go up to 50mA and the duration ranges from 50µs to 1000µs. Both the developed system and the array of electrodes can be seen in Figure 2.20 (c).

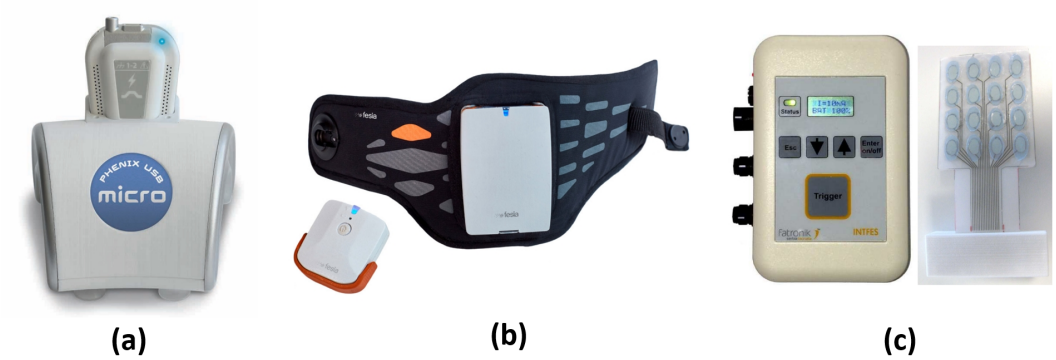

Figure 2.20: Commercial functional electrical stimulators. (a) *PHENIX USB Micro®*, (b) *FesiaWalk®* and (c) *FESarray®*. Adapted from Serbia (2011).

Table 2.4 was created to summarize the differences and characteristics of each commercial FES system presented.

Table 2.4: Commercial FES systems' characteristics

	Amplitude	Frequency	Pulsewidth	No. of Channels	Application
PHENIX®	0 to 100 mA	1 to 400 Hz	30 ms to 300 ms	2 (Multiplexed)	Wide Range
FesiaWalk®	0 to 80 mA	0 to 100 Hz	150 to 750 MIC	Electrode Matrix	Drop Foot
FESArray®	0 to 50 mA	1 to 50 Hz	50 to 1000 µs	Electrode Array	-

2.5.2 *Non-Commercial Systems*

The system created by Luzio de Melo (2014) is a modular stimulation system, *ISTim*, composed by four independent stimulation units, Modular Stimulation Unit (MSU)s, and a controller. The system can be seen in Figure 2.21 (a). The pulse generated by this stimulator can reach a frequency of up to 200 Hz, a pulse width of up to 503 µs and a pulse amplitude of up to 50 V. This system was created in order to fulfill a **market need of a small and wearable FES systems** that can be **programmed and usable in any pathology** that can be aided by FES, however it has not yet reached the market. The benefit, when compared to the commercial *PHENIX* stimulators, is that the PODs have two multiplexed stimulation channels each, while each ISTim comes with **four independent stimulation channels**. The system can be seen in Figure 2.21 (a).

Chen et al. (2004) developed a stimulator with **three selectable pulse frequency values**: 25 Hz, 35 Hz and 50 Hz. The stimulation amplitude ranges from 0 mA to 100 mA and the pulse width from 0 µs to 300 µs. The system, similarly to the *ISTim*, also has 4 independent stimulation channels, but in this stimulator **only the stimulation amplitude can be controlled independently** for each channel. Furthermore, the system is also portable, small and easily operated.

A wireless wearable functional electrical stimulator **controlled by an Android phone** with real-time-varying stimulation parameters, Edison-STIM, was designed by Wang et al. (2017) as a four-channel research prototype for post-stroke patients. The stimulus values range from 20 Hz to 80Hz, 100 µs to 600 µs and up to 60 V, for frequency, width and amplitude of the pulse, respectively. This stimulator was created with a **wrist-band concept**, in order to help stroke patients, as can be seen in Figure 2.21 (b).

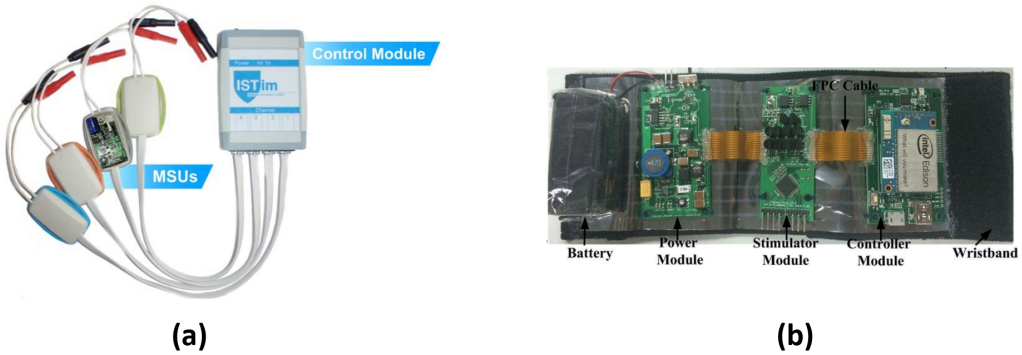

Figure 2.21: Non-commercial functional electrical stimulators. (a) *ISTim* and (b) *EDISON-Stim*. Adapted from Luzio de Melo (2014) and Wang et al. (2017).

Table 2.5 was created to summarize the differences and characteristics of each non-commercial FES system presented.

Table 2.5: Non-commercial FES systems' characteristics

	Amplitude	Frequency	Pulsewidth	No. of Channels	Application
ISTim	0 to 50 V	0 to 200 Hz	0 to 503 µs	4 (Fully Independent)	Wide Range
Chen et al. (2004)	0 to 100 mA	25 / 35 / 50 Hz	0 to 300 µs	4 (Amplitude Independent)	-
Edison-STIM	0 to 60 V	20 to 80 Hz	100 to 600 µs	4 (-)	Hand Movements

2.6 Discussion

The main goal of this project is to create a **DF correction system** that provides a **personalized experience for the user**, is **wearable and ergonomic** and ensures a **natural gait pattern**. Given that FES systems are divided into three components - **stimulator or actuator**, **sensor** and **control unit** - a literature research was made to determine what solution was best for each component. The most important aspect of the control unit is the control strategy implemented, therefore that was the focus of the research for this component. The results for each component are presented in the following sections.

Actuator

Given that **this project aims at providing a personalized user assistance that helps delay the onset of fatigue**, the stimulator should allow the **real-time update of the**

pulse parameters. Furthermore, knowing that the **pulse frequency is directly linked to muscle fatigue** (Gorgey et al. (2009), Gregory et al. (2007), Kesar et al. (2008)), the chosen pulse parameter to control in real-time should only the pulsewidth or the pulse amplitude. Considering the research aspect of this project and the risks inherent to implanted electrodes (Sheffler and Chae (2007)), **surface electrodes will be used**.

Another successful way to help delay the onset of fatigue, is the use of sequential or asynchronous stimulation (Pournezam et al. (1988), Popović and Malešević (2009), Nguyen et al. (2011), Maneski et al. (2013), Downey et al. (2014)) instead of conventional stimulation. However, **due to the small size of the *Tibialis Anterior* (TA) muscle, conventional stimulation will be used in this project**.

Considering the existing FES stimulators presented in Chapter 2.5, two were eligible to be used in this project: the commercial *PHENIX*® stimulator created by *VIVALTIS* and the non-commercial *ISTim* created by Luzio de Melo (2014). Since the Instituto Superior Técnico was able to provide one of the **Modular Stimulation Unit (MSU)s of the *ISTim Modular Stimulation Unit***, that was the chosen stimulator for this project. This stimulator is **portable and smaller than the palm of a hand**, allows the update of all the pulse parameters in real-time and can support USART communication, meaning it can communicate with any control unit that supports the same interface.

Sensor

Given this project **aims at correcting DF**, it is necessary to **detect the gait events**, therefore FSRs or an IMU could be used. However, it is also necessary to **obtain the real-time foot angle kinematics**, such as the foot angle and angular velocity. The FSR does not provide information about the joint's kinematic parameters, thus **an IMU was chosen for this project**.

Using only one sensor for both tasks effectively **reduces the number of sensor that have to be placed on the user**, thus helping create more ergonomic and efficient system that do not constrain user movements.

Control Strategy

After analyzing the control strategies, the **trajectory tracking control** was chosen instead of the EMG-based control strategy, **due to the complexity of the acquisition and processing of the bioelectric signal**. When it comes to the specific trajectory tracking control strategy, models combined with controllers yield the best results

(Quintern et al. (1997)). Therefore, that will be the configuration for the control strategy used for DF correction in this project.

Empirical models are preferred over **biomechanical models** for real-time control strategies, since they **require less parameters and need a less complex calibration routine**, while maintaining the same level of accuracy (Previdi (2002)). The **Neural Networks (NN) is the most common empirical model used in FES systems** and it generates good results when combined with a controller (Chang et al. (1997), Chen et al. (2004)). Furthermore, the literature research showed that models are usually paired with Proportional Integral Derivative (PID) or fuzzy controllers, being no indication of a significant difference between the their performance for fast tracking (Watanabe and Tadano (2017)). Thus, **the control strategy for this project will consist of a NN combined with a PID controller**. The specific NN chosen for this project will be explained in Chapter 4.

The choice of a trajectory tracking control helps delay the onset of fatigue by providing gradual stimulation that corresponds to the desired movement. However, in **order to generate natural movements, the reference trajectory should be based on natural movements**. Thus, the **reference trajectory** for this project will be **obtained from healthy subjects**, as it has proven to achieve good results (Seel et al. (2016b), Knutson et al. (2012), Ferrarin and D'Acquisto (1996)).

3

GENERAL OVERVIEW

This chapter provides an overview of the implemented system. It specifies the characteristics of each component, its role on the overall system and how the components communicate and complement each other. It ends with a system testing and a description of the necessary functionalities of the system.

3.1 INTRODUCTION

Functional Electrical Stimulation (FES) systems are meant to be **small and practical**, since they should be used on a daily basis to **help its users perform everyday tasks** that cannot be correctly performed otherwise. Therefore, the systems must also be **wearable** and not interfere with any of the users movements. FES systems for Drop Foot (DF) correction are comprised of a **stimulator** and electrodes, to stimulate the *Tibialis Anterior* (TA) muscle, a **sensor** to to acquire the foot kinematic parameters and a **Microcontroller Unit (MCU)**, to implement the control strategy.

The system designed for this project should provide a personalized assistance that helps reduce the onset of fatigue, compensates external disturbances and generates more natural movements. Hence, the stimulator must allow the **real-time update of pulse parameters**, so the provided stimulation can vary according to the desired movement; the sensor should provide real-time data that can be used to estimate the **foot angle and its angular velocity**; and the MCU should have enough peripherals to **communicate with the sensor and the stimulator**, have enough memory for the implementation of the control strategy, as well as for the gait event detection algorithm, while simultaneously being small and light.

3.2 SYSTEM OVERVIEW

The human average walking **step frequency is around 2 Hz**, being able to reach 2.5 Hz depending on the subject (Ji (2015), Kumar and Kumar (2017)). Therefore, the foot movement sampling rate should be 10 times higher in order to assure no aliasing occurs, which would be 25 Hz. Nonetheless, the sampling rate should be high enough to capture the varying dynamics of the foot movement during one step (Sprager and Juric (2015)), therefore, a **sampling frequency of 500 Hz** should be sufficient. The **signal acquisition** should also be done with a frequency 10 times higher than the sampling rate, which **should be no less than 5 kHz**. The system must comply with the time scales that can be seen in the diagram of Figure 3.1.

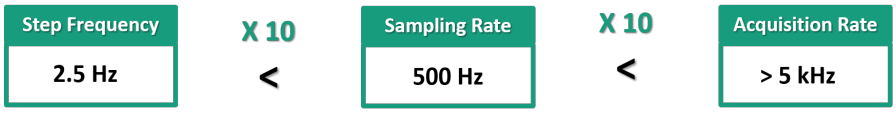

Figure 3.1: Time scale constraints for the system.

As stated in the previous chapter, a DF correction system is generally composed by a stimulator, a sensor and a MCU. In order to create a system personalized to the user's needs, it is necessary to model the electrically stimulated TA muscle. The **model will be created and tested using *MATLAB*®** running on an *ASUS*® computer with an *Intel*® *Core*™ i73537U processor at 2 GHz. Thus, the MCU should support USART communication to be able to communicate with the computer where *MATLAB*® is running. Furthermore, it should also feature enough peripherals to provide communication with the inertial sensor and the stimulator. Based on this, the system's components should follow the following requirements:

1. **MCU**
   (i) Small and light;
   (ii) Supports I^2C and USART communication;
   (iii) Features at least 2 USART ports;
   (iv) Operates at no lower than 5 kHz;
   (v) Provides sufficient memory to implement the control strategy;
2. **Stimulator**

(i) Small and light;

(ii) Allows for real-time update of pulse parameters with a frequency of at least 25 Hz;

(iii) Produces a biphasic pulse;

(iv) Supports USART communication;

3. **Inertial Sensor**

(i) Small and light;

(ii) Allows a sampling rate of 500 Hz;

(iii) Supports I^2C communication;

Based on these requirements the chosen components were the *STM NUCLEO-32F303K8®* MCU, used to implement the control strategy; the MSU from the ISTim Modular Stimulation System (Luzio de Melo (2014)), used to deliver the stimulation pulse to the TA muscle; the *MPU6050®* Inertial Measurement Unit (IMU) to acquire the foot kinematic parameters; and the *Future Technology Devices International Ltd.* (FTDI) USB to serial converter, used to support the communication between the MCU and *MATLAB®*. All the components for the designed DF correction system can be seen in Figure 3.2.

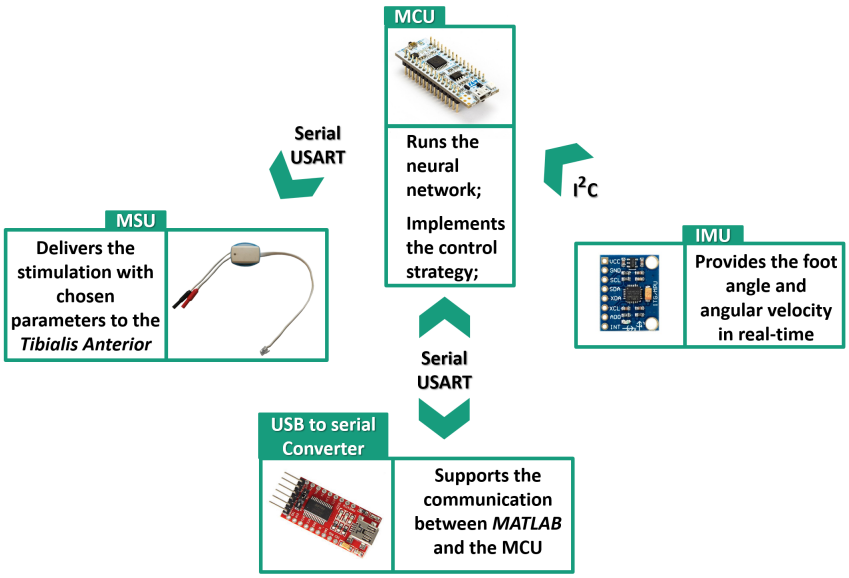

Figure 3.2: The DF correction system.

This system was designed to be **simple, lightweight and easy to use** on a daily basis. The components will be presented in depth in the next sections.

3.3 MICROCONTROLLER UNIT

The MCU **implements the control strategy** responsible for the **personalized DF correction strategy**. Therefore, it was required to be small and light, to support I^2C communication for the IMU and to support 2 USART communication peripherals for the stimulator and for the USB to serial converter. It was also required to operate at a minimum of 5 kHz and to have sufficient memory for the implementation of the model and the control strategy.

The chosen MCU was the *STM NUCLEO-32F303K8®*, since it is **small but has a high range of peripheric features**. It features I^2C and USART communication interfaces and provides 2 USART peripherals. It has an Arm® Cortex®-M4 32-bit CPU with 72 MHz maximum CPU frequency and features 64 Kbytes of Flash memory and 12 Kbytes of SRAM (STMicroelectronics (2018)). In Figure 3.3 it is possible to identify the used pinout of the MCU.

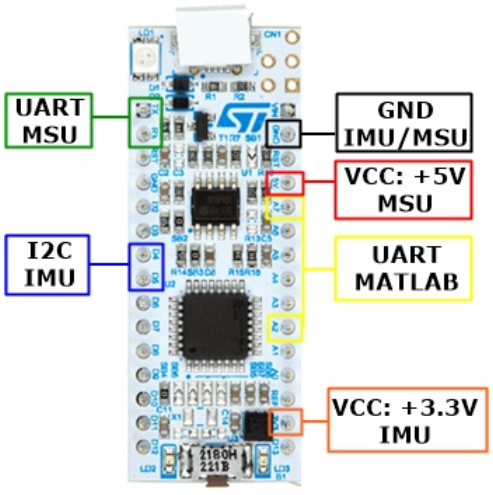

Figure 3.3: Pinout of the used peripherals in the MCU.

3.4 MODULAR STIMULATION UNIT

The **stimulator** is **responsible for applying the stimulation pulse to the TA muscle**, after its parameters are determined by the control strategy implemented in the MCU. Hence, it is important that this component **allows the real-time update of the pulse parameters**, produces a biphasic pulse, so there are no charge imbalances in the skin (de Souza et al. (2017)), and supports USART communication. It is also important that the stimulator is small and light, to allow for a **portable solution**.

Of the stimulators identified in section 2.5, two of them satisfy the requirements: the *PHENIX®* from *VIVALTIS* and the *ISTim Modular Stimulation Unit* created by Luzio de Melo (2014). Since the Instituto Superior Técnico was able to provide one of the MSUs of the *ISTim Modular Stimulation Unit*, that was the chosen stimulator for this project. This stimulator is **portable and smaller than the palm of a hand** and allows the update of all the pulse parameters in real-time. The full range of the MSU's parameter values can be seen in Table 3.1.

Table 3.1: Pulse parameter range available in the MSU.

	Pulse Parameters
Width	0 µs to 503 µs
Amplitude	0 V to 50 V
Frequency	0 Hz to 200 Hz

In section 2.2.1, it was stated that **frequency usually remains the same throughout the stimulation**, since it is directly linked to the increase of muscular fatigue. Hence, for this system the pulse parameter to be updated could either the pulse amplitude or the pulsewidth, since they are both related to muscle fibre recruitment. Given the pulse amplitude and pulsewidth range available in the MSU, the **pulsewidth spans through a wider range of values**. Therefore, that was the parameter chosen to be updated in the control strategy.

The MSU also delivers biphasic pulses, to prevent skin damage, and is able to update pulse parameters in **real-time with a frequency up to 250 Hz**. Given the human step frequency of 25 Hz, this is enough for this project. The MSU can be seen in Figure 3.4.

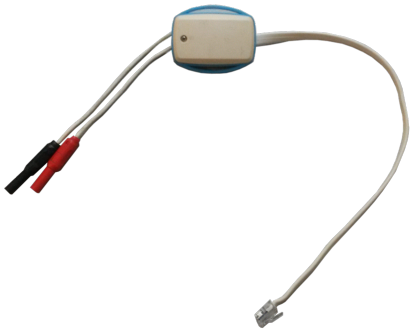

Figure 3.4: MSU used by the system.

There are two electrodes attached to the MSU, the indifferent electrode and the active electrode. For this system, the active electrode was placed on top of the motor point of the TA muscle and the indifferent electrode was placed over the *Common Peroneal* nerve, as can be seen in Figure 3.5.

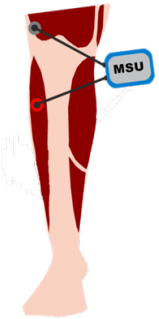

Figure 3.5: Electrode positioning to stimulate the *Tibialis Anterior* muscle. The red dot represents the active electrode.

The MSU communicates with the MCU through serial communication. The communication protocol consists of 5 bytes of data: the first byte is to signal that data will be sent/requested; the remaining 4 bytes contain the update values for each of the pulse's parameters: amplitude (A), frequency (F), and positive (P) and negative (N) widths. The baudrate for the serial data transmission is 111111 bits per second (defined by the manufacturer). The communication protocol can be seen in Figure 3.6.

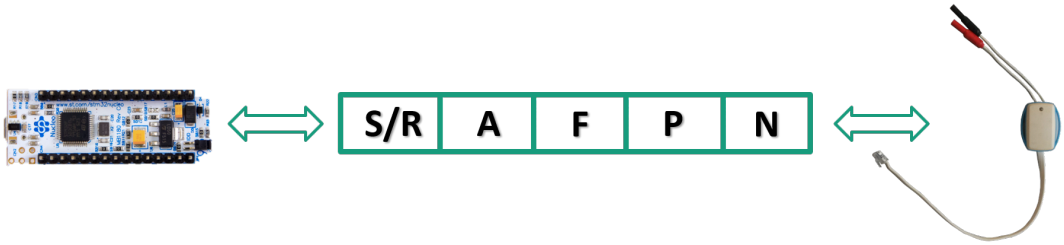

Figure 3.6: Communication protocol between MCU and MSU.

3.5 INERTIAL MEASUREMENT UNIT

In order to **provide feedback for the controller and to detect gait events**, it is necessary to have **real-time access to the foot's kinematic parameters**, particularly to the foot angle and its angular velocity. In order to obtain these kinematic parameters, a small and light component that was easily placed on the foot was necessary. It was also required that the component supported I^2C communication and allowed a sampling rate of 500 Hz.

The sensor that meets these requirements is an Inertial Measurement Unit (IMU). For this project, the *InvenSense Inc. MPU-6050®* IMU was used, as it has a 3-axis accelerometer and a 3-axis gyroscope and features an I^2C communication interface (Invensense (2013)). The MCU (master) and the IMU (slave) communicate through I^2C, with a bus speed of 400 kHz. The MCU receives the raw pitch, roll and yaw values from the accelerometer and gyroscope and uses them to calculate the foot angle. The acquisition is done with a **sampling frequency of 500 Hz**, which is in accordance to the time scale constraints of the system.

The foot angular velocity is the unfiltered gyroscope pitch value and the foot angle is calculated by fusing the data from the accelerometer and the gyroscope, using a complementary filter (Filippeschi et al. (2017)). The complementary filter is stated in Equation 1.

$$\theta = \alpha_g \times \theta_g + \alpha_a \times \theta_a \tag{1}$$

Where θ is the estimated foot pitch angle, θ_g is the foot pitch angle integrated from the gyroscope pitch axis, θ_a is the foot pitch angle estimated from the accelerometer axis values and α_g and α_a are the filter constants, that were tuned to 0.98 and 0.02, respectively.

There is a 5 second calibration routine, where the subject remains static in order to calculate the gyroscope offset and the pitch angle of the stationary IMU. The IMU was placed in the top of the foot (Anwary et al. (2018), Kwakkel et al. (2015)), inside of a black box, in a way that would not limit the subjects movements. The black box can be attached to the foot with a strap or with the user's shoelaces, for a more simplistic approach. The positioning of the sensor can be seen in Figure 3.7.

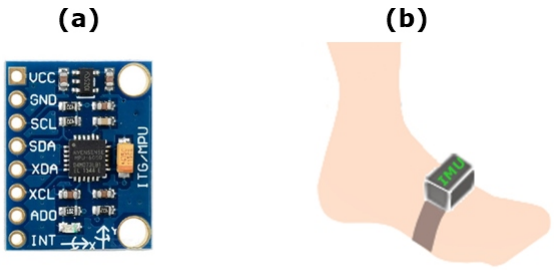

Figure 3.7: (a) *InvenSense Inc. MPU-6050®* IMU, (b) IMU foot placement.

3.6 USB TO SERIAL CONVERTER

The **model and the signals** used to acquire data for the model **were created in *MATLAB®***. Therefore it was necessary to send the signals in real-time to the MCU. To ensure the communication between the MCU and the computer, where the *MATLAB®* was running, the USB-RS232 *FTDI* Converter was used. The baudrate for the serial data transmission is 115200 bits per second.

The communication protocol consists of *MATLAB®* waiting for the character that signals the request for a signal (r) and then sending the signal to the MCU. When the MCU finishes receiving the signal it sends a character to indicate it received the signal successfully (e), and the communication is terminated. The communication protocol can be seen in Figure 3.8.

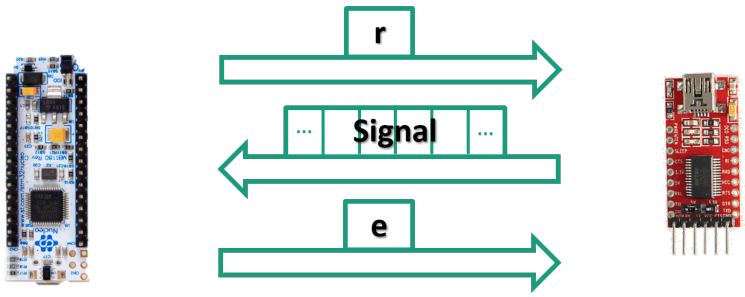

Figure 3.8: Communication protocol between MCU and *MATLAB*®.

3.7 SYSTEM TESTING

Tests were made in order to ensure that the system was respecting the required time constraints, since for a real-time DF correction control application, there cannot be unexpected time delays. In order to do this, an **oscilloscope was used to visualize the signals**.

The first test was to identify the **model's time response for one prediction**, as this is crucial for the time response of the control strategy. This test was done with the model operating alone, after it was first implemented in the MCU. The test was done by toggling a pin on the MCU to high when the model prediction function begins and toggling it back to off when it exits the function. The oscilloscope probe was connected to the pin and in Figure 3.9 the toggling of the pin can be seen.

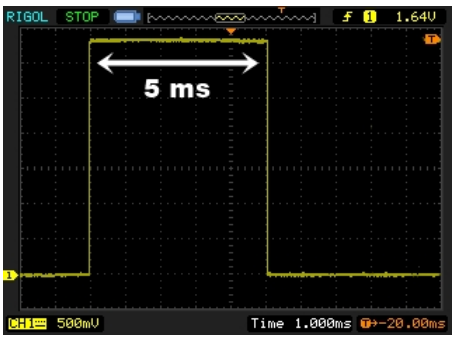

Figure 3.9: Neural network response time visualized with an oscilloscope.

Figure 3.9 shows that **the model needs 5 ms in order to make one prediction**, which means it has a **time response of 200 Hz**. Given the human step frequency of 2.5 Hz, this value is well within the acceptable limits.

The **control strategy** must take into account the response time of the model, therefore it **cannot operate faster than 200 Hz**. Given the lack of control loop response time information in the literature, the chosen response time was 125 Hz, since it respects the human step frequency of 2.5 Hz and also the response time of the model (200 Hz).

The response time of the control loop was tested with the system **operating in real-time DF correction mode**, in order to take into account the worst case scenario. The test was done by toggling a pin on the MCU everytime the control loop interruption occurred. The oscilloscope probe was connected to the pin and in Figure 3.10 the toggling of the pin can be seen, and therefore the time response of the control loop.

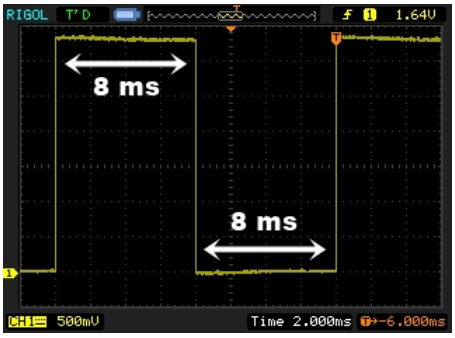

Figure 3.10: Control loop response time visualized with the oscilloscope.

Figure 3.10 shows that the pin is toggled every 8 ms, which means **the control loop is running at 125 Hz**, as expected.

Lastly, the IMU **sampling rate was tested with the system operating in real-time DF correction mode**, to ensure it was 500 Hz, as required by the time scales defined previously. For this project, the MCU clock speed was set to 64 MHz, which respects the acquisition rate set by the time scales of 5 KHz. The test was done by toggling a pin on the MCU everytime a sampling interruption occurred. The oscilloscope probe was connected to the pin. In Figure 3.11 the toggling of the pin can be seen and, therefore, the rate at which the IMU data was sampled.

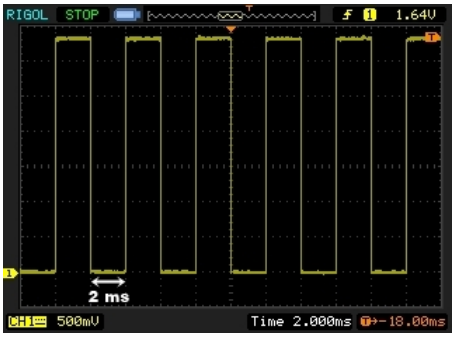

Figure 3.11: Sampling rate of the IMU visualized with an oscilloscope.

Figure 3.11 shows that the pin is toggled every 2 ms, which means the **IMU values are being sampled at at 500 Hz**, as expected.

3.8 PROJECT LAYOUT

Following the choice of the system's components, it is necessary to outline the subsequent steps to be taken in order to develop the DF correction control strategy. The **proposed trajectory tracking control strategy** can be seen in Figure 3.12 and it is divided in two main elements: the **NN model** and the **PD controller**, which will be presented in depth in Chapter 4 and Chapter 5, respectively.

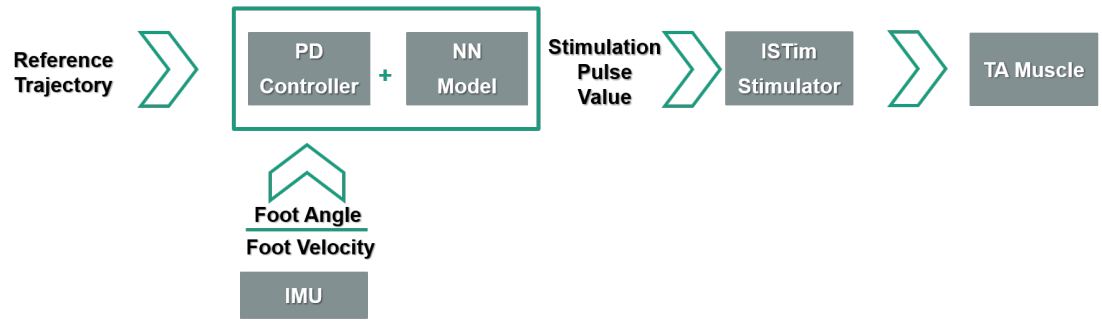

Figure 3.12: Control diagram of the proposed trajectory tracking control strategy.

In order to model the dynamics of the electrically stimulated muscle it is necessary to acquire real-time data of the foot angle correspondent to the stimulation pulse, that covers the full range of motion of the foot. This is necessary because DF affects the swing gait phase, which ranges from the lowest foot angle value, approximately -45°, to the highest, approximately 20°, in healthy subjects, as can be seen in Figure 3.13.

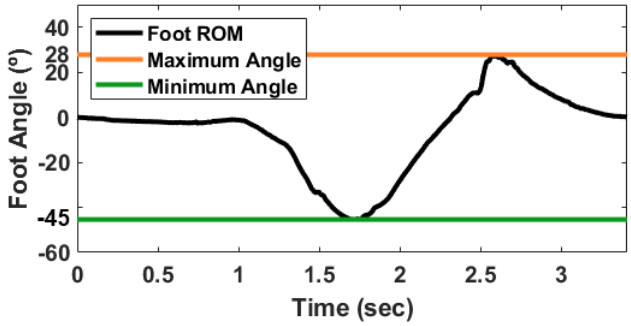

Figure 3.13: Foot ROM obtained with an IMU placed on the foot of a healthy subject walking at 1 km/h.

The **NN model** is responsible for **capturing the dynamics of the electrically stimulated TA muscle** and will be implemented in the MCU for the real-time control strategy, as stated previously. Since this model is **tailored to each user's needs**, a calibration should be done everytime a new user intends to use the system, to ensure the model is **personalized to the user's anatomical needs**. The **calibration** will be used to **apply different stimulus** to the user's TA muscle, so the full dynamics of the muscle can be captured by the model. In order to create the personalized model, the steps outlined in Figure 3.14 will be taken and properly documented throughout Chapter 4.

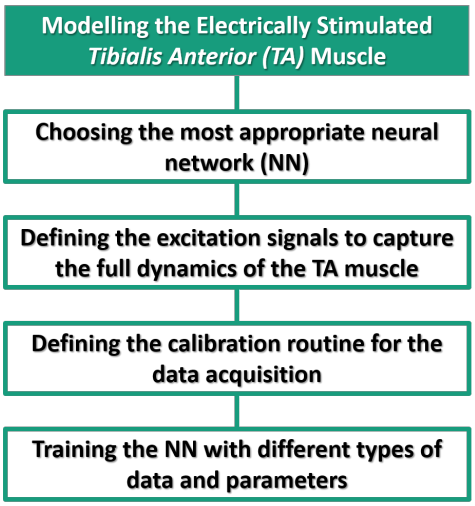

Figure 3.14: Steps to be taken in order to model the electrically stimulated TA muscle.

The **trajectory tracking control strategy** is responsible for **correcting DF during real-time gait**. In order to do this, it should use a **reference trajectory** that is based on **healthy gait patterns**, as to generate foot movements similar to natural ones. Since DF only affects one of the gait phases, the control strategy should only be applied when the gait cycle corresponds to that phase. Therefore, there is a necessity to **identify the gait events** in real-time, wearing the IMU that is also being used to acquire the foot kinematics, in order to **reduce the number of sensors placed on the subject**. The model created in Chapter 4 should be combined with a controller, in order to help **reduce fatigue and compensate for any external disturbances**. This will provide a more **robust and effective control strategy**.

The model should be validated alone and then paired with the controller, to compare their performances. Finally the implemented control strategy should be validated during real-time, to see if it able to correct DF. In order to create this control strategy, the steps outlined in Figure 3.15 will be taken and properly documented throughout Chapter 5.

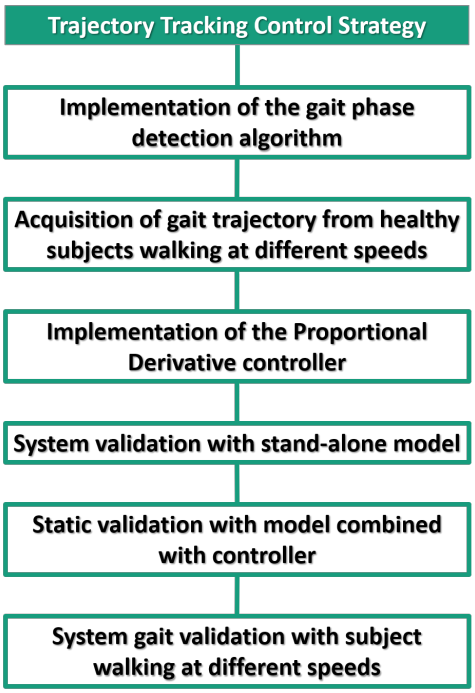

Figure 3.15: Steps to be taken in order to implement and validate the proposed control strategy.

4

MODELING ELECTRICALLY STIMULATED MUSCLES

This chapter focuses on modeling the dynamics of the electrically stimulated muscles. It starts with a brief introduction followed by the methods used to created the models. Afterwards, the results will be presented and the chapter will end with a discussion on the subject.

4.1 INTRODUCTION

The control strategy that is going to be used for this project is a **trajectory tracking control strategy**, using a **model combined with a Proportional Derivative (PD) controller**, as was stated in the previous chapters. Hence, it is necessary to determine which is the best option to **model the electrically stimulated *Tibialis Anterior* (TA) muscle**.

There are two types of approaches used to model the electrically stimulated muscles: **mechanistic or biomechanical** models and **empirical or black-box** models. Mechanistic models usually **have a large amount of parameters** that need to be tuned, since they are largely **based on the physical properties of the limb they are trying to model** (Previdi (2002)). For Functional Electrical Stimulation (FES) systems, empirical models only need the **pulse parameter used and the corresponding joint's movement kinematics**, in order to **find the relation between** them and create the desired model. Mechanistic models, such as biomechanical models or Hammerstein structures, are **more accurate and precise**, but the level of authenticity they entail is only achieved with complex calibration routines. Furthermore, the amount of parameters required to create this type of models is usually very high, which **can affect the real-time performance of the system** (Luzio de Melo (2014)). Empirical models are able to overcome these problems by **finding the relation between the inputs and outputs of the system**. This is done by **sacrificing the level of detail and parameters** required

to create the model when compared to mechanistic models, but the outcome is a **less complex model that is still able to perform in real-time**.

The model for this project is meant to **represent the inverse dynamics of the electrically stimulated TA muscle**, by predicting the pulsewidth to be applied to the muscle, given a desired joint kinematic trajectory. Empirical models require a **less complex calibration** routine, which is **important when modeling the muscles of subjects with disabilities**. They are **less complex**, when compared to mechanistic models, and thus **generally more suitable to be integrated in a real-time control strategy**. Therefore, an **empirical model was chosen** for this project.

4.2 METHODS

In this section a model is created with the purpose of being integrated in a trajectory tracking control strategy to control Drop Foot (DF). Firstly, the chosen model will be presented, followed by the signals used to train the Neural Networks (NN) and the data acquisition method used. The NN were created and trained in *MATLAB*® and the best performing Non-Linear Autoregressive Neural Network with Exogenous input (NARX Neural Network) was implemented in the Microcontroller Unit (MCU).

4.2.1 *Neural Network*

NNs have been extensively used in Functional Electrical Stimulation (FES) research projects to model electrically stimulated muscles, be it for upper limb movements (Fujita et al. (1998), Imatz-ojanguren et al. (2016), Popov et al. (2015)) or for lower limb movements (Chang et al. (1997), Chen et al. (2004), Azura et al. (2016), Previdi (2002), Yassin et al. (2017), Yilei et al. (2006)), given they **can model the non-linear behaviour of the electrically stimulated muscles**. Although, in the past, it was more common to use feedforward neural networks with FES (Chen et al. (2004) Chang et al. (1997) Fujita et al. (1998)), the most **recent projects use recurrent neural networks, in particular NARX Neural Networks** (Azura et al. (2016) Yassin et al. (2017) Yilei et al. (2006) Previdi (2002) Popov et al. (2015) Imatz-ojanguren et al. (2016)). Considering that the main goal of this project is to **correct DF during real-time gait** and since the use of a **non-linear model provides a more accurate model** for the control of the full range of motion of a joint (Previdi (2002)), **a NARX Neural Network was chosen** to model the electrically stimulated TA muscle in this project.

Non-Linear Autoregressive with Exogenous input (NARX) **models** are a class of discrete-time non-linear systems that **establish non-linear relationships between past observations and future outputs** (Previdi (2002), Lin et al. (1996)). These models are useful for FES research purposes because of the **small number of required parameters and their ability to represent the nonlinear dynamic behaviour** of the electrically stimulated muscle (Previdi and Carpanzano (2003)). This model is represented by Equation (2):

$$y(t) = f(u(t), u(t-1), ..., u(t-n), y(t-1), ..., y(t-m)) + e(t) \tag{2}$$

where *y(t)* is the output predicted by the model, *u(t)* is the input and *e(t)* represents disturbances and modelling errors at time t. f is the non-linear function that describes the system's behavior and n and m are the regression orders of the input and output, respectively. **When the function f is represented by a *Multilayer Perceptron (MLP)***, a feedforward NN, **the result is a NARX Neural Network**. The NARX Neural Network is a type of *Recurrent Neural Network (RNN)* that only has feedback between the output and input layers (Lin et al. (1997)). In order to benefit from the **characteristics of the NARX model** while also taking **advantage of the adaptability of neural networks**, the **chosen model is a NARX Neural Network**. A diagram of the NARX Neural Network can be seen in Figure 4.1.

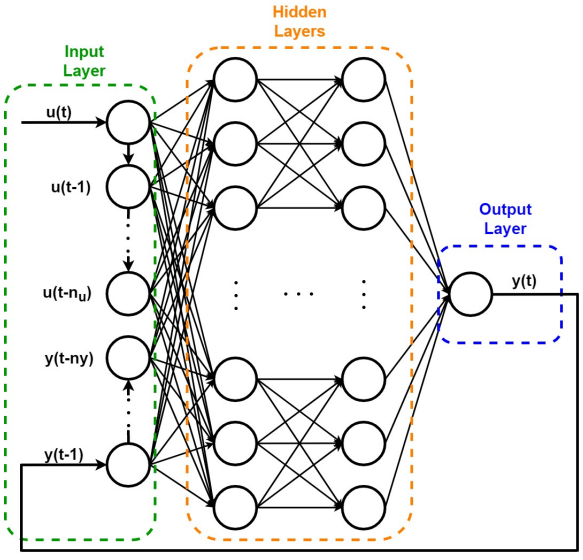

Figure 4.1: NARX Neural Network diagram.

The NARX Neural Network can operate in two modes: **Series-Parallel** mode and **Parallel** mode (Maria and Barreto (2007)). In **Series-Parallel** mode the values that are fed back into the NN are real values output by the system. This mode is represented in Equation (2) and in Figure 4.2, where the output predicted by the model is represented by $\hat{y}(t)$.

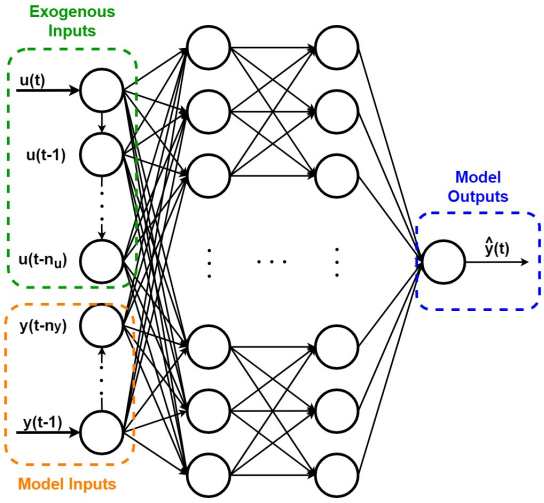

Figure 4.2: Series-Parallel mode NARX Neural Network diagram.

In **Parallel** mode the values estimated by the model are fed back into the NN as inputs in the correct regression order. This mode is represented by Equation (2), where the outputs predicted by the model are represented by $\hat{y}(t)$ in Figure 4.3.

NARX Neural Networks are generally trained in **Series-Parallel** mode, so that the weights are updated accordingly, but in real-time control they are usually used in **Parallel** mode. Thus, for this project, the **NN will be trained in Series-Parallel mode** and afterwards it **will be used in Parallel mode for real-time prediction**.

In order to have a basis for performance comparison, initially a **direct model** was created, having as input the pulsewidth, given it spans through a wider range of values on the chosen stimulator, (as explained in section 3.4), and as output the foot angle. Afterwards, the **basic inverse model** was created, which has as input the foot angle and as output the pulsewidth. Finally, a **dynamic inverse model** was created. This model uses as input, both the foot angle and the foot angular velocity. The three models will be presented in the following sections and the data present in the figures was normalized using Equation 3, where y represents the normalized value, X

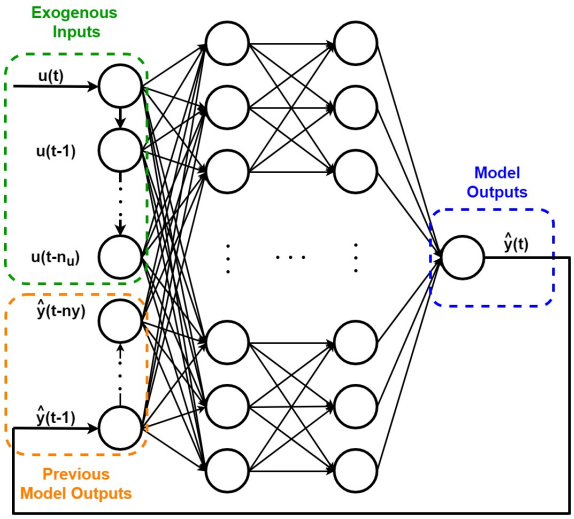

Figure 4.3: Parallel mode NARX Neural Network diagram.

represents the array of data to be normalized and x represents the value within the array to be normalized.

$$y = \frac{x - min(X)}{max(X) - min(X)} \tag{3}$$

Direct Model

The **direct model** was created using the **applied pulsewidth as exogenous input** and the **resulting foot angle as output**, to **train the NARX Neural Network**. It is the direct model because it **models the behaviour of the TA muscle after being electrically stimulated with different pulsewidths**. The model is represented by Equation 4, which is based on Equation 2.

$$\theta(t) = f(PW(t), PW(t-1), ..., PW(t-n), \theta(t-1), ..., \theta(t-m)) + e(t) \tag{4}$$

where $\theta(t)$ is the foot angle predicted by the model, $PW(t)$ is the pulsewidth input and $e(t)$ represents disturbances and modelling errors at time t. f is represented by a MLP and n and m are the regression orders of the input and output, respectively. A diagram of this model is represented in Figure 4.4.

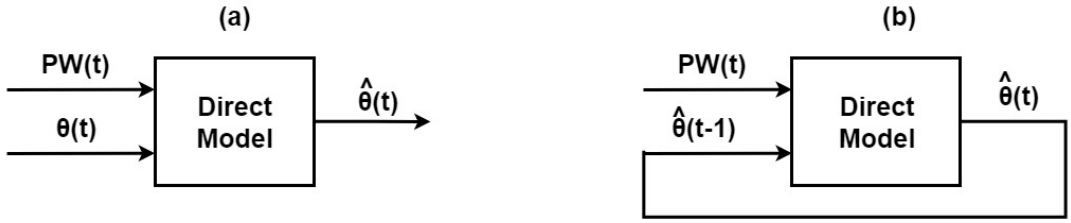

Figure 4.4: Direct model NARX Neural Network diagram for: (a) training and (b) real-time prediction.

Basic Inverse Model

The **basic inverse model** was created using the **foot angle as exogenous input** and the **applied pulsewidth as output**, to train the NARX Neural Network. It is the inverse model because it **models the inverse relationship of the electrically stimulated TA muscle**. This means that, **given a desired foot angle the model outputs the pulsewidth that must be applied**. The model is represented by Equation 5.

$$\hat{PW}(t) = f(\theta(t), \theta(t-1), ..., \theta(t-n), PW(t-1), ..., PW(t-m)) + e(t) \tag{5}$$

where $\hat{PW}(t)$ is the pulsewidth predicted by the model, $\theta(t)$ is the foot angle input and $e(t)$ represents disturbances and modelling errors at time t. f is represented by a MLP and n and m are the regression orders of the input and output, respectively. A diagram of this model is represented in Figure 4.5.

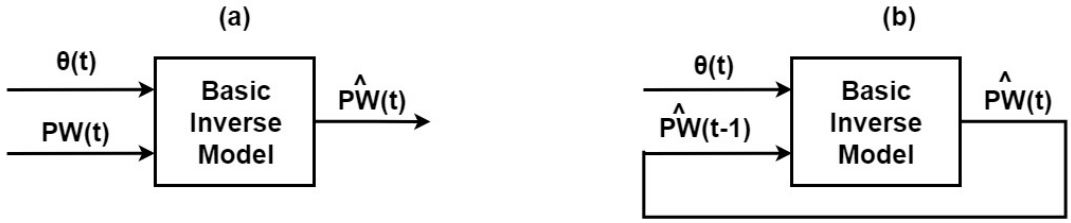

Figure 4.5: Basic inverse model NARX Neural Network diagram for: (a) training and (b) real-time prediction.

There is a **delay from the moment the stimulation pulse is applied until the TA muscle responds to the stimulus** (Chang et al. (1997)). Given that the NARX Neural Network is used for time series prediction, the **pulsewidth was shifted 1 second in order to remove this delay**, so the NN can properly be trained with the data. This process can be seen in Figure 4.6.

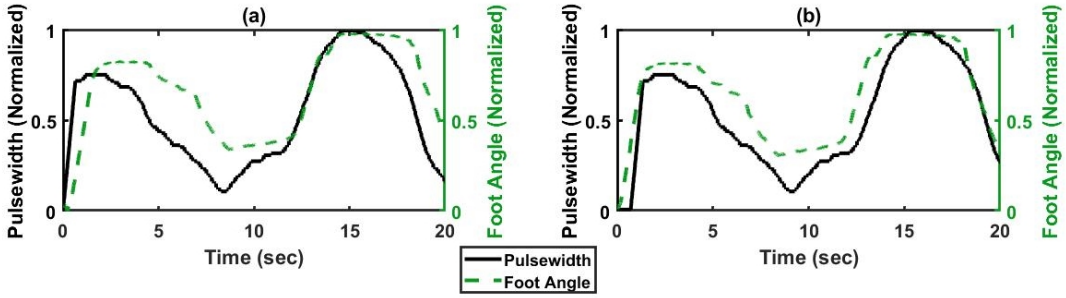

Figure 4.6: Response time removal on training data: (a) original data and (b) data with response time delay removed.

Dynamic Inverse Model

The **dynamic inverse model** was created using **both the foot angle and its angular velocity as exogenous input**. As output the applied pulsewidth that generated the foot movement was used to train the NARX Neural Network. It is the dynamic inverse model because it **uses two kinematic foot parameters**, the angle and the angular velocity. The model is represented by Equation 6.

$$\text{(t)} = \text{f}(\theta(t), \theta(t-1), ..., \theta(t-n), \dot{\theta}(t), \dot{\theta}(t-1), ..., \dot{\theta}(t-n), PW(t-1), ..., PW(t-m)) + e(t) \quad (6)$$

where $\hat{PW}(t)$ is the pulsewidth predicted by the model, $\theta(t)$ is the input foot angle, $\dot{\theta}(t)$ is the input foot angular velocity and $e(t)$ represents disturbances and modelling errors at time t. f is represented by a MLP and n and m are the regression orders of the input and output, respectively. A diagram of this model is represented in Figure 4.7.

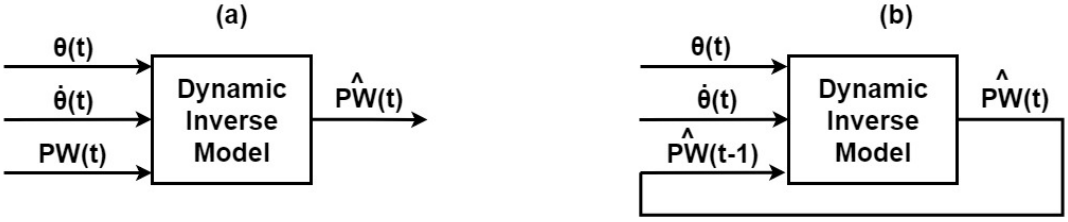

Figure 4.7: Dynamic inverse model NARX Neural Network diagram for: (a) training and (b) real-time prediction.

As in the case of the basic inverse model depicted in Figure 4.6, the pulsewidth was also shifted for the dynamic training data, in order to remove the delay of the muscle response.

4.2.2 *Model Excitation Signals*

The **selection of signals used to train the NARX Neural Network** is very important, since the stimulus is applied directly to the patient's leg. Therefore, a **gradual recruitment of the muscle fibers** is preferred over abrupt recruitment, which is especially true in the current case of DF correction because the **foot movement is progressive**. Furthermore, abrupt muscular stimulation with high amplitude values **may cause the onset of fatigue sooner as well as cause discomfort for the patient** (Le et al. (2010)).

The signals must be able to generate the whole range of joint movements, in order for the model to **capture the full Range of Motion (ROM) of the foot**. There are some signals that are able to achieve this such as white noise (Farahat and Herr (2005)), Triangular Ramps (TR), Staircase Ramps (STR), *Pseudo-Random Binary Sequences (PRBS)* (Schauer and Hunt (2000)), Pseudo-Random Multi-Level Sequences (PRMS) (Previdi and Carpanzano (2003), Previdi et al. (2005)) and Filtered Random Noise (FRN). PRMS are more adequate than PRBS, since they are distributed throughout the whole range of the joint movement.

Since the model is meant to express the dynamic behaviour of the electrically stimulated muscle, **dynamic excitation signals are the most appropriate for model identification purposes** (Le et al. (2010)). The only signals with dynamic behaviour are the white noise, the PRBS, the PRMS and the FRN. PRMS is a deterministic signal similar to white noise which covers the full range of motion. FRN is a signal resultant of low-pass filtering white noise. Based on this, **the candidate input signals are FRN and PRMS**, which are depicted in Figure 4.8 a) and Figure 4.8 b), respectively.

An **offset and gain are applied** to both signals to ensure they **stay within the full ROM of each subject**. These offset and gain values are based on the **minimum pulsewidth** value that generates a foot motion for each subject and the **saturation pulsewidth** value, where the foot angle stops increasing despite the pulsewidth continues to increase. These values **differ from subject to subject** and may even **differ for the same subject under different conditions**. Hence, after the minimum and saturation values are obtained, **personalized PRMS and FRN signals** are created.

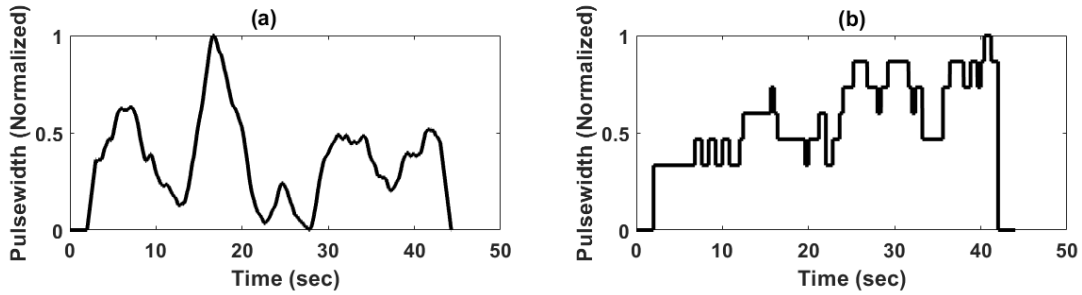

Figure 4.8: Excitation signals selected: a) FRN and b) PRMS.

In order to obtain the minimum and saturation values, a **TR, is applied in the beginning of every experiment**. The TR increases linearly from 0 µs to 200 µs and then decreases back to 0 µs, as can be seen in Figure 4.9.

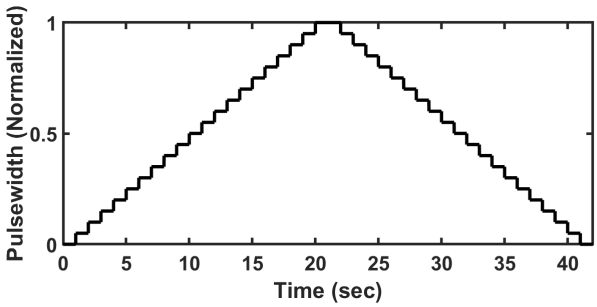

Figure 4.9: TR applied at the beginning of every experiment.

The procedure done to acquire training data for the NARX Neural Network is described in the next section.

4.2.3 *Model Data Acquisition*

In order to personalize the model to the user's TA muscle characteristics, there needs to be a calibration routine done for each user. This allows the acquisition of data specific to the user, by applying different signals to the TA muscle and recording the corresponding foot kinematic parameters. This data is then used to train the model, thus assuring that the model is personalized to the user's needs. This is necessary because, as mentioned previously, electrically stimulated muscles have a time-variant dynamic that varies depending on the subjects, their physical condition and muscular

fatigue (Gorgey et al. (2009)). Thus, this section describes the model data acquisition calibration routine, necessary to tailor the model to the user's anatomic characteristics.

Since **during the swing phase no external forces, besides gravity, are applied to the foot**, the experimental setup must take this into account. Therefore the subject was **placed in a sitting position that kept the foot from touching the ground** and allowed the ankle to move without restriction. An IMU was strapped to the foot, in order to acquire the kinematic parameters of the foot. The setup can be seen in Figure 4.10. The subject was a 23 year old neurologically intact female, since the **muscle response between healthy subjects and impaired subjects is very similar** (Chang et al. (1997)).

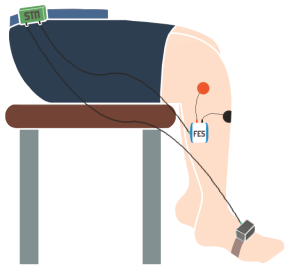

Figure 4.10: Model data acquisition experimental setup.

For this project, **the pulse amplitude and frequency remain constant and the pulsewidth is controlled**. The frequency is set at 30 Hz for every subject, since it should not have a value that is too low that it generates muscular twitches, but not too high that it promotes the early onset of fatigue (Downey et al. (2015b)). The **pulse amplitude must be adjusted according to the subject**. In order to do this, firstly a constant pulse of 70 µs is applied to the TA muscle and the amplitude is increased slowly starting at 0 V. **When the muscle reaches a steady contraction**, that means the **adequate amplitude** value has been reached and it remains constant throughout the rest of the trials. For this subject, the adequate pulse amplitude value was 28 V.

Afterwards, it is necessary to **determine the subject's minimum and saturation pulsewidth values**. In order to do this, the TR seen in Figure 4.9 is applied. The **minimum pulsewidth** is assumed to be the one that **causes an increase of 0.5° of the foot angle**. The **saturation pulsewidth is achieved when the foot angle stops increasing**, despite the pulsewidth continues to increase. The process can be seen in Figure 4.11.

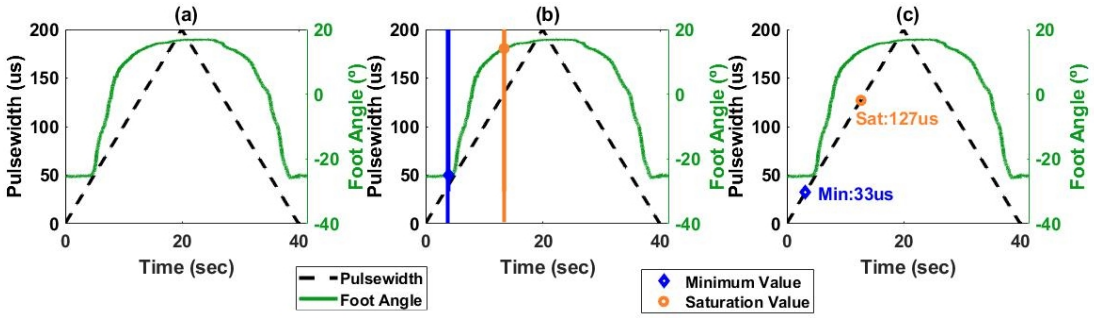

Figure 4.11: Identification of minimum and saturation pulsewidth values: (a) subject's foot angle data acquired when the TR pulse is applied, (b) minimum and saturation angle values identified and (c) minimum and saturation correspondent pulsewidth values.

The **FRN and PRMS pulses**, explained in the previous section, are then **created based on the determined minimum and saturation pulsewidth** values. In order to assess the robustness of the model, **both pulses were created with different behaviours**. FRN at 0.1 Hz, 0.2 Hz and 0.3 Hz, to represent **slow, intermediate and fast movement transitions**, respectively, and PRMS created with slow movement transitions and fast movement transitions. These transitions are meant to **generate slower or faster foot movements, thus generating a diverse range of data**. The created signals can be seen in Figure 4.12.

The signals in Figure 4.12 were applied to the subject's TA muscle and the corresponding foot kinematic parameters were recorded, with the setup shown in Figure 4.10. **Each FRN and PRMS signal generates a muscular response which translates into a foot movement**. **Three trials were made for each pulse type**, in order to gather a **wide range of data for the model creation**. The signals applied to the TA muscle as well as the corresponding foot angle data obtained from one trial can be seen in Figure 4.13.

After the training data was obtained, the direct model, basic inverse model and dynamic inverse model were trained with it. The results obtained from the trained models will be examined in the following section.

4.3 RESULTS

The **performance of the NARX Neural Network models** was assessed in terms of **percentage based on a *Goodness of Fit (GOF)*, measured with *Normalized Root***

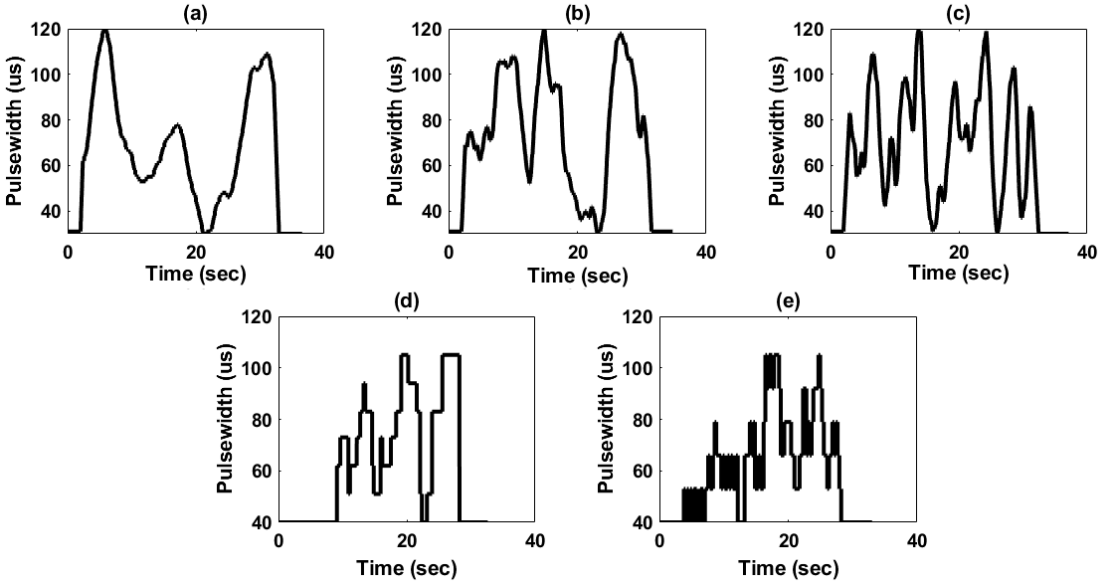

Figure 4.12: Input signals used to stimulate the TA muscle: (a) FRN with slow transitions, (b) FRN with intermediate transitions, (c) FRN with fast transitions, (d) PRMS with slow transitions and (e) PRMS with fast transitions.

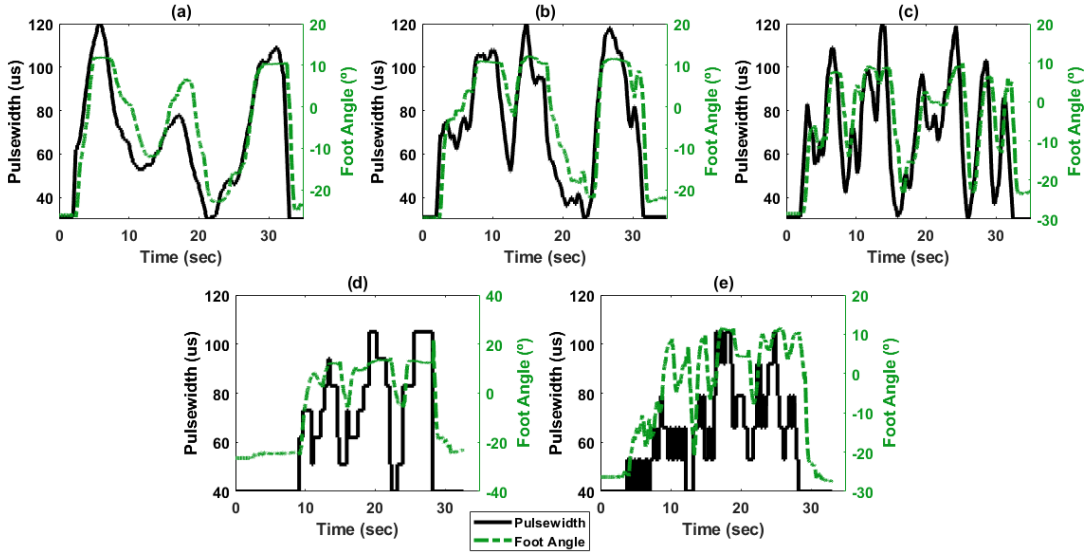

Figure 4.13: Input signals used to stimulate the TA muscle and correspondent foot angle: (a) FRN with slow transitions, (b) FRN with intermediate transitions, (c) FRN with fast transitions, (d) PRMS with slow transitions and (e) PRMS with fast transitions.

Mean Square Error (NRMSE) (Le et al. (2010), Luzio de Melo (2014)). This metric is represented in Equation 7:

$$Goodness\ of\ Fit = \left(1 - \left(\frac{\|yref - y\|}{\|yref - \overline{yref}\|}\right)\right) \times 100 \tag{7}$$

where *yref* represents the reference data and y represents the model output. The GOF ranges between $-\infty$, which symbolizes very poor fit, and 100 %, which symbolizes a perfect fit.

The **models were trained using the data acquired in the previous section**, after it was normalized using Equation 3, and the training of the was done offline, using *MATLAB*®. For the training of the NARX Neural Network the **data was divided in blocks, leaving 70% for training, 15% for validation and 15% for testing**, given the high amount of training data. The activation function used on the MLP was the *hyperbolic tangent* and the training algorithm used was the *Levenberg-Marquardt*. The **weights were initialized randomly**, between -1 and 1, and the **NARX Neural Network was trained with 2 different stopping criteria**: upon reaching 500 training epochs or if the validation error increases 6 times in a row. The validation MSE was calculated by comparing the expected values with those output by the NARX Neural Network. A flowchart of the training algorithm can be seen in Figure 4.14, where *Val_MSE* represents the validation error of the current training epoch, *P_Val_MSE* represents the validation error of the previous training epoch and *Val_Fail* represents the number of consecutive increases in validation error.

Tests were made for each type of model, with a **varying number of neurons (5, 10 and 20) and hidden layers (1 and 2) of the NARX Neural Network**, this was done to see if an increasing number of neurons in each hidden layer, and an increase in hidden layers, generates a NARX Neural Network with a better performance. **For each type of signal three prediction trials were done**.

In order to **assess the robustness of the models** trained with fast, medium and slow FRN and PRMS, **validation tests were made**. This was done by **using a model trained with one type of signal (fast, medium or slow) and then using this model to predict the remaining type of signals**. The tests were done with NARX Neural Networks with 20 neurons in each hidden layer and for models with 1 and 2 hidden layers. The **regression orders were set to *m*=*n*=2**, since in Previdi and Carpanzano (2003) the MSE of the NARX Neural Network with m=n=2, only increased 0.003 when compared to the model that performed better, with m=3 and n=4.

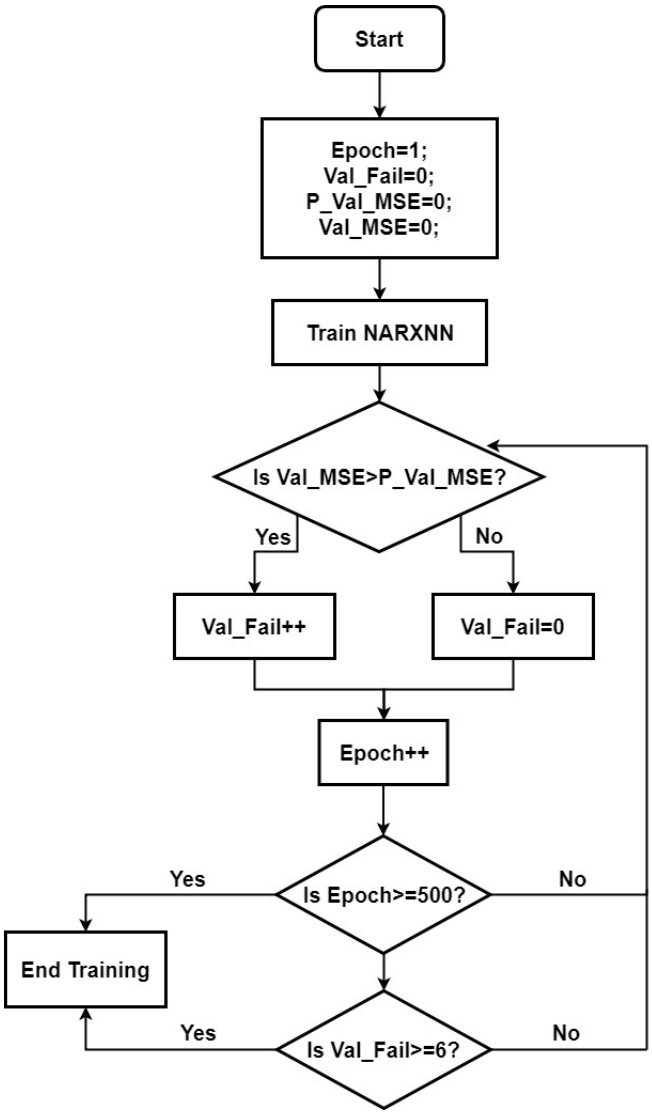

Figure 4.14: Flowchart of the training algorithm.

4.3.1 *Direct Model*

The input of the NARX Neural Networks used to create the direct model is the pulsewidth applied to the subject's TA muscle and the output is the corresponding foot angle. In Figure 4.15 the results for the NARX Neural Networks trained with the signals from the first trial can be seen. The model is able to predict the foot angle with high accuracy for models trained with FRN, with 85.20%, 90.43% and 82.85% accuracy, for slow, medium and fast transitions, respectively. When it comes to the PRMS the accuracy drops to 65.43% and 53.16%, for slow and fast transitions, respectively. The results for all the trials of the models trained with FRN can be seen in Table 4.1 and the results for all the trials of the models trained with PRMS can be seen in Table 4.2.

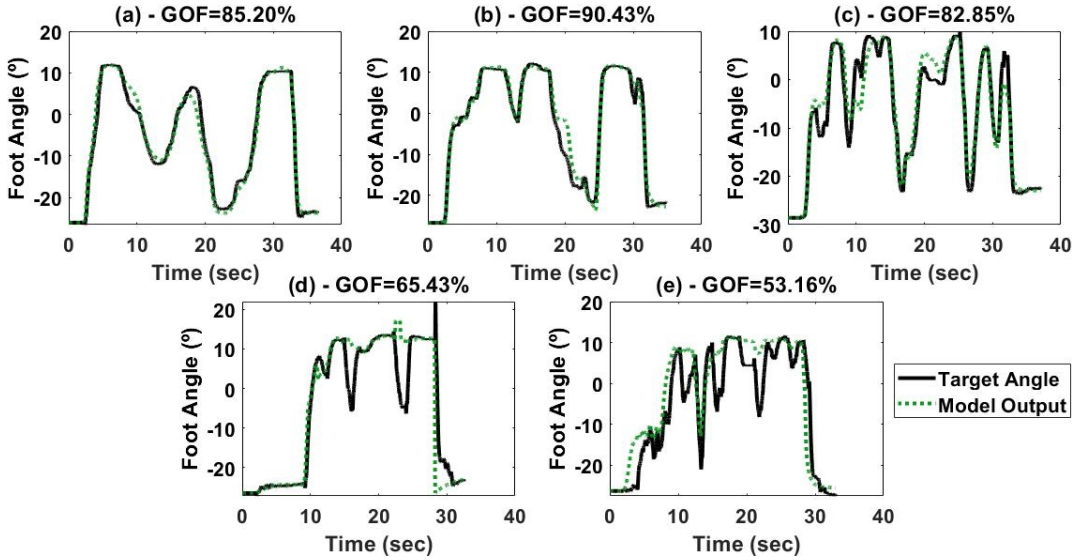

Figure 4.15: Direct model results for first trial with 1 hidden layer and 5 neurons: (a) FRN with slow transitions, (b) FRN with intermediate transitions, (c) FRN with fast transitions, (d) PRMS with slow transitions and (e) PRMS with fast transitions.

Based on the results of Table 4.1 it can be concluded that the **NARX Neural Networks with 2 hidden layers perform better for every number of neurons in the hidden layers**. However, the **difference in accuracy between NARX Neural Network with 1 and 2 hidden layers is low** for signals with medium transitions, with a difference of 3.34%, 2.01% and 1.56% for 5, 10 and 20 neurons respectively. For signals with slow transitions this difference increases to 7.77%, 12.03% and 17.16% for 5, 10 and 20 neurons respectively. For signals with fast transitions these differences are low for 10 and 20 neurons, with an accuracy of 1.93% and 2.27%, respectively. For

Table 4.1: Results for direct model with 5, 10 or 20 neurons and 1 or 2 hidden layers, trained with FRN signals.

No. Neurons	No. Layers	Trial 1	Trial 2	Trial 3	Average	Transitions
5	1	78.57%	61.41%	75.02%	71.67%	Fast
	2	82.85%	69.71%	83.64%	**78.73%**	
10	1	81.89%	60.00%	83.20%	75.03%	
	2	83.63%	66.96%	80.28%	**76.96%**	
20	1	79.78%	66.34%	84.58%	76.90%	
	2	83.39%	68.36%	85.75%	**79.17%**	
5	1	90.08%	83.53%	82.06%	85.22%	Medium
	2	90.43%	87.11%	88.15%	**88.56%**	
10	1	92.99%	87.46%	87.43%	89.29%	
	2	94.20%	90.74%	88.95%	**91.30%**	
20	1	93.70%	88.99%	83.47%	88.72%	
	2	94.58%	89.87%	86.40%	**90.28%**	
5	1	84.10%	58.91%	79.89%	74.30%	Slow
	2	85.20%	79.47%	81.53%	**82.07%**	
10	1	79.91%	80.56%	28.92%	51.09%	
	2	80.19%	59.29%	49.88%	**63.12%**	
20	1	84.48%	55.60%	38.64%	51.09%	
	2	85.09%	53.63%	66.03%	**68.25%**	

[a] Best results for each No. of neurons are colored green.

NARX Neural Networks with 5 neurons this difference increases to 7.06%. Hence if a model trained with FRN with medium transitions is used in the control strategy, it can be composed of only 1 hidden layer while if it is trained with FRN with slow transitions it should be composed of 2 hidden layers, since it results in a more accurate model.

When it comes to the number of neurons in each hidden layer, Table 4.1 shows that there is **no significant difference in the performance of the model depending on the number of neurons of the hidden layer**. The maximum performance difference for models with 2 hidden layers trained with medium transitions is only 2.74%, between 10 neurons and 5 neurons in each layer.

Similarly to what happened with the models trained with FRN signals, it can be seen in Table 4.2 that **models with 2 hidden layers perform better than models with 1 hidden layer**, with the highest accuracy difference of 38.39% for the models with 20 neurons trained with fast transitions. Models with 2 hidden layers perform similarly despite the number of neurons in the hidden layer, with a decrease of 4.15% when reducing from 20 neurons to 10 for models trained with fast transitions. Overall,

models trained with PRMS have a worst performance than models trained with FRN, with a decrease in performance of 25.63% for models with 20 neurons and 2 hidden layers trained with signals with fast transitions and a decrease in performance of 26.67% for models with 20 neurons and 2 hidden layers trained with signals with slow transitions.

Table 4.2: Results for direct model with 5, 10 or 20 neurons and 1 or 2 hidden layers, trained with PRMS signals.

No. Neurons	No. Layers	Trial 1	Trial 2	Trial 3	Average	Transitions
5	1	48.69%	64.44%	-53.58%	19.85%	Fast
	2	54.18%	71.07%	31.34%	**52.20%**	
10	1	46.72%	60.81%	31.35%	46.29%	
	2	60.37%	53.81%	33.99%	**49.39%**	
20	1	52.70%	52.24%	-61.00%	14.65%	
	2	53.16%	77.16%	30.31%	**53.54%**	
5	1	-1.52%	68.78%	0.12%	22.46%	Slow
	2	77.02%	61.76%	-5.76%	**44.34%**	
10	1	68.33%	67.37%	-2.89%	44.27%	
	2	83.03%	57.45%	-3.79%	**45.56%**	
20	1	65.39%	58.57%	-1.98%	40.66%	
	2	65.43%	64.24%	-4.93%	**41.58%**	

[a] Best results for each No. of neurons are colored green.

The results of the validation tests to assess the robustness of the models trained with FRN signals can be seen in Table 4.3. For both types of models, with 1 hidden layer and with 2, the **models trained with signals with slow transitions are the ones that are able to predict other types of signals better**. The difference is small for the prediction of fast signals, with only an increase in accuracy of 4.23% and 1.87%, for models with 1 and 2 hidden layers, respectively, when compared to models trained with medium transitions. For the prediction of medium signals, this difference increases to 6.57% and 7.46%, for models with 1 and 2 hidden layers, respectively, when compared to models trained with fast transitions.

Table 4.3: Results for robustness tests for models trained with FRN signals.

	2 Hidden Layers			1 Hidden Layer		
Transitions	Fast	Medium	Slow	Fast	Medium	Slow
Fast	85.08%	65.71%	69.45%	78.71%	59.66%	63.96%
Medium	62.68%	94.41%	69.66%	57.32%	87.40%	55.01%
Slow	**64.55%**	**73.17%**	84.28%	**61.55%**	**66.23%**	82.34%

[a] Best prediction results for each type of transition are colored green.
[b] Grey boxes indicate results for signals of the same type.

The results of the validation tests to assess the robustness of the models trained with PRMS signals can be seen in Table 4.4. It is clear that the **models with 2 hidden layers are able to predict different types of signals with more accuracy**, with an increase in performance of 20.38% for the prediction of signals with slow transitions and an increase of 9.78% for the prediction of signals with fast transitions.

Table 4.4: Results for robustness tests for models trained with PRMS signals.

	2 Hidden Layers		1 Hidden Layer	
Transitions	Fast	Slow	Fast	Slow
Fast	51.43%	57.74%	51.13%	47.96%
Slow	36.77%	67.76%	16.39%	61.20%

[a] Best prediction results for each type of transition are colored green.
[b] Grey boxes indicate results for signals of the same type.

Overall, **models trained with PRMS have low prediction accuracy**, with the highest prediction average of 53.54% (Table 4.2), for models with 2 hidden layers and 20 neurons in each layer. The **highest prediction average for models trained with FRN is 91.30%** (Table 4.1), for models trained with 2 hidden layers and 10 neurons in each layer. This likely happens because **FRN has a gradual behaviour**, which makes it easier to model, while **PRMS have sudden abrupt changes**. Given that **natural muscular movement also consists of continuous transitions, such as FRN**, henceforth **PRMS will be discarded**, and only FRN will be used to train the basic inverse model and the dynamic inverse model.

4.3.2 *Basic Inverse Model*

The **input of the NARX Neural Network used to create the basic inverse model is the foot angle and the output is the pulsewidth applied to the subject's TA muscle** that caused the foot movement. In Figure 4.16 the results for the NARX Neural Network trained with the signals from the first trial can be seen. The model is able to predict the applied pulsewidth with satisfactory accuracy, with 78.99%, 68.45% and 62.64% accuracy, for slow, medium and fast transitions, respectively. The results for all the trials of the model trained with FRN can be seen in Table 4.5.

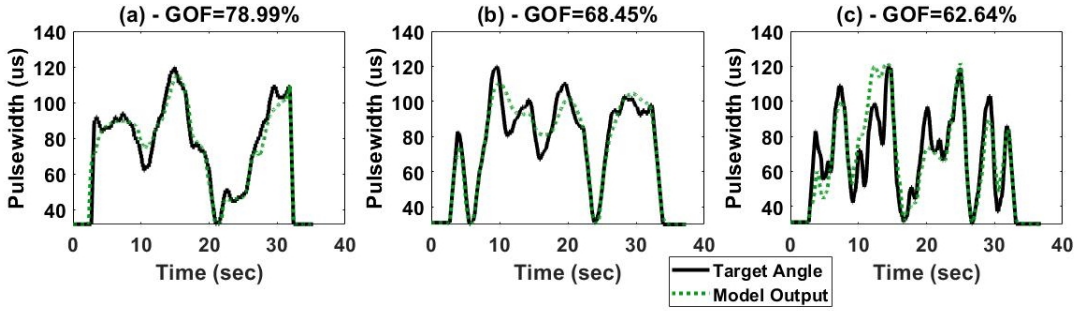

Figure 4.16: Basic inverse model results for first trial with 2 hidden layers and 5 neurons: (a) FRN with slow transitions, (b) FRN with intermediate transitions, (c) FRN with fast transitions.

Based on the results of Table 4.5 it can be concluded that the **NARX Neural Networks with 2 hidden layers perform better for every number of neurons in the hidden layers**. The difference in accuracy between models with 1 and 2 hidden layers is significant, especially for models trained with slow transitions, with an average decrease in performance of 25.36%, 43.59% and 18.68%, for models with 5, 10 and 20 neurons, respectively. For models with 2 hidden layers, the ones with 20 neurons in each layer generate the best average results for all cases. However, the difference between models with 20 neurons and models with 10 or 5 neurons was very small, having the highest average difference of 2.2% for models trained with slow transitions, and 1.46% for models trained with medium differences.

The results of the validation tests to assess the robustness of the models trained with FRN signals can be seen in Table 4.6. For both types of models, trained with 1 hidden layer and with 2 hidden layers, the **models trained with signals with medium transitions are the ones that are able to predict other types of signals better**. For the prediction of slow signals, the difference in prediction accuracy from models trained

Table 4.5: Results for basic inverse model with 5, 10 or 20 neurons and 1 or 2 hidden layers, trained with FRN signals.

No. Neurons	No. Layers	Trial 1	Trial 2	Trial 3	Average	Transitions
5	1	61.31%	53.02%	57.69%	57.34%	Fast
	2	62.96%	55.82%	62.64%	**60.47%**	
10	1	53.51%	49.95%	-24.31%	26.38%	
	2	57.85%	54.96%	63.34%	**58.72%**	
20	1	58.74%	52.93%	65.44%	59.04%	
	2	62.23%	58.20%	62.33%	**60.92%**	
5	1	71.17%	65.50%	63.01%	66.56%	Medium
	2	72.94%	66.77%	68.45%	**69.39%**	
10	1	78.18%	66.18%	62.89%	69.08%	
	2	78.43%	67.96%	65.25%	**70.55%**	
20	1	77.04%	62.83%	54.48%	64.68%	
	2	80.10%	70.92%	61.52%	**70.85%**	
5	1	46.33%	36.16%	56.77%	46.42%	Slow
	2	67.68%	68.66%	78.99%	**71.78%**	
10	1	45.24%	-57.71%	74.30%	20.61%	
	2	45.14%	72.07%	75.40%	**64.20%**	
20	1	33.81%	52.50%	77.69%	54.67%	
	2	71.08%	70.37%	78.61%	**73.35%**	

[a] Best results for each No. of neurons are colored green.

with fast and medium signals is small for models with 2 hidden layers and more significant for models with 1 hidden layer, reaching 3.57% and 6.78%, respectively. For the prediction of fast signals, the difference in prediction accuracy from models trained with slow and medium signals is more significant, reaching 8.96% and 26.37%, for models with 2 hidden layer and 1 hidden layer, respectively. Hence, **models with 2 hidden layers appear to be more robust when it comes to the predicting other types of signals**. Models trained with **fast transitions are able to predict signals with medium transitions better than models trained with slow transitions**, by a small difference of 1.92% for models with 2 hidden layers and a significant difference of 13.4% for models with 1 hidden layer.

Table 4.6: Results for robustness tests for models trained with FRN signals.

	2 Hidden Layers			1 Hidden Layer		
Transitions	Fast	Medium	Slow	Fast	Medium	Slow
Fast	64.35%	**57.12%**	56.06%	55.61%	**49.21%**	47.33%
Medium	**55.04%**	78.60%	**59.63%**	**53.01%**	75.93%	**54.11%**
Slow	46.08%	55.20%	76.91%	26.64%	35.81%	68.25%

[a] Best prediction results for each type of transition are colored green.

[b] Grey boxes indicate results for signals of the same type.

Overall, in the case of the **basic inverse model**, **NARX Neural Networks with 2 hidden layers are able perform better** than those with 1 hidden layer, despite the number of neurons in each layer. Furthermore, they are also **able to more accurately predict other types of signals, when compared to models with 1 hidden layer**. Basic inverse models **should be trained with signals with medium transitions**, given they are able to predict other types of signals more accurately.

4.3.3 *Dynamic Inverse Model*

The **inputs of the NARX Neural Network used to create the dynamic inverse model are the foot angle and its angular velocity, and the output is the pulsewidth applied to the subject's TA muscle that caused the foot movement**. In Figure 4.17 the results for the NARX Neural Network trained with the signals from the first trial can be seen. The **model is able to predict the applied pulsewidth with good accuracy**, with 89.05%, 93.9% and 69.49% accuracy, for slow, medium and fast

transitions, respectively. The results for all the trials of the model trained with FRN can be seen in Table 4.7.

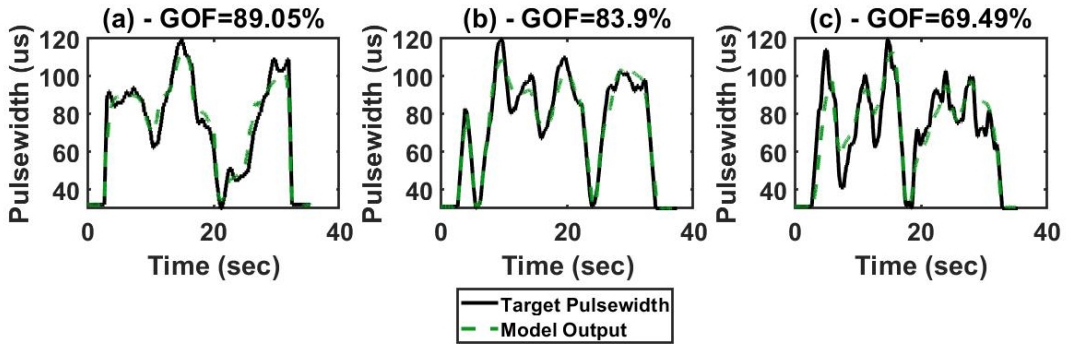

Figure 4.17: Dynamic inverse model results for first trial with 2 hidden layers and 20 neurons: (a) FRN with slow transitions, (b) FRN with intermediate transitions, (c) FRN with fast transitions.

Based on the results of Table 4.7, it can be seen that, **similarly to what happened with the basic inverse model**, the **models with 2 hidden layers perform better for all types of signals**. Furthermore, **the dynamic inverse model is able to predict the signals with higher accuracy when compared to the basic inverse model**, by comparing the results of Table 4.5. For models with 20 neurons and 2 hidden layers, with the dynamic inverse models the performance increases 7.15%, 5.6% and 8.06%, for models trained fast, medium and slow transitions, respectively, when compared to the same basic inverse model.

The results of the validation tests to assess the robustness of the models trained with FRN signals can be seen in Table 4.6. For both types of models, with 1 hidden layer and with 2 hidden layers, the **models trained with signals with fast transitions are the ones that are able to predict other types of signals better**. For models with 2 hidden layers, the models trained with fast transitions are able to increase the prediction accuracy of signals with medium transitions by 8.4%, when compared to models trained with signals with slow transitions, and increase the prediction accuracy of signals with slow transitions by 6.72%, when compared to models trained with signals with medium transitions.

Furthermore, when comparing Table 4.6 with Table 4.8, it can be seen that **the dynamic inverse model is able to perform better when predicting different types of signals**, with an increase of 2.29% for signals with fast transitions, an increase of

Table 4.7: Results for dynamic inverse model with 5, 10 or 20 neurons and 1 or 2 hidden layers, trained with FRN signals.

No. Neurons	No. Layers	Trial 1	Trial 2	Trial 3	Average	Transitions
5	1	61.74%	51.89%	54.35%	55.9%	Fast
	2	63.75%	53.14%	55.25%	**57.38%**	
10	1	64.03%	49.21%	51.81%	55.02%	
	2	66.01%	66.64%	60.57%	**64.41%**	
20	1	60.34%	52.70%	67.14%	60.06%	
	2	69.49%	64.27%	70.44%	**68.07%**	
5	1	53.05%	70.51%	66.18%	63.25%	Medium
	2	72.42%	65.44%	72.81%	**70.22%**	
10	1	70.52%	63.26%	76.43%	70.07%	
	2	84.38%	67.67%	62.26%	**71.44%**	
20	1	81.31%	68.48%	75.65%	75.15%	
	2	83.90%	73.95%	71.49%	**76.45%**	
5	1	58.83%	64.38%	71.30%	64.84%	Slow
	2	84.78%	68.58%	78.53%	**77.30%**	
10	1	87.15%	73.32%	71.48%	77.32%	
	2	86.89%	73.18%	81.86%	**80.64%**	
20	1	88.06%	73.91%	78.41%	80.13%	
	2	89.05%	72.65%	82.54%	**81.41%**	

[a] Best results for each No. of neurons are colored green.

Table 4.8: Results for robustness tests for models trained with FRN signals.

	2 Hidden Layers			1 Hidden Layer		
Transitions	Fast	Medium	Slow	Fast	Medium	Slow
Fast	68.20%	**72.89%**	**68.09%**	66.23%	**64.62%**	**45.38%**
Medium	**57.33%**	80.48%	61.37%	**40.52%**	80.01%	44.52%
Slow	34.25%	64.49%	88.13%	24.38%	53.62%	72.13%

[a] Best prediction results for each type of transition are colored green.
[b] Grey boxes indicate results for signals of the same type.

Table 4.9: Time response for one prediction for the inverse models with 2 hidden layers.

	No. of Neurons		
Inverse Model	20	10	5
Basic	6.5 ms	**6 ms**	6.5ms
Dynamic	7.5 ms	**7 ms**	7.5 ms

[a] Best prediction results for each type of transition are colored green.

15.77% for signals with medium transitions and 8.46% for signals with slow transitions, when compared to the same basic inverse model.

Since the chosen **model will be used in a real-time trajectory tracking control strategy**, it is important to **analyze the time response of the models for one prediction**. Hence, in Table 4.9 the time span of one prediction for the basic inverse model and the dynamic inverse model can be seen. The results show that for both inverse models, the **best time response is for the models with 10 neurons in each hidden layer**. Since dynamic inverse models proved to be the best models for signal prediction and given that the average walking step frequency is around 2.5 Hz (section 3.2), a **dynamic inverse model with 2 hidden layers and 10 neurons in each hidden layer was chosen to be implemented in the control strategy**.

4.4 DISCUSSION

NARX Neural Networks have been used previously to model upper body muscles for hand flexion (Popov et al. (2015)), to model quadriceps muscles (Chang et al. (1997), Yassin et al. (2017)) and to model the TA muscle (Chen et al. (2004)). However, to the best of the author's knowledge, a dynamic inverse NARX Neural Network model that uses 2 different inputs has not yet been used to model the TA muscle. Hence, **the**

innovative aspect of this project is the dynamic inverse model, that **uses the foot angle and the foot's angular velocity to model the TA muscle**.

Neural Network

The **chosen NN for this project was a NARX Neural Network**, because is **establishes non-linear relationships between past observations and future outputs** (Previdi (2002), Lin et al. (1996)), thus being **able to model the non-linear dynamic behaviour of electrically stimulated muscles** (Previdi and Carpanzano (2003)). Three models were created for this project: a **direct model**, that uses a NARX Neural Network with the pulsewidth applied to the TA muscle as input and the corresponding foot angle as output; a **basic inverse model**, that uses a NARX Neural Network with the pulsewidth applied to the TA muscle as output and the corresponding foot angle as input; and a **dynamic inverse model**, that uses a NARX Neural Network with the pulsewidth applied to the TA muscle as output and the corresponding foot angle and angular velocity as inputs.

Model Data Acquisition

In order to **adapt the models to the anatomic characteristics of each user**, a **calibration method** was proposed. It can be done with disabled subjects, since it **consists only of being sat down on a chair without having the foot touch the floor**. A TR is first applied, in order to find the minimum and saturation pulsewidth values of the subject, that are then used to create the FRN and PRMS signals to apply to the muscle, so that they capture the full ROM of the subject's foot. **FRN and PRMS are dynamic signals**, therefore being **appropriate to model the dynamics of the electrically stimulated muscle** (Le et al. (2010)).

Results

The **models were created with different parameters**, using NARX Neural Networks with 1 or 2 hidden layers and 5, 10 or 20 neurons, to determine which NARX Neural Network configuration generated better predictions. **Different types of FRN and PRMS signals were used to train the models**, having slow, medium and intermediate transitions, to create a wider range of data.

The **PRMS were discarded** after being used to train the direct model, because they **produced models with low prediction accuracy**. This was likely because of their

abrupt behaviour, when **compared to the gradual behaviour of FRN**, that resembles the continuous and also **gradual natural muscular movement**.

The **dynamic inverse model is able to predict the pulsewidth values with more accuracy, when compared to the basic inverse model**, with an increase in accuracy of 7.15%, 5.6% and 8.06%, for models trained with fast, medium and slow transitions, respectively. The prediction time responses of the inverse models were also studied, showing that both models had the lowest response time for NARX Neural Networks with 10 neurons. Thus, since there is only 1 ms difference in response time, from the basic inverse model to the dynamics model, and knowing that the dynamic inverse model provided higher average accuracy predictions for all cases, **the model chosen for the control strategy was a dynamic model with 2 hidden layers and 2 neurons**.

5

TRAJECTORY TRACKING CONTROL STRATEGY

In this chapter the implemented control strategy and steps taken to implement it are discussed. The importance of gait event detection and muscular response time delay removal for the control strategy are explained, followed by a brief description of how it was implemented. Subsequently, the dynamic inverse model created in Chapter 4 is validated for trajectory tracking and then paired with a Proportional Derivative (PD) controller, so that the trajectory tracking control strategy can be validated. Lastly, the trajectory tracking control strategy for Drop Foot (DF) correction is validated with a healthy subject with a treadmill at different speeds. The Chapter ends with a discussion of the obtained results.

5.1 INTRODUCTION

This project **aims at providing a personalized assistance for DF gait patients**, that helps delay the onset of fatigue and ensures a foot movement similar to the natural one. The literature analysis in Chapter 2 demonstrated that **combining a model with a controller provides the best tracking performance**, since the **controller is able to compensate for any modeling errors** that inevitably occur in real-time and the **model avoids time delays** inherent to the controller (Quintern et al. (1997)). Furthermore, it led to the choice of a **Trajectory Tracking control strategy** over an Electromyography (EMG)-based control strategy, due to the complexity of the acquisition and processing of the bioelectric signal of the latter.

The trajectory tracking control strategy makes the foot follow a desired trajectory, which in this case will be foot angle and foot angular velocity trajectories correspondent to the swing phase, since this is the gait phase affected by DF. The reference trajectories input to the control strategy will be created **using the foot trajectories of healthy subjects during real-time gait**, so that the **foot of DF subjects**

mimics healthy gait patterns. This will **generate a biological-like movement** for the ankle of DF subjects.

5.2 METHODS

In this section the methods used to create the **trajectory tracking control strategy** are presented. Firstly, the gait phase detection algorithm is explained, followed by the steps taken to create the reference trajectory with the gait of healthy subjects. Afterwards, the implemented control strategy is presented.

5.2.1 *Gait Phase Detection*

Gait it composed of two main phases: the **stance phase**, which is the phase when the foot maintains contact with the ground, and the **swing phase**, which is the phase during which the foot leaves the ground (Umberger (2010)). Since **dorsiflexion is the movement of raising the foot upwards**, caused by the contraction of the *Tibialis Anterior* (TA) muscle, and DF causes an inability to contract the TA muscle, DF only affects the swing phase of gait. Starting from stance, the gait event that marks the transition into the swing phase is the **toe-off**, when the foot leaves the ground. The gait event that marks the end of the swing phase is the **heel strike**, when the foot makes the first contact with the ground. The gait cycle can be seen in Figure 5.1.

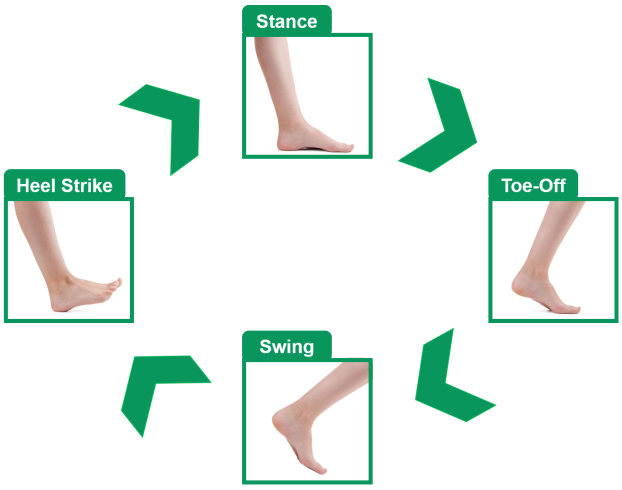

Figure 5.1: Gait cycle diagram.

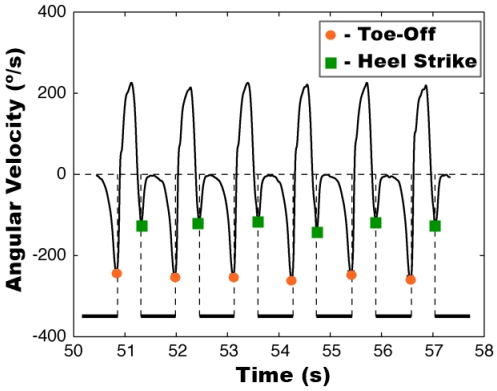

Figure 5.2: Typical foot angular velocity during gait. Adapted from Sabatini et al. (2005).

Since **DF only affects the swing phase of gait**, it is necessary to **identify when the swing phase ends and when it begins**, during real-time gait. For this purpose, the toe-off and heel strike gait phases were identified during real-time gait, **using the IMU placed on the foot**. The **foot's angular velocity** was used to determined the toe-off and heel strike events, using a simplified version of the gait event detection algorithm designed in Figueiredo et al. (2018). A typical foot angular velocity during gait can be seen in Figure 5.2.

Starting at the stance phase, when the **angular velocity drops below a threshold value, *TRl***, it signifies the **toe-off event** and, therefore, the start of the swing phase. Then, after the foot velocity reaches a positive value, when the **angular velocity drops below another threshold value, *TRh***, it signifies the **heel strike** event has happened and, therefore, the swing phase has ended. The diagram for the gait event detection algorithm can be seen in Figure 5.3.

In order to **test the algorithm**, a **healthy subject walked on a treadmill at three different speeds: 1 km/h, 1,5 km/h and 2 km/h**. The threshold values used were -2,1 rad/s and -3 rad/s, for *TRh* and *TRl*, respectively. The algorithm proved successful for all speeds tested. In Figure 5.4 the **algorithm was tested with the subject walking at 1 km/h and can detect the toe-off and heel-strike events based on the thresholds**, *TRh* and *TRl*.

It is important to emphasize that **the model has a delay that is specific for each subject and based on the muscular response time**. Therefore, in order to reach the correct foot angle in the correspondent gait phase, it is important to **anticipate this delay**. This was achieved by **starting stimulation slightly earlier than the toe-off**, how earlier was determined by the response time of each subject. The subject's **response**

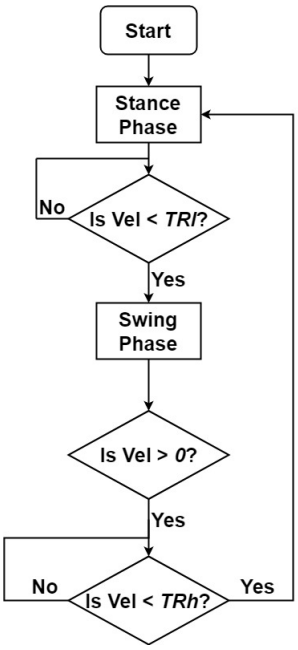

Figure 5.3: Gait event detection algorithm flowchart. *Vel* represents the foot angular velocity.

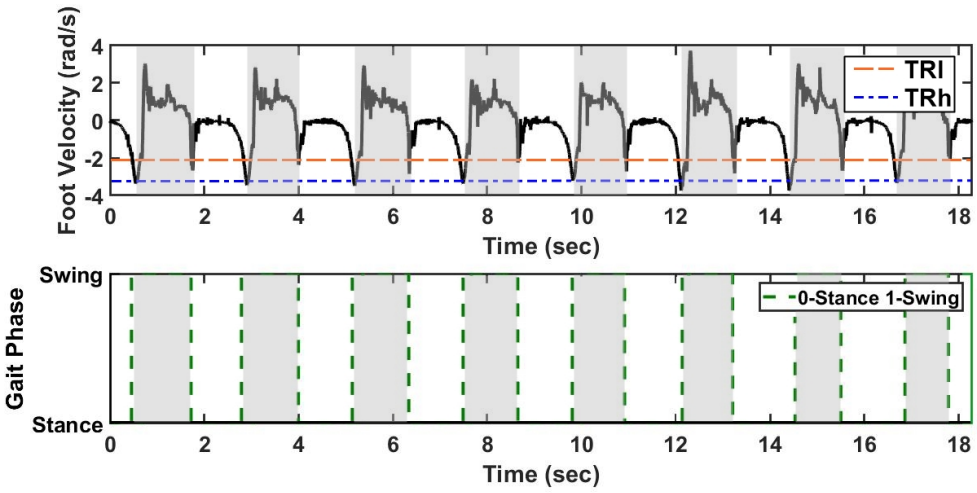

Figure 5.4: Real-time implementation of the gait event detection algorithm with a subject walking on a treadmill at 1 km/h: a) Foot angular velocity and b) Gait phase detection. The grey areas represent the swing phase and white areas represent the stance phase.

time is **found by determining how long after the stimulation is sent, does the foot begin to move**. The response time determination for the healthy test subject can be seen in Figure 5.5.

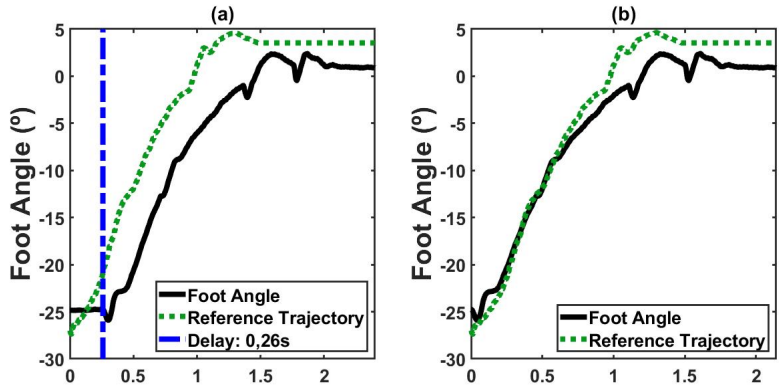

Figure 5.5: Test subject delay determination and removal: (a) determination of subjects response time and (b) removal of subjects response time.

The **removal of the delay** caused by the muscular response time was **achieved through the gait event detection algorithm**. The first step is used to determine the **duration of the stance phase, between heel strike and toe-off**. Being T_{st} the duration of the stance phase, T_{to} the beginning of toe-off and pT_{hs} the beginning of the previous heel strike, the calculation of the duration of the stance phase can be seen in Equation 8.

$$T_{st} = T_{to} - pT_{hs} \tag{8}$$

After this, the control is applied after the heel strike, as early before the toe-off as the corresponding delay, knowing the full duration of the stance phase. Being T_d the time delay of the subject and T_{stim} the time after heel-strike when the stimulation must start to be applied, the calculation of T_{stim} is explicit in Equation 9.

$$T_{stim} = T_{st} - T_d \tag{9}$$

The stimulation is afterwards terminated upon each heel strike. **During the first step the duration of the stance phase, T_{st}, is calculated and the stimulation is only applied after the first step.** The flowchart in Figure 5.12 can be used to better understand the real-time delay removal strategy.

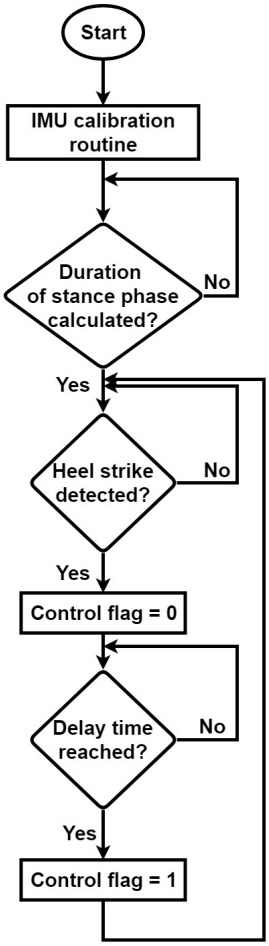

Figure 5.6: Delay removal strategy flowchart.

In order to test the algorithm, a **healthy subject walked on a treadmill at three different speeds: 1 km/h, 1,5 km/h and 2 km/h**. There was no stimulation applied to the subject on these trials. The algorithm proved successful for all speeds. One of the trials can be seen in Figure 5.7.

5.2.2 *Reference Trajectory Acquisition*

The use of FES for DF correction is mostly used with constant values, that are higher than the necessary at moments, causing the early onset of fatigue. Furthermore, it does not create a natural movement, since the **biological movement has a gradually increasing movement instead of a coarse one**. This is why a **reference trajectory based on the movements of healthy subjects** is important, to help **create a movement**

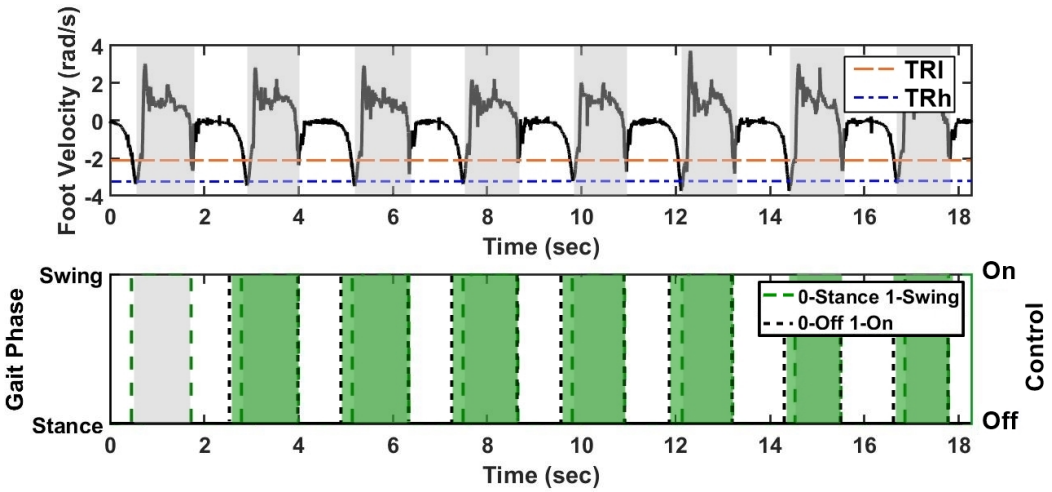

Figure 5.7: Real-time implementation of the delay removal gait event detection with a subject walking on a treadmill at 1.5 km/h: a) Foot angular velocity and b) Gait phase detection and control strategy duration. The grey areas represent the swing phase, the white areas represent the stance phase and the green areas represent when stimulation is applied.

as close to the biological one as possible. The gait reference trajectory for the control strategy was obtained from **10 healthy subjects walking on a treadmill** at different speeds. The subject's characteristics are presented in Table 5.1.

Table 5.1: Characteristics of the subjects used for the reference trajectory

	Male	Female
Number of subjects	6	4
Age	24.83 ±2.22	24 ±1.83
Weight (kg)	68.16 ±6.76	57.25 ±3.2
Height (cm)	175.5 ±2.94	161.75 ±3.68

In order to acquire the gait trajectory, **an IMU was placed on the foot of the subjects**. They were asked to walk on a treadmill, with no slope, at the speeds of 1 km/h, 1.5km/h and 2 km/h. The **foot angle and foot angular velocity were acquired in real-time**, for 10 steps for each speed.

The **trajectory of one full step** of each trial was taken randomly for each subject, considering each step begins and ends when the both the foot velocity and the foot angle are at 0° and 0 rad/s, respectively. At each moment, **the average value of**

each sample was determined to create the reference trajectory. The resulting acquired trajectories for each speed can be seen in Figure 5.8.

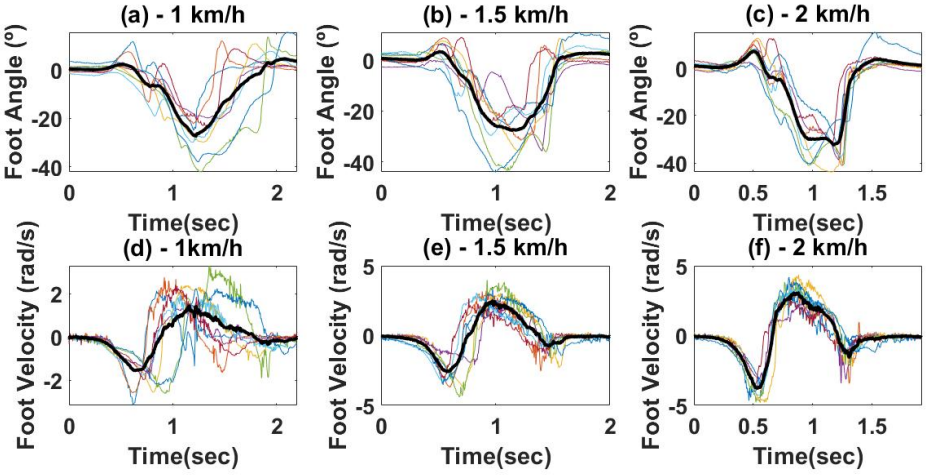

Figure 5.8: Acquired gait trajectories and calculated average: (a) and (d) foot angle and velocity for 1 km/h, respectively; (b) and (e) foot angle and velocity for 1,5 km/h, respectively; (c) and (f) foot angle and velocity for 2 km/h, respectively. The thin lines show each subject's step and the thick line represents the reference trajectory.

Since **DF only affects the swing phase of gait**, the reference trajectory input to the controller corresponds only to the swing phase of the reference trajectories. The final reference trajectories can be seen in Figure 5.9.

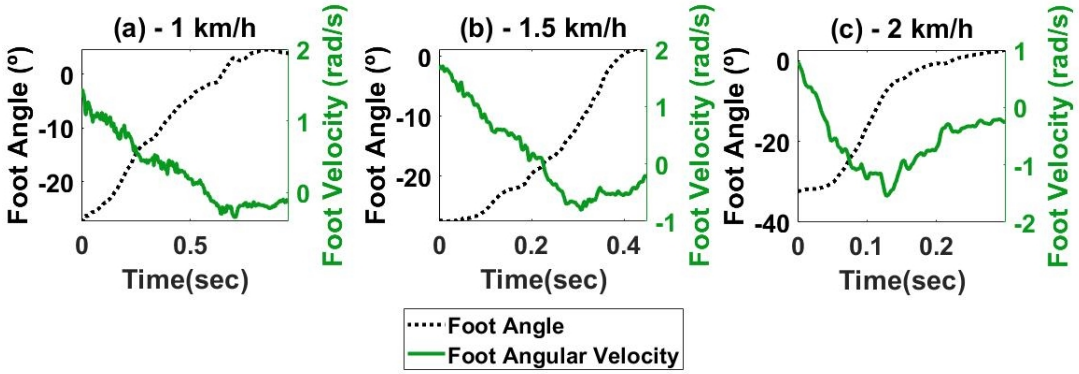

Figure 5.9: Control gait reference trajectories for swing phase: (a) 1 km/h speed, (b) 1,5 km/h and (c) 2 km/h.

5.2.3 *Control Strategy*

For the **control strategy a PD controller was chosen to pair with the dynamic inverse NARX Neural Network model**, created in section 4.2.1. The PD controller was used due to the relative simplicity in implementation and tuning. A diagram for the PD controller can be seen in Figure 5.10. The **IMU placed on the foot provides the foot angle,** θ, used to calculate the error and the **angular velocity of the foot,** $\dot{\theta}$.

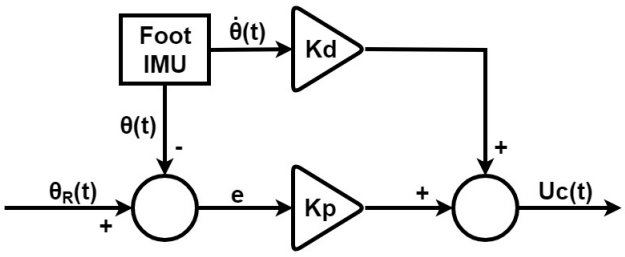

Figure 5.10: PD controller diagram.

For the PD controller, if the error value, *e(t)*, is represented by Equation 10

$$e(t) = \theta_R(t) - \theta(t) \tag{10}$$

where $\theta_R(t)$ is the desired trajectory angle and $\theta(t)$ is the real foot angle measured by the IMU, then the PD control is represented by Equation 11

$$U_c(t) = e(t) * Kp + \dot{\theta}(t) * Kd \tag{11}$$

where $U_c(t)$ is the control variable output by the controller, *e(t)* is the error value of Equation 10, $\dot{\theta}(t)$ is the foot's angular velocity, and *Kp* and *Kd* are the proportional and derivative gains, respectively.

The dynamic inverse NARX Neural Network model is represented by Equation 12, which is derived from Equation 2.

$$U_m(t) = f(\theta_R(t), ..., \theta_R(t-n), \dot{\theta}_R(t), ..., \dot{\theta}_R(t-n), P\hat{W}(t-1), ..., P\hat{W}(t-m)) \tag{12}$$

where U_m is the variable output by the model, θ_R is the desired foot angle trajectory, $\dot{\theta}_R$ is the desired foot angular velocity trajectory and $P\hat{W}$ is the pulsewidth value predicted by the NARX Neural Network.

The final control variable that is sent to the stimulator, U_s, is a sum of the pulsewidth value predicted by the model, U_m, and the control variable from the PD controller, U_c. This is given by Equation 13.

$$U_s(t) = U_m(t) + U_c(t) \tag{13}$$

The control loop used for the trajectory tracking strategy, using the PD controller paired with the dynamic inverse NARX Neural Network model, **allows real-time foot angle feedback, thus being able to overcome external disturbances**. This control strategy, which is given by Equation 13, can be seen in Figure 5.11.

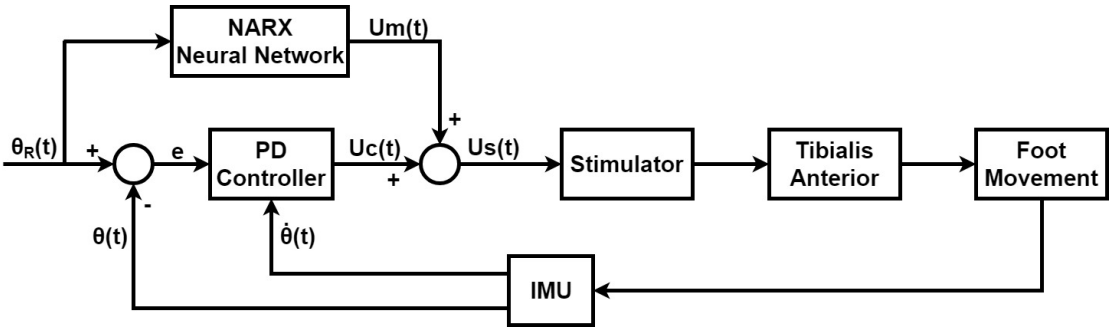

Figure 5.11: Trajectory tracking control diagram of NARX Neural Network with PD controller.

The flowchart presented in Figure 5.12, can be used to better understand the implemented control system.

In order to **establish a comparison for the performance of the implemented trajectory tracking control strategy**, an **open-loop** control strategy using **only the dynamic inverse NARX Neural Network model** was used. This strategy is represented by Equation 12 and a diagram can be seen in Figure 5.13.

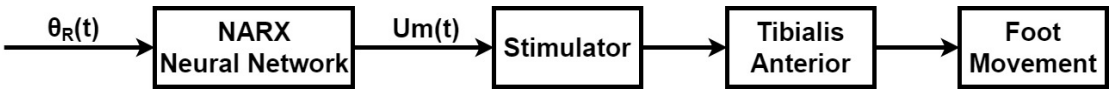

Figure 5.13: Trajectory tracking strategy with NARX Neural Network diagram.

The same **trajectory was input to the open-loop control strategy and to the trajectory tracking control strategy, to compare the performance of both strategies**. The validation are described in the following section.

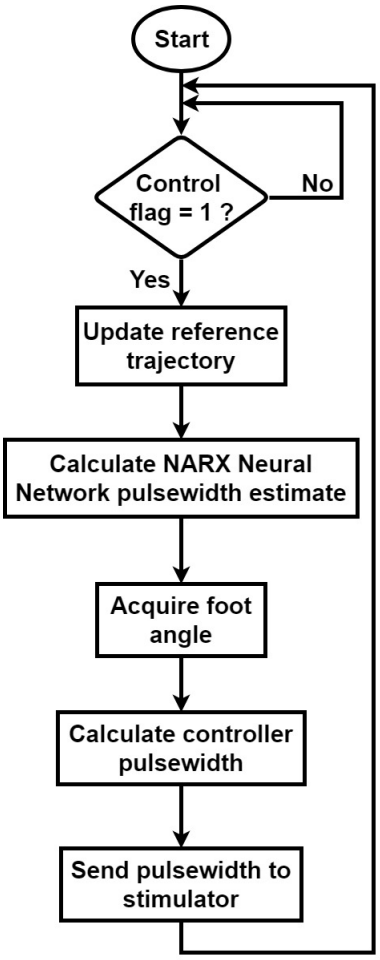

Figure 5.12: Trajectory tracking control strategy flowchart.

5.2.4 *Validation Protocols*

Two configurations were used to test the trajectory tracking control strategy: a **static configuration**, with the subject sitting on a chair, and a **gait configuration**, with the subject walking on a treadmill. The static configuration was **used to determine if the control strategies were able to track the reference trajectories** and to **compare the performance of the open-loop control strategy with the trajectory tracking control strategy**. The trajectory tracking control strategy was also tested in a static configuration with a **weight strapped to the foot**, to see if the control strategy was **able to compensate external disturbances**. The gait configuration was **used to determine if the trajectory tracking control strategy was able to correct DF during real-time gait**.

The open-loop control strategy and trajectory tracking control strategy were both tested in a static configuration, while only the trajectory tracking control strategy was tested in a gait configuration. The protocols for each validation will be described next. However, **for every validation protocol there are steps that need to be taken** in order to setup the system on the user, as follows:

1ST **STEP -** Shave the *Common Peroneal* nerve area and the *Tibialis Anterior* area.

2ND **STEP -** Place the active electrode on the motor point of the *Tibialis Anterior* muscle and the indifferent electrode on the *Common Peroneal* nerve, as can be seen in Figure 5.14 (a).

3RD **STEP -** Place the IMU on top of the foot, whether strapped to the shoe laces or with a strap, as can be seen in Figure 5.14 (b).

4TH **STEP -** Find the minimum and maximum threshold values for each subject, by applying a TR signal, as described in section 4.2.3.

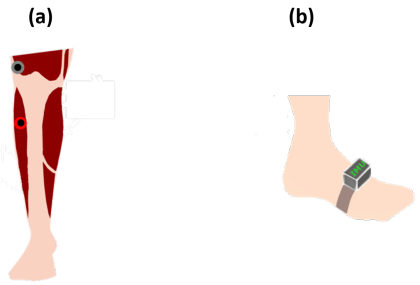

Figure 5.14: Validation setup steps: (a) Electrode placement (active electrode is red) and (b) IMU placement.

Unrestrained Open-Loop Control Static Validation

since **during the swing phase no external forces, besides gravity, are applied to the foot**, the static validation protocol tries to emulate the conditions during swing phase. Therefore the **subject was placed in a sitting position that kept the foot from touching the ground** and allowed the ankle to move without restriction. The setup can be seen in Figure 5.15.

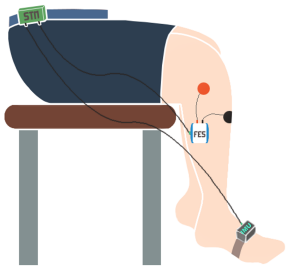

Figure 5.15: Static validation setup.

This validation was done **using the open-loop control strategy**, that uses the dynamic inverse NARX Neural Network model. The strategy was validated with the reference trajectory for **three different speeds: 1 km/h, 1.5 km/h and 2 km/h**. This is done to **see if the model is able to predict the pulsewidth correspondent to desired reference trajectories accurately**. The performance of the open-loop control strategy is done by **comparing the real foot angle trajectory with the desired trajectory**, measured using the Goodness of Fit (GOF) given in Equation 7.

Unrestrained Trajectory Tracking Control Static Validation

The same protocol used to validate the open-loop control was used for the static validation of the trajectory tracking control, that uses a **PD controller paired with the dynamic inverse NARX Neural Network model**. This control strategy was validated with the reference trajectory for 1 km/h, 1.5 km/h and 2 km/h. This was done to **see if the control strategy was able to follow the reference trajectories accurately**. The performance assessment of the trajectory tracking control strategy is also done by comparing the real foot angle trajectory with the desired trajectory, and is measured using the GOF given in Equation 7.

Weighted Trajectory Tracking Control Static Validation

In order to **determine the robustness of the PD controller and its ability to overcome external disturbances**, it was validated for the same three speeds, 1 km/h, 1.5 km/h and 2 km/h, with a **weight strapped to the foot**.

The weight weighed 0.4 kg and it was **strapped with velcro around the foot, so that it was evenly distributed** and so that it would not put too much strain on the foot. The validation setup can be seen in Figure 5.16.

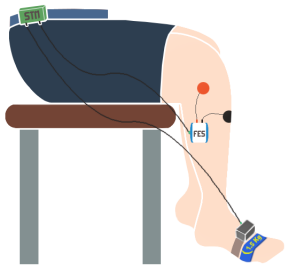

Figure 5.16: Weighted static validation setup.

Trajectory Tracking Control Gait Validation

The **gait validation** was done with a **healthy subject on a treadmill walking at 3 speeds: 1 km/h, 1.5 km/h and 2 km/h**. The trajectory tracking control strategy was **tested in real-time gait to see if it was able to track the correspondent swing trajectory and correct DF gait**. The validation setup can be seen in Figure 5.17.

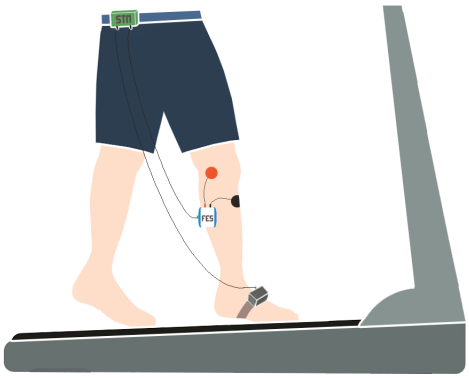

Figure 5.17: Setup of the real-time gait control validation on a treadmill.

During the validation trials, **the healthy subject was instructed not to lift the foot during the swing phase**, leaving it loose, **behaving like a DF patient**. This was done to see if the system was ready to be validated on DF subjects.

In order to have a term of comparison, a **healthy subject was asked to walk on a treadmill like a DF patient**: trying his best not to lift the foot during the swing phase, therefore dragging it on the floor. This creates a **pseudo-DF gait** that can be **compared with the subject's gait when applying the trajectory tracking control strategy in real-time**. The resulting angle trajectory can be seen in Figure 5.18, which shows that the main differences between healthy gait and DF gait is that **upon heel strike the foot angle is below** 0° for DF gait and also that the **foot drags on the floor when toe-off should occur**.

The results of all the validations described in this section will be presented in the next section.

5.3 RESULTS

The system was validated with a healthy 23 year old female subject with 162 cm and 60 kg. The threshold values found in the system calibration, explained in section 4.2.3, are 30 µs and 120 µs, for the minimum and threshold values, respectively. The **parameters for the PD controller were tuned manually** and the values for each gain were 1.5 and 0.7, for the kp and the kd, respectively.

Note that, in the presented results, the delay resultant of the subject's muscular response time, T_d, has already been removed, so the performance of the validated

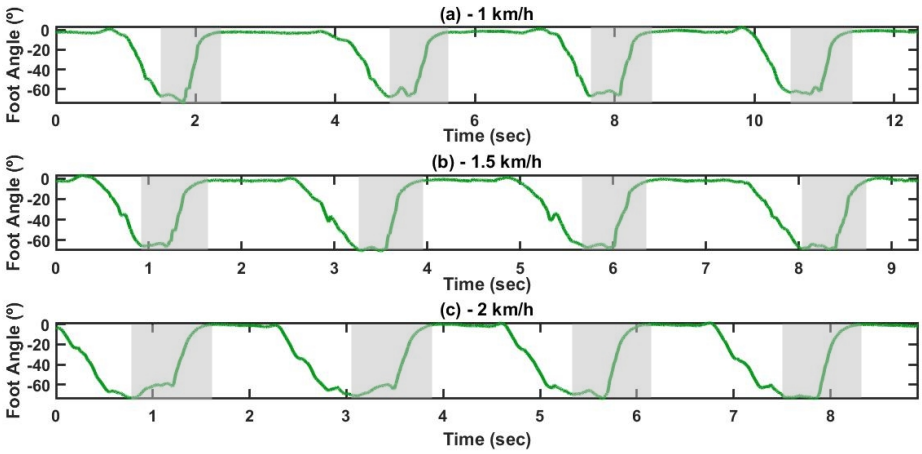

Figure 5.18: Forced DF gait acquired from a healthy subject. (a) 1 km/h speed, (b) 1.5 km/h speed and (c) 2 km/h speed. The grey areas represent the swing phase.

control strategies can be correctly determined. This delay was determined in section 5.2.2.

5.3.1 *Unrestrained Open-Loop Control Static Validation*

The **dynamic inverse NARX Neural Network model** was tested in an **open-loop control strategy** to see if it was able to **accurately predict the pulsewidth** that must be applied to the TA muscle, in order to follow the desired trajectory. The results for this validation, done for the trajectories of 1 km/h, 1.5 km/h and 2 km/h, can be seen in Figure 5.19.

The model was **able to predict the trajectory for 1 km/h accurately, with 68.16% accuracy**, as shown in Figure 5.19 (a). This shows that the **model is adapted to the user's characteristics**, since without any feedback, it is able to place the foot close to the desired positions. For the **1.5 km/h trajectory**, however, the model **was not able to predict the necessary pulsewidth** accurately, with an **accuracy of only 23.86%**, seen in Figure 5.19 (b). This low accuracy is mostly because **the trajectory for 1.5 km/h increases the desired foot angle faster than the 1 km/h trajectory**, but the **model predicts a pulsewidth pattern very similar to the 1 km/h trajectory**, as can be seen in Figure 5.19 (d) and (e). This results in the **foot not being able to accompany the desired trajectory**. When it comes to the 2 km/h trajectory, the **model is able to increase the predicted pulsewidth values, when compared to the 1 km/h and 1.5**

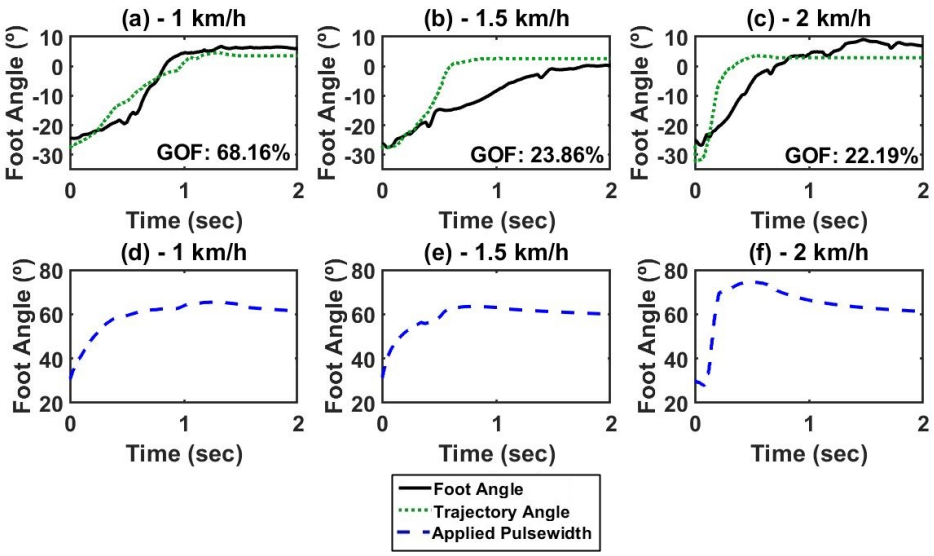

Figure 5.19: Performance of open-loop control. Reference foot angle trajectory and real foot angle for (a) 1 km/h, (b) 1.5 km/h and (c) 2 km/h. Applied pulsewidth for (d) 1 km/h, (e) 1.5 km/h and (f) 2 km/h.

km/h trajectories, as seen in Figure 5.19 (d), (e) and (f). The **model's prediction tries to match the abrupt increase in the desired foot angle trajectory**, however this increase is not sufficient and the control strategy accuracy is only 22.19%, as can be seen in Figure 5.19 (c).

5.3.2 *Unrestrained Trajectory Tracking Control Validation*

After the open-loop control validation, the **dynamic inverse NARX Neural Network model was paired with the PD controller** in order to validate the trajectory tracking control strategy. The control strategy was tested for the 1 km/h, 1.5 km/h and 2 km/h speeds and the results can be seen in Figure 5.20.

This control is **able to track the trajectories for the 1 km/h and 1.5 km/h speeds, with accuracies of 77.87% and 63.32%**, respectively. When it comes to the **2 km/h speed**, the control strategy has a **low accuracy of only 23.72%**. This happens because the **initial foot angle is higher than the initial reference angle**, which does not happen for the 1 km/h and 1.5 km/h trajectories, as can be seen in Figure 5.20 (d), (e) and (f). Therefore **during the first 100 ms only the minimum pulsewidth was applied**. When the reference trajectory then increases abruptly, so does the applied pulsewidth.

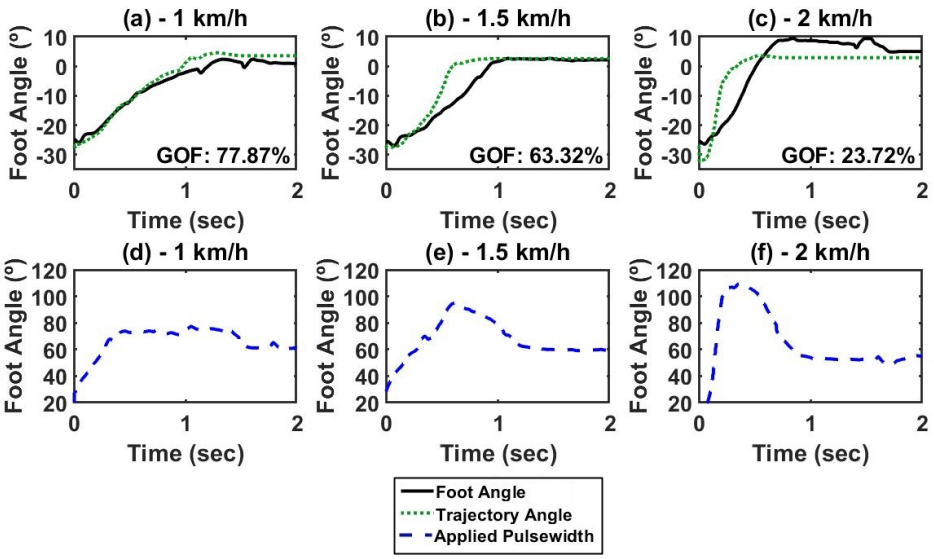

Figure 5.20: Performance of trajectory tracking control. Reference foot angle trajectory and real foot angle for (a) 1 km/h, (b) 1.5 km/h and (c) 2 km/h. Applied pulsewidth for (d) 1 km/h, (e) 1.5 km/h and (f) 2 km/h.

However, this **increase is not applied soon enough** and thus the **foot angle does not reach the desired reference angle** in time, as can be seen in Figure 5.20 (c).

A **comparison of the open-loop control strategy and the trajectory tracking control strategy** can be seen in Figure 5.21. The **PD controller is able to improve the performance of the dynamic inverse model** in open-loop configuration, by **correcting the model's predictions based on the real-time foot angle and foot angular velocity**. For the 1 km/h speed the tracking performance is increased by 9.71%; for the 1.5 speed trajectory the tracking performance is increased by 39.46%; and for the 2 km/h speed the performance is increased only by 1.53%.

The **tracking performance for the 2 km/h speed remains similar** with and without the addition of the PD controller, since the abrupt increase in the applied pulsewidth occurs at the same time, as can be seen in Figure 5.21 (f).

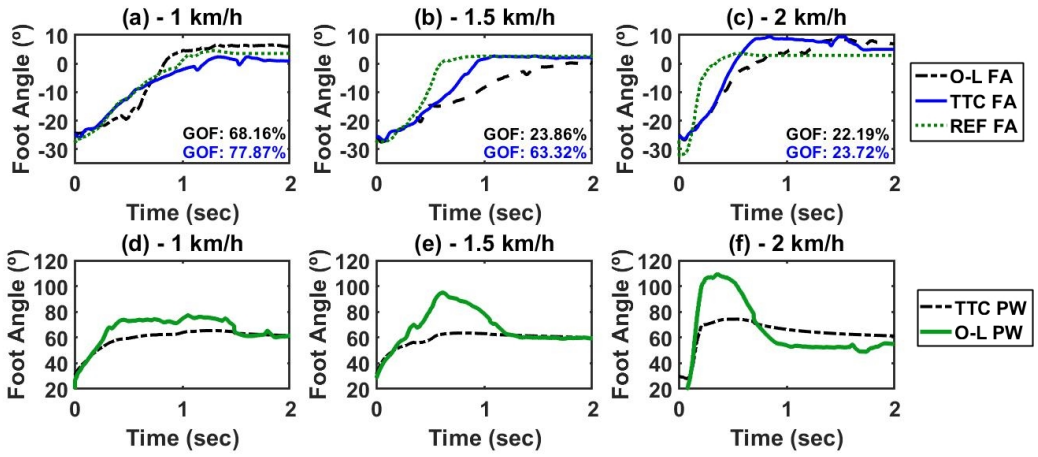

Figure 5.21: Performance comparison between open-loop and trajectory tracking control. Reference foot angle trajectory and real foot angle for (a) 1 km/h, (b) 1.5 km/h and (c) 2 km/h. Applied pulsewidth for (d) 1 km/h, (e) 1.5 km/h and (f) 2 km/h. O-L stands for open-loop control, TTC stands for trajectory tracking control, PW stands for pulsewidth and FA stands for foot angle.

5.3.3 *Weighted Trajectory Tracking Control Static Validation*

In order to **test the robustness of the trajectory tracking control strategy and its ability to compensate for external disturbances**, an **external disturbance (0.4 kg weight) was strapped to the subject's foot**. The validation was done for 1 km/h, 1.5 km/h and 2 km/h speeds, and the results can be seen in Figure 5.22. For the 1 km/h speed, although **in the beginning the foot was not able to follow the trajectory correctly**, the **controller was able to increase the applied pulsewidth so that the foot was able to match the reference trajectory**, as can be seen in Figure 5.22 (a).

The **tracking accuracy for the 1.5 km/h speed was very satisfactory, at 59.87%**. The foot angle was able to follow the reference trajectory very closely, as can be seen in Figure 5.22 (b). Since the **2 km/h trajectory** is the one that **increases more abruptly**, in order to compensate for this disturbance **the applied pulsewidth reached the saturation threshold value of 120 μs** as can be seen in Figure 5.22 (f). However, this was **not enough to make the foot track the reference trajectory accurately**, indicating that the **weight restrains fast movements**.

The comparison between the performance of the unrestrained and weighted trajectory tracking control was compared in Figure 5.23. For the 1 km/h speed, the **performance of the unrestrained control is better, with an increase of 40.5%**. This

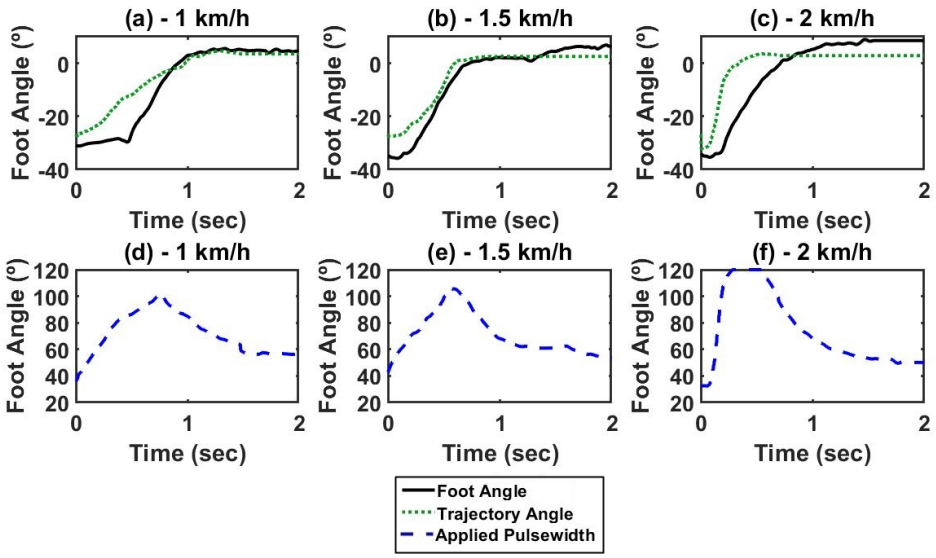

Figure 5.22: Weighted trajectory tracking control with dynamic inverse model paired with PD controller.

was **due to the slow start caused by the weight**. However, at 1 s, the **foot was able to follow the rest of the trajectory accurately**, as can be seen in Figure 5.23 (a).

For the **1.5 km/h speed** the **performance accuracy is very similar**, only **increasing by 3.45%** when the weight is not used. This shows the **trajectory tracking control is able to compensate external disturbances**, as expected. The difference between the control performance for **the 2 km/h** speed trajectory is 35.43%, improving when the weight is not used. However, for the weighted control the subject's saturation pulsewidth value was reached.

5.3.4 *Trajectory Tracking Control Gait Validation*

After assessing the performance of the trajectory tracking control in static configurations, the **control strategy was tested in a real-time gait configuration**. The **trials were done on a treadmill** and, as stated previously, the **subject was instructed to let his foot as loose as possible** during the swing phase, to **mimic the behaviour of DF patient's feet**. For the first trial, the treadmill was set to 1 km/h and the subject was asked to walk 10 steps. The results of this validation can be seen in Figure 5.24.

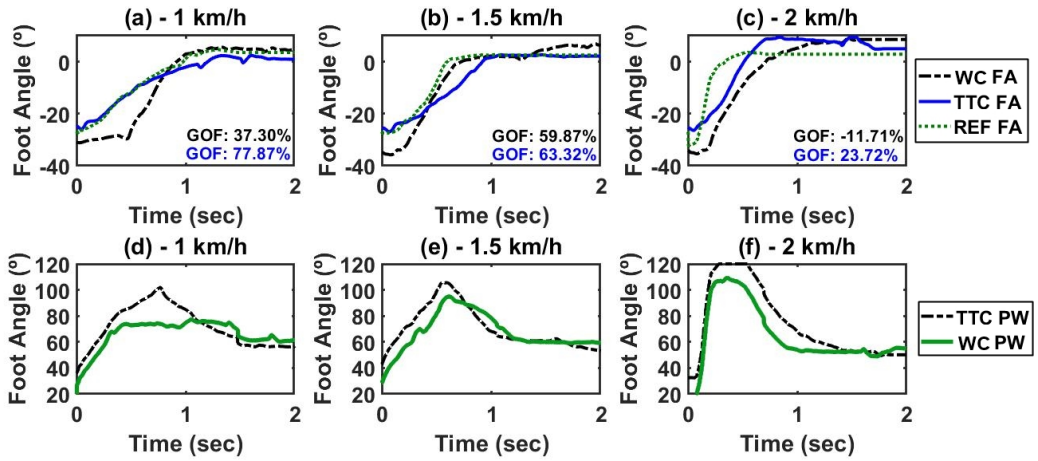

Figure 5.23: Performance comparison between unrestrained and weighted trajectory tracking control. Reference foot angle trajectory and real foot angle for (a) 1 km/h, (b) 1.5 km/h and (c) 2 km/h. Applied pulsewidth for (d) 1 km/h, (e) 1.5 km/h and (f) 2 km/h. WC stands for weighted control, TTC stands for trajectory tracking control, PW stands for pulsewidth and FA stands for foot angle.

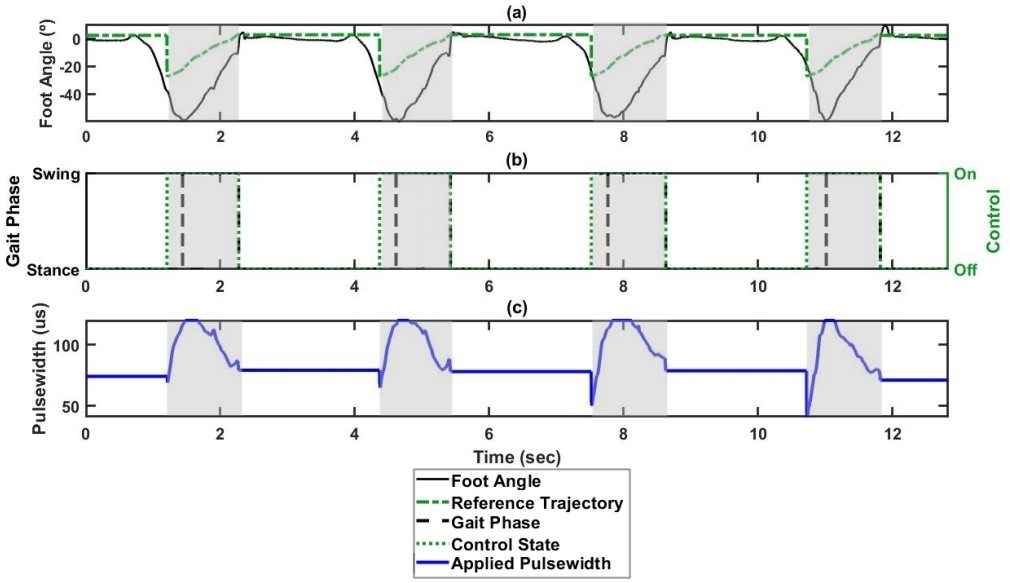

Figure 5.24: Real-time trajectory tracking control strategy validation at 1 km/h: (a) Foot angle and reference trajectory, (b) Gait event detection and control activation and (c) Applied pulsewidth. The grey areas represent the stages when the stimulation is applied (control strategy is on).

By analyzing Figure 5.24 (a), it can be seen that at the beginning of the swing phase, the real foot angle is 20º lower than the reference trajectory. In order **to compensate this disturbance, the controller is able to increase the applied pulsewidth**, as can be seen in 5.24 (c). **As the foot angle approaches the desired trajectory the applied pulsewidth decreases**, as expected, in order **to prevent the early onset of fatigue**.

The **pseudo-DF gait and the gait corrected with FES were compared**, in order to see if the control strategy was able to improve the gait pattern of DF patients. The red rectangle in Figure 5.25 shows that, while **in the DF gait the foot is not able to rise above 0º at heel strike**, when the **trajectory tracking control strategy is applied**, the **foot is able to track the desired trajectory, thus raising above 0º and generating a foot movement similar to the healthy one**.

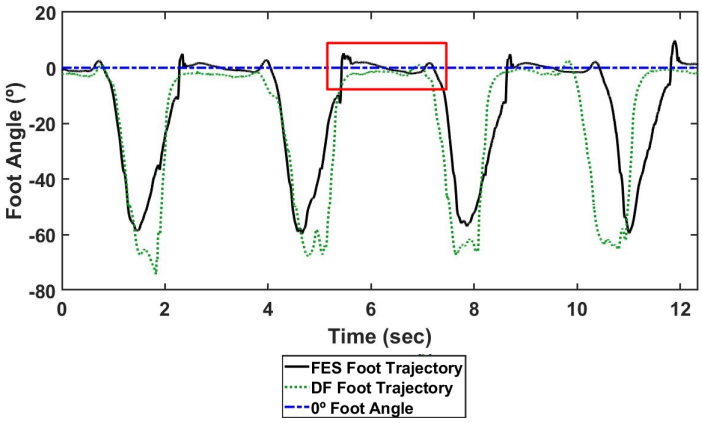

Figure 5.25: Comparison between DF gait and gait corrected with FES at 1 km/h.

The control was then **tested on the treadmill at a speed of 1.5 km/h**. The subject was, once again, instructed to let the foot relaxed and loose during the swing phase. The results of this validation can be seen in Figure 5.26.

Once again, the **initial swing foot angle is lower than the initial reference angle**, therefore the controller increases the applied pulsewidth until the difference decreases. The **pulsewidth is not constant throughout the swing phase**, it **changes according to the discrepancy between the desired trajectory and the real foot angle**, as can be seen in Figure 5.26 (c). The foot angle is able to reach the desired reference angles before the heel strike, thus generating a more natural movement.

By comparing the pseudo-DF gait with the gait corrected by the control strategy, it can be seen that **the angle at heel strike increases with the DF correction strategy**. This will **prevent subjects from dragging their feet on the ground** during gait, thus

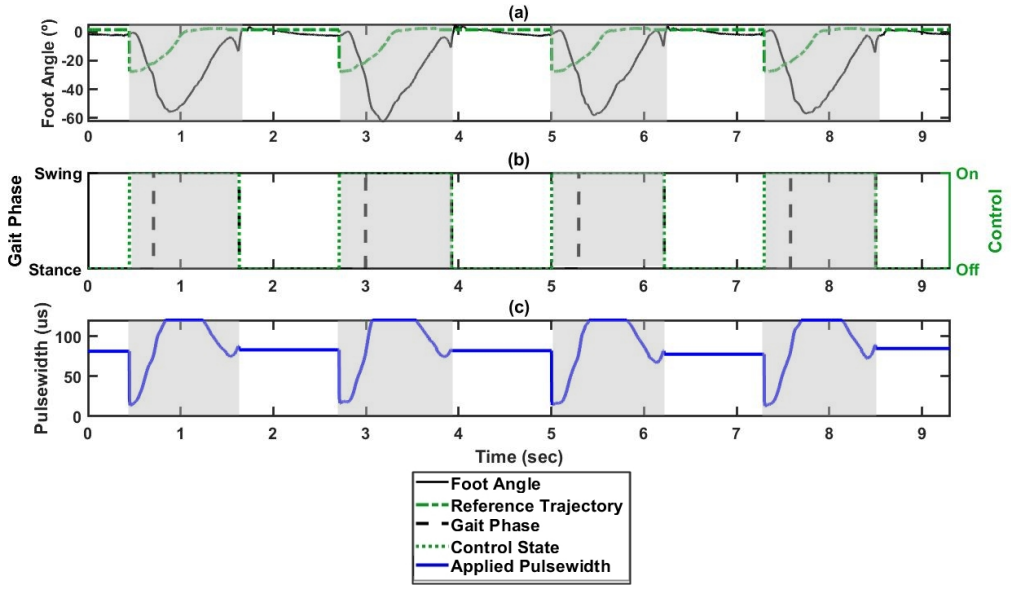

Figure 5.26: Real-time trajectory tracking control strategy validation at 1.5 km/h: (a) Foot angle and reference trajectory, (b) Gait event detection and control activation and (c) Applied pulsewidth. The grey areas represent the stages when the stimulation is applied (control strategy is on).

decreasing the likelihood of tripping and falling when walking. The comparison can be seen in the red rectangle of Figure 5.27.

Finally, the control strategy was tested with the subject **walking on a treadmill at 2 km/h**, with the corresponding reference trajectory being input to the controller. The results of this validation were similar to the ones for the slower speeds and can be seen in Figure 5.28. However, **the applied pulsewidth stays longer at the maximum threshold tolerated by the subject** due to the increase in the reference angle being more abrupt, when compared to the 1 km/h and 1.5 km/h trajectories. Regardless, upon heel strike the foot angle is higher than 0°, as desired.

The comparison with the pseudo-DF gait, shows that not only is the **foot angle higher upon heel strike with the implemented correction strategy**, but it also **helps reduce the step length**, as can be seen in Figure 5.29. This happens because **the foot is no longer dragging on the floor**, making it easier for the subject to walk.

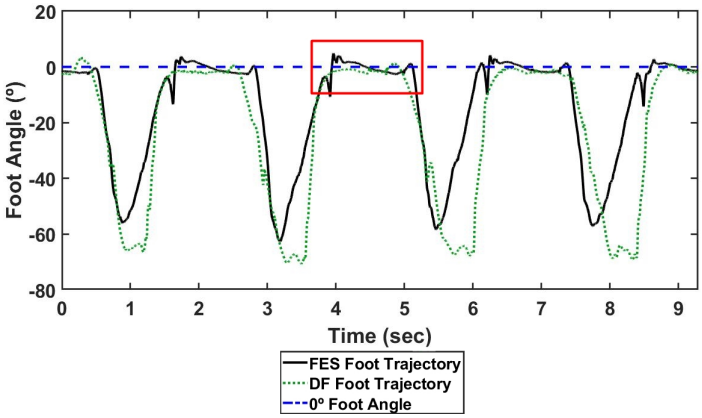

Figure 5.27: Comparison between DF gait and gait corrected with FES at 1.5 km/h.

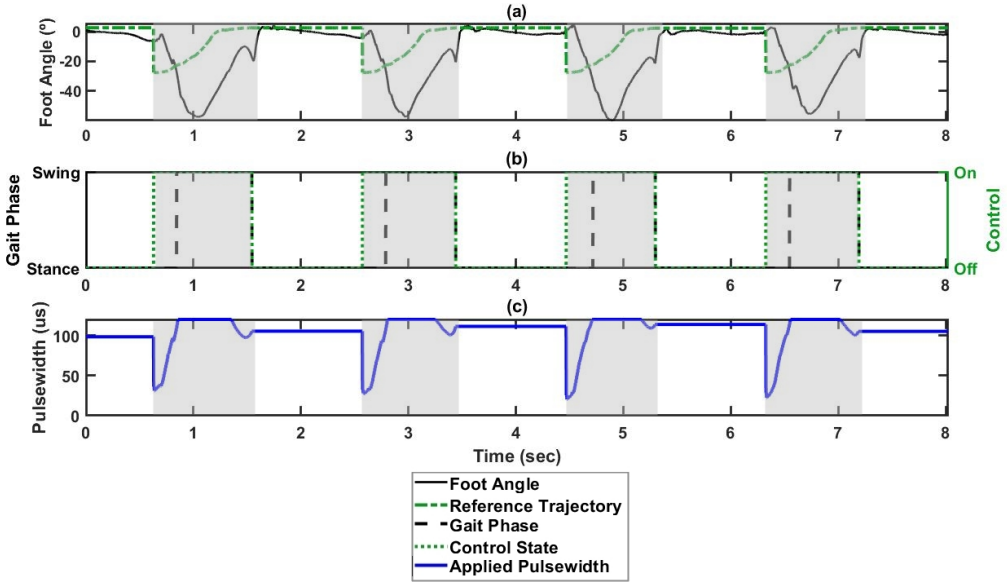

Figure 5.28: Real-time trajectory tracking control strategy validation at 2 km/h: (a) Foot angle and reference trajectory, (b) Gait event detection and control activation and (c) Applied pulsewidth. The grey areas represent the stages when the stimulation is applied (control strategy is on).

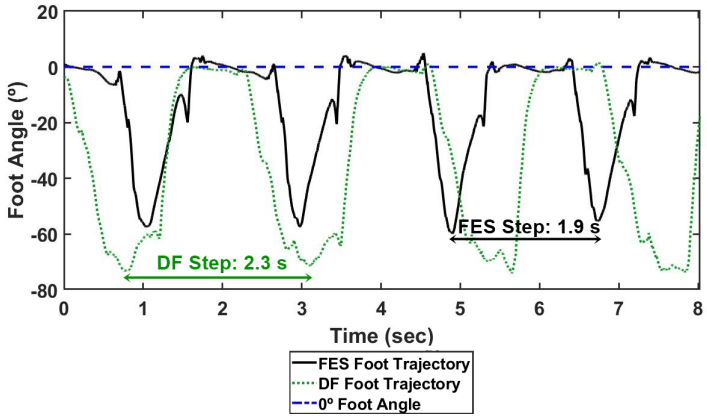

Figure 5.29: Comparison between DF gait and gait corrected with FES at 2 km/h.

5.4 DISCUSSION

In this section, a **trajectory tracking control strategy for DF correction was proposed**. An identical control strategy with a basic inverse model was used to control the knee angle (Chen et al. (2004)). However, to the best of the authors' knowledge, **this is the first time a reference trajectory created from the gait of healthy subjects was used in a trajectory tracking control strategy, composed by a dynamic inverse NARX Neural Network model of the TA muscle and a PD controller, in order to correct DF.**

Gait Phase Detection

A **gait phase detection strategy was implemented**, in order to **determine the gait events that mark the beginning and end of the swing phase**: the toe-off and heel strike, respectively. The algorithm proved successful for the speeds of 1 km/h, 1.5 km/h and 2 km/h. Furthermore, since there is a time delay since the stimulus is applied until the movement begins, a delay removal method was also created. This **method was based on the duration of the subject's stance phase**, that was determined in the beginning of each trial. During the real-time gait validation this **algorithm was able to start stimulation earlier than toe-off, thus removing the time delay successfully**.

Results

Two configurations were used to test the trajectory tracking control strategy: a **static configuration**, with the subject sitting on a chair, and a **gait configuration**, with the subject walking on a treadmill. The static configuration was **used to determine if the control strategies were able to track the reference trajectories** and to **compare the performance of the open-loop control strategy with the trajectory tracking control strategy**. The gait configuration was **used to determine if the trajectory tracking control strategy was able to correct DF during real-time gait**.

For the open-loop validation, the **dynamic inverse model predicted the correct pulsewidth values for the 1 km/h trajectory accurately**, resulting in the foot following the desired trajectory with an **accuracy of 68.16%**. This showed **the model was tailored to the user's characteristics**. However, for the 1.5 km/h and 2 km/h trajectories it was not able to predict the necessary pulsewidth, likely because the trajectories had more abrupt increases when compared to the 1 km/h trajectory. One way to solve this problem would be to **stimulate the TA muscle with signals with more variations, by using FRN filtered at higher frequencies**, and then using the acquired data to train the model. However, **when increasing the frequency it is necessary to take into account the comfort of the subject and its physiological limitations, since signals with fast variations may cause discomfort and involuntary reflexes** (Le et al. (2010)).

By pairing the **PD controller with the dynamic inverse model**, the **tracking accuracy increased by 9.71%, 39.46% and 1.53%** for the 1 km/h, 1.5 km/h and 2 km/h trajectories, respectively. For the 2 km/h trajectory the increase in accuracy was minimal because **the initial foot angle angle was higher than the initial reference trajectory**, thus creating a delayed pulsewidth increase that translates in a delay in reaching the desired trajectory. **This was solved in the real-time gait validation**.

The **trajectory tracking control strategy** was also **validated with a 0.4 kg weight strapped to the foot**, to **test its robustness and ability to compensate for external disturbances**. For the **1.5 km/h trajectory**, the **control strategy was able to match the performance of the unrestrained validation**, decreasing only by 3.45%, thus **being able to compensate the external disturbances**.

Lastly, the **real-time gait validation** was done, to **test if the trajectory tracking control strategy was able to correct DF gait in real-time**. It was **tested with a healthy subject on a treadmill at three speeds: 1 km/h, 1.5 km/h and 2 km/h**. During the swing phase, **the control strategy was able to increase and decrease the applied pulsewidth according to the reference trajectory**, instead of providing a constant

stimulation pulse throughout the swing phase, in order to **help delay the onset of fatigue**. For every speed, **a pseudo-DF gait pattern was compared to the foot angle generated by the trajectory tracking control strategy in real-time**. This showed that, contrary to the DF gait, the **foot was able to rise above** 0°**, generating a foot movement similar to the healthy one**. This **prevents the subjects from dragging the foot on the ground, thus decreasing the likelihood of falling and tripping when walking**. The implemented control strategy was also **able to reduce step length**.

The validation results show the system can be used for real-time DF correction, since the muscular behaviour of healthy and paretic muscles is very similar (Chang et al. (1997)).

6

CONCLUSIONS

In this thesis a **novel Drop Foot (DF) correction control strategy** was developed, with the purpose of **increasing the quality of life** of subjects with gait impairments.

In Chapter 2 the study of Functional Electrical Stimulation (FES) methods to help subjects with motor disabilities, used in the commercial and research areas, helped to **identify what approach had yet been taken for DF correction**. An **empirical model** was chosen over a mechanistic one to **model the electrically stimulated *Tibialis Anterior* (TA) muscle**, due to the less complex calibration methods while maintaining the same accuracy. Furthermore, the favorable results found in the literature and the recent rise in the use of artificial intelligence methods for more user centered FES rehabilitation techniques, made the **Non-Linear Autoregressive Neural Network with Exogenous input (NARX Neural Network)** the chosen model in this project.

In Chapter 3 the requirements for the components and the system time scales were laid out, and the chosen components were able to respect these requirements. The result is a **light and small system**, that is **easily wearable and inserted into daily activities**. The use of the Inertial Measurement Unit (IMU) for the acquisition of foot kinematics **limits the number of sensors placed on the subject**, increasing its simplicity, which **increases user comfort** and facilitates the setup of the system. The tests, visualized with the oscilloscope, confirmed that the system is able to **perform the control strategy with a frequency of 125 Hz**, respecting the time constraint the human step frequency of 25 Hz.

In Chapter 4 Non-Linear Autoregressive Neural Network with Exogenous input (NARX Neural Network) models with different parameters were created, in order to determine which type of model is more suitable to be used in the real-time control strategy. The results indicated that the **models** should be **trained with dynamic signals** that **mimic the gradual behaviour of the biological movements** for more robust and accurate solutions.

The **innovative feature** of this strategy is the **dynamic inverse model** that uses the **foot angle as well and the angular velocity** to model the electrically stimulated TA muscle, for DF correction. This results in a more robust model, when compared to the basic inverse model, that can be used in the **real-time tracking of reference trajectories**. Furthermore, the **implemented calibration method** necessary to **create the personalized model** for each subject is simple enough to be carried out with DF patients, neither being very **time consuming nor putting too much physical strain** on the subjects. **The chosen model to implement in the trajectory tracking control strategy was a dynamic inverse model with 2 hidden layers and 10 neurons in each layer**.

The main constraint of this system is the response time of the muscle to the delivered stimulation. In order to overcome this obstacle a **time delay removal strategy** was implemented. The measurement of the duration of the stance phase allows an early beginning of the stimulation, so that the foot can start moving upon toe-off, thus **following the reference trajectory when expected**. Furthermore, in order to generate a movement as **close to the healthy one as possible**, the reference trajectories used in the trajectory tracking control strategy were acquired from **healthy subjects walking at different speeds**, as shown in Chapter 5.

Additionally, the **combination of the dynamic inverse model with the Proportional Derivative (PD) controller** increased the accuracy of the reference trajectory tracking, when compared to the dynamic inverse model in open-loop, and allowed the **tracking of the reference trajectory during real-time gait**. For any of the speeds with which the control strategy was validated on a treadmill, 1 km/h, 1.5 km/h and 2 km/h, **the control strategy was able to correct DF**, by having the foot at a positive angle every time heel strike occurred. This **prevents the subjects from dragging the foot on the ground, thus decreasing the likelihood of falling and tripping when walking**. Overall, the **trajectory tracking control strategy was able to correct DF at different speeds in real-time gait**, as can be seen in Chapter 5.

This project was able to answer all the research questions proposed in Chapter 1, throughout this dissertation.

How to provide a personalized experience for each user?

To **provide a personalized experience** for the user the designed system uses a model, in particular a **NARX Neural Network**. This model is able to **capture the dynamics of the electrically stimulated TA** muscle of each user, by acquiring **user-specific data using a calibration routine**.

How to provide a comfortable long-lasting experience for each user?

In order to provide a comfortable experience for the user, the system used **light and small components**, so it would not constraint any user movements. Furthermore, a long-lasting experience is only possible if the muscular fatigue is delayed. Therefore, in this project a **trajectory tracking control strategy, composed by a PD controller paired with a dynamic inverse NARX Neural Network model**, was used. Thus, **only the necessary stimulation pulse is applied at any given moment, depending on the desired reference trajectory**.

How to ensure a natural gait pattern?

To ensure a **natural gait pattern** the reference trajectory was obtained from **healthy subjects walking at different speeds**. This way, the DF gait is corrected not with a constant stimulation pulse, but with a **gradual movement that matches the natural one**.

6.1 FUTURE WORK

The first step to be taken next is the **validation of the system with DF patients**. Furthermore, in order to allow a complete freedom of movements, an **wireless IMU** should be implemented. This would improve the wearability of the system, as well as **simplify the user's setup**. In the future, more stimulators could be integrated in the system, in order to treat motor disabilities that use more than one muscle and are, therefore, more complex.

Another aspect to be taken into account for future improvements to the system is the speed selection. As it is, there is a manual change in the reference trajectory depending on the chosen treadmill speed. However, it will be important to **calculate the velocity in real-time** and **adapt the reference trajectory**, seeing as the system is meant to be worn for **daily activities**. In order to do that, more gait trajectories with healthy subjects will have to be acquired and a relation between then will have to be found. This task can possibly be done with machine learning. Additionally, the stance phase duration should be updated at every step, so the system's response time delay removal is even more effective.

The system was only tested with a healthy subject, therefore, in the first step the subject would walk correctly, so the system could determine the duration of the stance phase. When the system is validated with DF patients, during the **swing phase of the first step a constant pulse with the subject's saturation threshold value** should

be applied, so the system can determine the correct stance phase duration and the control strategy can be applied correctly during the rest of the gait (Seel et al. (2016b)).

Another important feature to be added to the system would be the **control of plantarflexion**, the movement of lowering the foot and toes, which is the antagonist movement of dorsiflexion. Usually, DF patients are also affected by slap foot, which is an inability to perform the plantarflexion movement in a controlled manner (Tu et al. (2017)). This world create a **more robust DF correction system**, by being able to **control the antagonist pair of muscles in real-time gait**.

BIBLIOGRAPHY

Arif Reza Anwary, Hongnian Yu, and Michael Vassallo. Optimal Foot Location for Placing Wearable IMU Sensors and Automatic Feature Extraction for Gait Analysis. *IEEE Sensors Journal*, 18(6):2555 – 2567, 2018. doi: 10.1109/JSEN.2017.2786587.

Nor Azura, Saadi Bin, Ahmad Kamaruddin, Norazan Mohamed, and Noorhamizah Binti Mohamed. The Quadriceps Muscle of Knee Joint Modelling Using Neural Network Approach : Part 1. pages 52–57, 2016.

A. L. Basith, A. Arifin, F. Arrofiqi, T. Watanabe, and M. Nuh. Embedded fuzzy logic controller for functional electrical stimulation system. *2016 International Seminar on Intelligent Technology and Its Applications (ISITIA)*, pages 89–94, 2016. doi: 10.1109/ISITIA.2016.7828639. URL http://ieeexplore.ieee.org/document/7828639/.

O Brend, C Freeman, and M French. Multiple-Model Adaptive Control of Functional Electrical Stimulation. *IEEE Transactions on Control Systems Technology*, 23(5): 1901–1913, 2015. ISSN 1063-6536. doi: 10.1109/TCST.2015.2394508.

F Brunetti, Á Garay, J C Moreno, and J L Pons. Enhancing functional electrical stimulation for emerging rehabilitation robotics in the framework of hyper project. *IEEE International Conference on Rehabilitation Robotics*, 2011. ISSN 19457898. doi: 10.1109/ICORR.2011.5975370.

Jane Burridge, Morten Haugland, Birgit Larsen, Ruth M Pickering, Niels Svaneborg, Helle K Iversen, P Br??gger Christensen, Jens Haase, Jannick Brennum, and Thomas Sinkjaer. Phase II trial to evaluate the ActiGait implanted drop-foot stimulator in established hemiplegia. *Journal of Rehabilitation Medicine*, 39(3):212–218, 2007. ISSN 16501977. doi: 10.2340/16501977-0039.

G. C. Chang, J. J. Luh, G. D. Liao, J. S. Lai, C. K. Cheng, B. L. Kuo, and T. S. Kuo. A neuro-control system for the knee joint position control with quadriceps stimulation. *IEEE Transactions on Rehabilitation Engineering*, 5(1):2–11, 1997. ISSN 10636528. doi: 10.1109/86.559344.

Mo Chen, Bian Wu, Xinxin Lou, Ting Zhao, Jianhua Li, Zhisheng Xu, Xiaoling Hu, and Xiaoxiang Zheng. A self-adaptive foot-drop corrector using functional electrical stimulation (FES) modulated by tibialis anterior electromyography (EMG) dataset. *Medical Engineering and Physics*, 35(2):195–204, 2013. ISSN 13504533. doi: 10.1016/j.medengphy.2012.04.016. URL http://dx.doi.org/10.1016/j.medengphy.2012.04.016.

Yu Luen Chen, Shih Ching Chen, Weoi Luen Chen, Chin Chih Hsiao, Te Son Kuo, and Jin Shin Lai. Neural network and fuzzy control in FES-assisted locomotion for the hemiplegic. *Journal of Medical Engineering and Technology*, 28(1):32–38, 2004. ISSN 03091902. doi: 10.1080/03091900310001211523.

D C de Souza, M C Gaiotto, G N Nogueira Neto, M C F de Castro, and P Nohama. Power amplifier circuits for functional electrical stimulation systems. *Research on Biomedical Engineering*, 33(2):144–155, 2017. ISSN 24464740. doi: 10.1590/2446-4740.07716.

Barbara M Doucet, Amy Lam, and Lisa Griffin. Neuromuscular electrical stimulation for skeletal muscle function. *The Yale journal of biology and medicine*, 85:201–215, 2012. ISSN 1551-4056. doi: 10.1007/BF02371250. URL http://www.pubmedcentral.nih.gov/articlerender.fcgi?artid=3375668{&}tool=pmcentrez{&}rendertype=abstract.

Ryan J. Downey, Mark Tate, Hiroyuki Kawai, and Warren E. Dixon. Comparing the force ripple during asynchronous and conventional stimulation. *Muscle and Nerve*, 50(4):549–555, 2014. ISSN 10974598. doi: 10.1002/mus.24186.

Ryan J. Downey, Matthew J. Bellman, Hiroyuki Kawai, Chris M. Gregory, and Warren E. Dixon. Comparing the Induced Muscle Fatigue Between Asynchronous and Synchronous Electrical Stimulation in Able-Bodied and Spinal Cord Injured Populations. *IEEE Transactions on Neural Systems and Rehabilitation Engineering*, 23(6):964–972, 2015a. ISSN 15344320. doi: 10.1109/TNSRE.2014.2364735.

Ryan J. Downey, Teng Hu Cheng, Matthew J. Bellman, and Warren E. Dixon. Closed-Loop Asynchronous Neuromuscular Electrical Stimulation Prolongs Functional Movements in the Lower Body. *IEEE Transactions on Neural Systems and Rehabilitation Engineering*, 23(6):1117–1127, 2015b. ISSN 15344320. doi: 10.1109/TNSRE.2015.2427658.

Arthur Eberstein and Sharon Eberstein. eberstein1996_denervated.pdf. *Medicine & Science in Sports & Exercise*, 28(12):1463 – 1469, 1996.

Waleed Farahat and Hugh Herr. A method for identification of electrically stimulated muscle. *Conference proceedings : ... Annual International Conference of the IEEE Engineering in Medicine and Biology Society. IEEE Engineering in Medicine and Biology Society. Conference*, 6:6225–6228, 2005. ISSN 1557-170X. doi: 10.1109/IEMBS.2005.1615918.

M Ferrarin and E D'Acquisto. An experimental PID controller for knee movement restoration with closed loop FES system. *... in Medicine and ...*, pages 453–454, 1996. ISSN 05891019. doi: 10.1109/IEMBS.1996.657039. URL http://ieeexplore.ieee.org/xpls/abs{_}all.jsp?arnumber=657039.

Joana Figueiredo, Paulo Félix, Luís Costa, Juan C Moreno, Senior Member, and Cristina P Santos. Gait Event Detection in Controlled and Real-life Situations : Repeated Measures from Healthy Subjects. *IEEE Transactions on Neural Systems and Rehabilitation Engineering*, 26(10):1945–1956, 2018. doi: 10.1109/TNSRE.2018.2868094.

Alessandro Filippeschi, Norbert Schmitz, Markus Miezal, Gabriele Bleser, Emanuele Ruffaldi, and Didier Stricker. Survey of Motion Tracking Methods Based on Inertial Sensors : A Focus on Upper Limb Human Motion. pages 1–40, 2017. doi: 10.3390/s17061257.

K. Fujita, K. Shiga, and H. Takahashi. Learnig control of hand posture with neuralnetwork in fes for hemiplegics. *IEEE International Conference in Medicine and Biology Society*, 20(5):2588–2589, 1998.

Gavin Giovannoni and George Pepper. Time matters in multiple sclerosis. Technical report, Brain Health, 2015.

Kyler M Godwin, Joan Wasserman, and Sharon K Ostwald. Cost Associated with Stroke: Outpatient Rehabilitative Services and Medication. 18(Suppl 1):676–684, 2011. doi: 10.1310/tsr18s01-676.

Ashraf S. Gorgey, Christopher D. Black, Christopher P. Elder, and Gary A. Dudley. Effects of Electrical Stimulation Parameters on Fatigue in Skeletal Muscle. *Journal of Orthopaedic & Sports Physical Therapy*, 39(9):684–692, 2009. ISSN 0190-6011. doi: 10.2519/jospt.2009.3045. URL http://www.jospt.org/doi/10.2519/jospt.2009.3045.

Chris M. Gregory, Warren Dixon, and C. Scott Bickel. Impact of varying pulse frequency and duration on muscle torque production and fatigue. *Muscle and Nerve*, 35(4):504–509, 2007. ISSN 0148639X. doi: 10.1002/mus.20710.

Mitsuhiro Hayashibe, Qin Zhang, and Christine Azevedo-Coste. Dual predictive control of electrically stimulated muscle using biofeedback for drop foot correction. *IEEE International Conference on Intelligent Robots and Systems*, pages 1731–1736, 2011. ISSN 2153-0858. doi: 10.1109/IROS.2011.6048654.

J. C. Hsieh, C. C. Chen, S. C. Chen, Y. L. Chen, Y. C. Li, Y. Y. Shih, and T. S. Kuo. Novel control for ambulation function restoration in a non-invasive functional electrical stimulation system. *IFMBE Proceedings*, 25(9):464–467, 2009. ISSN 16800737. doi: 10.1007/978-3-642-03889-1-124.

Kenneth J Hunt, Marko Munih, Nick De N Donaldson, and Fiona M D Barr. Investigation of the Hammerstein Hypothesis in the Modeling of Electrically Stimulated Muscle. 45(8):998–1009, 1998.

Eukene Imatz-ojanguren, Eloy Irigoyen, David Valencia-blanco, and Thierry Keller. electrical stimulation in able-bodied and hemiplegic subjects. 0:1–9, 2016. doi: 10.1016/j.medengphy.2016.06.008.

Invensense. MPU-6000 and MPU-6050 Product Specification, 2013.

Tianjian Ji. Frequency and velocity of people walking. (February), 2015.

Catherine A Johnson, Jane H Burridge, Paul W Strike, Duncan E Wood, and Ian D Swain. The Effect of Combined Use of Botulinum Toxin Type A and Functional Electric Stimulation in the Treatment of Spastic Drop Foot After Stroke : A Preliminary Investigation. 85(June):902–909, 2004. doi: 10.1016/j.apmr.2003.08.081.

Lise A Johnson and Andrew J Fuglevand. Mimicking muscle activity with electrical stimulation. *Journal of Neural Engineering*, 8(1):016009, 2011. ISSN 1741-2560. doi: 10.1088/1741-2560/8/1/016009. URL http://stacks.iop.org/1741-2552/8/i=1/a=016009?key=crossref.e3c62ce45c474d193a0fbb65b8b2b125.

Trisha Kesar, Li Wei Chou, and Stuart A. Binder-Macleod. Effects of stimulation frequency versus pulse duration modulation on muscle fatigue. *Journal of Electromyography and Kinesiology*, 18(4):662–671, 2008. ISSN 10506411. doi: 10.1016/j.jelekin.2007.01.001.

Bhawna Khattar, Alakananda Banerjee, Rajsekhar Reddi, and Anirban Dutta. Feasibility of Functional Electrical Stimulation-Assisted Neurorehabilitation following Stroke in India: A Case Series. *Case Reports in Neurological Medicine*, 2012: 1–7, 2012. ISSN 2090-6668. doi: 10.1155/2012/830873. URL http://www.hindawi.com/journals/crinm/2012/830873/.

J. Knutson, M. Harley, T. Hisel, S. Hogan, M. Maloney, and J Chae. Contralaterally Controlled Functional Electrical Stimulation for Upper Extremity Hemiplegia: An Early-Phase Randomized Clinical Trial in Subacute Stroke Patients. *Neurorehabil Neural Repair*, 26(3):239–246, 2012. doi: 10.1177/1545968311419301.Contralaterally.

Prakash Kumar and Anil Kumar. Modeling of Longitudinal Human Walking Force Using Self- Sustained Oscillator Modeling of Longitudinal Human Walking Force Using Self-Sustained Oscillator. (November), 2017. doi: 10.1142/S0219455418500803.

S P Kwakkel, S Godha, and G Lachapelle. Foot and Ankle Kinematics During Gait Using Foot Mounted Inertial System. (January), 2015.

Fengmin Le, Ivan Markovsky, Christopher T. Freeman, and Eric Rogers. Identification of electrically stimulated muscle models of stroke patients. *Control Engineering Practice*, 18(4):396–407, 2010. ISSN 09670661. doi: 10.1016/j.conengprac.2009.12.007. URL http://dx.doi.org/10.1016/j.conengprac.2009.12.007.

Zhan Li, Mitsuhiro Hayashibe, David Andreu, and David Guiraud. Real-time closed-loop FES control of muscle activation with evoked EMG feedback. *International IEEE/EMBS Conference on Neural Engineering, NER*, 2015-July(1):623–626, 2015. ISSN 19483554. doi: 10.1109/NER.2015.7146700.

M. Liberson, W. T.; Holmquest, H. J.; Scot, D.; Dow. Functional electrotherapy: Stimulation of the peroneal nerve synchronized with the swing phase of the gait of hemiplegic patients. *Archives of physical medicine and rehabilitation*, 42:101 – 105, 1961.

Tsungnan Lin, Bill G Horne, Peter Tiiio, C Lee Giles, and Senior Member. Learning Long-Term Dependencies in. I(6):1329–1338, 1996.

Tsungnan Lin, C Lee Giles, Bill G Horne, and S Y Kung. A Delay Damage Model Selection Algorithm for NARX Neural Networks. 45(11):2719–2730, 1997.

John Low, B a Hons, Ann Reed Ba, and Mary Dyson. Electrotherapy Explained Second edition Foreword by Electrical stimulation of nerve and muscle. *Director*.

Paulo Luzio de Melo. *A Novel Functional Electrical Stimulation System and Strategies for Motor Rehabilitation*. PhD thesis, Universidade de Lisboa - Instituto Superior Técnico, 2014.

Jovana Malešević, Suzana Dedijer Dujović, Andrej M. Savić, Ljubica Konstantinović, Aleksandra Vidaković, Goran Bijelić, Nebojša Malešević, and Thierry Keller. A decision support system for electrode shaping in multi-pad FES foot drop correction. *Journal of NeuroEngineering and Rehabilitation*, 14(1):1–14, 2017. ISSN 17430003. doi: 10.1186/s12984-017-0275-5.

Lana Z. Popović Maneski, Nebojša M. Malešević, Andrej M. Savić, Thierry Keller, and Dejan B. Popović. Surface-distributed low-frequency asynchronous stimulation delays fatigue of stimulated muscles. *Muscle & Nerve*, 48(6):930–937, 2013. ISSN 0148639X. doi: 10.1002/mus.23840. URL http://doi.wiley.com/10.1002/mus.23840.

P J Maria and Guilherme A Barreto. Long-Term Time Series Prediction with the NARX Network : An Empirical Evaluation. (March 2007), 2007.

P. L. Melo, M. T. Silva, J. M. Martins, and D. J. Newman. Technical developments of functional electrical stimulation to correct drop foot: Sensing, actuation and control strategies. *Clinical Biomechanics*, 30(2):101–113, 2015. ISSN 18791271. doi: 10.1016/j.clinbiomech.2014.11.007. URL http://dx.doi.org/10.1016/j.clinbiomech.2014.11.007.

L. Meng, B. Porr, and H. Gollee. Technical developments of functional electrical stimulation to restore gait functions: Sensing, control strategies and current commercial systems. *Yi Qi Yi Biao Xue Bao/Chinese Journal of Scientific Instrument*, 38(6):1319–1334, 2017. ISSN 02543087.

Robert Nguyen, Kei Masani, Silvestro Micera, Manfred Morari, and Milos R. Popovic. Spatially Distributed Sequential Stimulation Reduces Fatigue in Paralyzed Triceps Surae Muscles: A Case Study. *Artificial Organs*, 35(12):1174–1180, 2011. ISSN 0160564X. doi: 10.1111/j.1525-1594.2010.01195.x.

P. Hunter Peckham and Jayme S. Knutson. Functional Electrical Stimulation for Neuromuscular Applications. *Annual Review of Biomedical Engineering*, 7(1):327–360, 2005. ISSN 1523-9829. doi: 10.1146/annurev.bioeng.6.040803.140103. URL http://www.annualreviews.org/doi/10.1146/annurev.bioeng.6.040803.140103.

N S Popov, D J Ĉ, M Stankovi, G M Krajoski, and D Staniši. Development of a Closed Loop FES System Based on NARX Radial Based Network. pages 70–74, 2015. doi: 10.1007/978-981-287-573-0.

Lana Z. Popović and Nebojša M. Malešević. Muscle fatigue of quadriceps in paraplegics: Comparison between single vs. multi-pad electrode surface stimulation. *Proceedings of the 31st Annual International Conference of the IEEE Engineering in Medicine and Biology Society: Engineering the Future of Biomedicine, EMBC 2009*, pages 6785–6788, 2009. ISSN 1557-170X. doi: 10.1109/IEMBS.2009.5333983.

M. Pournezam, B. J. Andrews, R. H. Baxendale, G. F. Phillips, and J. P. Paul. Reduction of muscle fatigue in man by cyclical stimulation. *Journal of Biomedical Engineering*, 10 (2):196–200, 1988. ISSN 01415425. doi: 10.1016/0141-5425(88)90100-8.

F. Previdi. Identification of black-box nonlinear models for lower limb movement control using functional electrical stimulation. *Control Engineering Practice*, 10(1): 91–99, 2002. ISSN 0967-0661. doi: 10.1016/S0967-0661(01)00128-9. URL http://www.sciencedirect.com/science/article/pii/S0967066101001289.

F Previdi, K J Hunt, M H Fraser, E Ferchland, and J Raisch. Online identification and nonlinear control of the electrically stimulated quadriceps muscle. 13:1207–1219, 2005. doi: 10.1016/j.conengprac.2004.10.006.

Fabio Previdi and Emanuele Carpanzano. Design of a Gain Scheduling Controller for Knee-Joint Angle Control by Using Functional Electrical Stimulation. 11(3):310–324, 2003.

Shuang Qiu, Feng He, Jiabei Tang, Jiapeng Xu, Lixin Zhang, Xin Zhao, Hongzhi Qi, Peng Zhou, Xiaoman Cheng, Baikun Wan, and Dong Ming. Intelligent algorithm tuning PID method of function electrical stimulation using knee joint angle. *Conference proceedings : ... Annual International Conference of the IEEE Engineering in Medicine and Biology Society. IEEE Engineering in Medicine and Biology Society. Annual Conference*, 2014:2561–2564, 2014. ISSN 1557170X. doi: 10.1109/EMBC.2014.6944145.

J Quintern, R Riener, and S Rupprecht. Comparison of simulation and experiments of different closed- loop strategies for functional electrical stimulation: Experiments in paraplegics. *Artificial Organs*, 21(3):232–235, 1997.

Jan Rueterbories, Erika G. Spaich, and Ole K. Andersen. Gait event detection for use in FES rehabilitation by radial and tangential foot accelerations. *Medical Engineering and*

Physics, 36(4):502–508, 2014. ISSN 18734030. doi: 10.1016/j.medengphy.2013.10.004. URL http://dx.doi.org/10.1016/j.medengphy.2013.10.004.

Angelo M Sabatini, Chiara Martelloni, Sergio Scapellato, and Filippo Cavallo. Assessment of Walking Features From Foot Inertial Sensing. *IEEE transactions on bio-medical engineering*, 52(March):486–494, 2005. doi: 10.1109/TBME.2004.840727.

T. Schauer and K. Hunt. Linear Modelling and Controller Design for the Single Limb Movement of Paraplegics using FES. *IFAC Proceedings Volumes*, 33(3):7–12, 2000. ISSN 14746670. doi: 10.1016/S1474-6670(17)35480-0. URL http://dx.doi.org/10.1016/S1474-6670(17)35480-0.

Thomas Seel, Thomas Schauer, and Jörg Raisch. Iterative learning control for variable pass length systems. *IFAC Proceedings Volumes (IFAC-PapersOnline)*, 18(PART 1): 4880–4885, 2011. ISSN 14746670. doi: 10.3182/20110828-6-IT-1002.02180.

Thomas Seel, Cordula Werner, Jörg Raisch, and Thomas Schauer. Iterative learning control of a drop foot neuroprosthesis - Generating physiological foot motion in paretic gait by automatic feedback control. *Control Engineering Practice*, 48:87–97, 2016a. ISSN 09670661. doi: 10.1016/j.conengprac.2015.11.007. URL http://dx.doi.org/10.1016/j.conengprac.2015.11.007.

Thomas Seel, Cordula Werner, and Thomas Schauer. The adaptive drop foot stimulator – Multivariable learning control of foot pitch and roll motion in paretic gait. 38: 1205–1213, 2016b. doi: 10.1016/j.medengphy.2016.06.009.

Fatronik Serbia. INTFES: A multi-pad electrode system for selective transcutaneous electrical muscle stimulation. pages 2–4, 2011. URL http://ifess.org/proceedings/IFESS2011/IFESS2011{_}004{_}Velik.pdf.

Lynne R. Sheffler and John Chae. Neuromuscular electrical stimulation in neurorehabilitation. *Muscle & Nerve*, 35(5):562–590, 2007. ISSN 0148639X. doi: 10.1002/mus.20758. URL http://doi.wiley.com/10.1002/mus.20758.

Daniel Simonsen, Erika G. Spaich, John Hansen, and Ole K. Andersen. Design and Test of a Closed-Loop FES System for Supporting Function of the Hemiparetic Hand Based on Automatic Detection using the Microsoft Kinect sensor. *IEEE Transactions on Neural Systems and Rehabilitation Engineering*, 4320(c):1–1, 2016. ISSN 1534-4320. doi: 10.1109/TNSRE.2016.2622160. URL http://ieeexplore.ieee.org/document/7707366/.

Sebastijan Sprager and Matjaz B Juric. *Inertial Sensor-Based Gait Recognition: A Review*. 2015. ISBN 3861241935. doi: 10.3390/s150922089.

STMicroelectronics. Stm32f303k8. https://www.st.com/en/microcontrollers/stm32f303k8.html, 2018. [Online; accessed 20-November-2018].

Xikai Tu, Jiaxin Li, Jian Li, Chen Su, Shali Zhang, Haoran Li, Jingyan Cao, and Jiping He. Model-Based Hybrid Cooperative Control of Hip-Knee Exoskeleton and FES Induced Ankle Muscles for Gait Rehabilitation. *International Journal of Pattern Recognition and Artificial Intelligence*, 31(09):1759019, 2017. ISSN 0218-0014. doi: 10.1142/S0218001417590194. URL http://www.worldscientific.com/doi/abs/10.1142/S0218001417590194.

Brian R Umberger. Stance and swing phase costs in human walking. (March): 1329–1340, 2010.

Roos Van Swigchem, Vivian Weerdesteyn, Hanneke J. Van Duijnhoven, Jasper Den Boer, Tjemme Beems, and Alexander C. Geurts. Near-normal gait pattern with peroneal electrical stimulation as a neuroprosthesis in the chronic phase of stroke: A case report. *Archives of Physical Medicine and Rehabilitation*, 92(2):320–324, 2011. ISSN 00039993. doi: 10.1016/j.apmr.2010.10.038. URL http://dx.doi.org/10.1016/j.apmr.2010.10.038.

L. Venugopalan, P. N. Taylor, J. E. Cobb, and I. D. Swain. Upper limb functional electrical stimulation devices and their man–machine interfaces. *Journal of Medical Engineering & Technology*, 39(8):471–479, 2015. ISSN 0309-1902. doi: 10.3109/03091902.2015.1102344. URL http://www.scopus.com/inward/record.url?eid=2-s2.0-84947044971{&}partnerID=tZOtx3y1{%}5Cnhttp://www.tandfonline.com/doi/full/10.3109/03091902.2015.1102344.

Hai Peng Wang, Ai Wen Guo, Yu Xuan Zhou, Yang Xia, Jia Huang, Chong Yao Xu, Zong Hao Huang, X. Lü, and Zhi Gong Wang. A wireless wearable surface functional electrical stimulator. *International Journal of Electronics*, 104(9):1514–1526, 2017. ISSN 13623060. doi: 10.1080/00207217.2017.1312708. URL http://dx.doi.org/10.1080/00207217.2017.1312708.

Takashi Watanabe and Takumi Tadano. Design of Closed-Loop Fuzzy FES Controller and Tests in. (9):2261–2264, 2017.

Ihsan Mohd Yassin, Rozita Jailani, Megat Syahirul, Amin Megat, Rahimi Baharom, and Abu Huzaifah. Comparison between Cascade Forward and Multi-Layer Perceptron Neural Networks for NARX Functional Electrical Stimulation (FES) -Based Muscle Model. 7(1):215–221, 2017.

Hojun Yeom and Young-Hui Change. Autogenic EMG-Controlled Functional Electrical Stimulation for Ankle Dorsiflexion Control. *J Neurosci Methode*, pages 118–225, 2011. ISSN 0002-8177; 1943-4723. doi: 10.1016/j.jneumeth.2010.08.011.Autogenic.

Wu Yilei, Song Qing, Yang Xulei, and Lan Li. Recurrent Neural Network Control of Functional Electrical Stimulation Systems. pages 400–404, 2006.